Master's thesis

NTNU
Norwegian University of Science and Technology
Faculty of Medicine and Health Sciences
Department of Clinical and Molecular Medicine

Hanna Riina Elina Pulli

Deciphering the pathomolecular mechanisms underlying thoracic aortic aneurysm formation in syndromic patients

Master's thesis in Molecular Medicine
Supervisor: María Galán
Co-supervisor: Cristina Rodriguez Sinovas, Marit Walbye Anthonsen
May 2022

NTNU
Kunnskap for en bedre verden

Hanna Riina Elina Pulli

Deciphering the pathomolecular mechanisms underlying thoracic aortic aneurysm formation in syndromic patients

Master's thesis in Molecular Medicine
Supervisor: María Galán
Co-supervisor: Cristina Rodriguez Sinovas, Marit Walbye Anthonsen
May 2022

Norwegian University of Science and Technology
Faculty of Medicine and Health Sciences
Department of Clinical and Molecular Medicine

NTNU
Kunnskap for en bedre verden

Abstract

A thoracic aortic aneurysm (TAA) is local dilatation that occurs in the major blood vessel from which blood flows to the aorta. In the worst case, weakened dilation can lead to rupture. Clinical decision making for the management of thoracic aortic aneurysms is based on diameter monitoring and surgery. Novel drugs to prevent, stop or revert the dilation of the aortic wall are urgently needed. This study aimed to identify new therapeutic targets among those related to the endoplasmic reticulum (ER) and mitochondrial stress to handle aortic aneurysms in syndromic patients.

This study included three study groups; syndromic patients and non-syndromic patients, which were divided into bicuspid and genetic patients. Healthy donors formed the control group. Aortic wall tissue specimens for RNA extraction were collected from 43 patients. Gene expression was investigated by Illumina RNA sequencing to identify the differentially expressed genes (DEGs). Using bioinformatic analysis, the most significant DEGs were selected and analyzed. DEGs were validated with a quantitative real-time polymerase chain reaction. To measure circulating levels of selected candidate genes, including markers of ER stress and mitochondrial biogenesis, an enzyme-linked immunosorbent assay was performed for serum samples. In addition, to examine changes in the aortic wall structure, histological analyzes were performed.

Among the top-50 DEGs, we identified four genes exclusively upregulated in bicuspid TAA patients and eight genes exclusively upregulated in syndromic and genetic TAA patients. One gene was identified as upregulated in the damaged tissue of all three patient groups. DEGs were associated with many enriched inflammation pathway clusters. However, enriched pathway clusters related to homeostasis, mitochondria, and extracellular matrix were also noted. Enrichment and upregulation of chosen ER stress and mitochondrial biogenesis markers suggest that ER stress is somehow involved in TAA development. Clear differences in the circulating protein levels among patient groups could not be seen. Histological staining's strengthen the existing perception that dissimilar pathological features found in the wall of TAA are associated with patterns of aortic remodelling according to the dissimilar groups of the study.

Acknowledgements

This master project was performed during the years 2021-2022 in cooperation with the Department of Group of Regulatory Mechanisms in Cardiovascular Remodeling of the Sant Pau Institute of Biomedical Research and with the Institution of Clinical and Molecular Medicine (IKOM) of the Faculty of Medicine and Health Sciences, Norwegian University of Science and Technology (NTNU). Laboratory work was performed at the Sant Pau Institute of Biomedical Research, Barcelona.

I would like to thank my main supervisor María Galán for her instructions at the laboratory and her general guidance during this project and during the process of writing my thesis. I would not be able to do this without your help. I would also like to sincerely thank my co-supervisors, Cristina Rodriguez Sinovas and Marit Walbye Anthonsen, for all the advice and guidance during this whole process.

Finally, I want to thank for everyone working in the laboratory. I loved working with you. A special thanks to Lidia Puertas, who was always there to answer my questions, provided me with protocols and gave me technical assistance in the lab. Your help was invaluable.

Pulli, Hanna
Trondheim, May 2022

Table of Contents

List of Figures

List of Tables

List of Abbreviations

AAA	Abdominal aortic aneurysms
BAV	Bicuspid aortic valve
BiP	Immunoglobulin binding protein
DEG	Differentially expressed genes
ECM	Extracellular matrix
FEEL	Elastic fibre fragmentation/loss
EFD	Elastic fibre disorganization
EFTO	Elastic fibre thinning out
ER	Endoplasmic reticulum
FBN1	Fibrillin-1 gene
FDR	False discovery rate
GO	Gene Ontology
GSEA	Gene set enrichment analysis
LDS	Loeys-Diets syndrome
LMC	Laminar medial collapse
MD	Medial degeneration
MEMA	Mucoid extracellular matrix accumulation
MFS	Marfan syndrome
RNA-seq	RNA sequencing
SMC	Smooth muscle cell
TAA	Thoracic aortic aneurysm
TGF- β	Transforming growth factor- β
UPR	Unfolded protein response
vEDSs	Vascular Ehlers-Danlos syndrome
XBP1	X-box binding protein

1. Introduction

1.1. Aorta structure and definition

The aorta is the largest artery in the human body. An aortic aneurysm is one well-known pathogenesis of the aorta. The aorta can be divided into five anatomical segments (1). These are the aortic root, ascending aorta, aortic arch, descending aorta, and the subdiaphragmatic abdominal aorta (not shown in the figure) (Fig.1). These segments have distinct functional activities (1). Most significant cardiovascular malformations in the aorta are seen in the proximal segments (1).

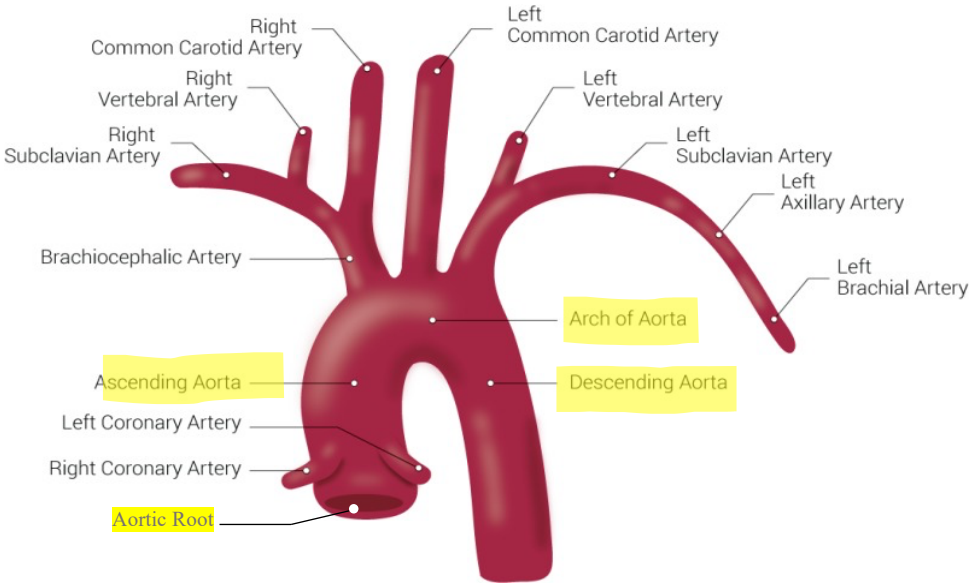

Figure 1. Structure of the thoracic aorta. Figure modified from illustration contributed by Beckie Palmer. Bookshelf ID: NBK537319 (2) .

The main cellular components of the aorta are elastin and collagen fibres, smooth muscle cells (VSMC), and a proteoglycan-rich ground substance which make the aorta an elastic artery (3). The aorta is composed of three-layer; intima, media and adventitia (Fig. 2). The intima is the innermost layer and thus is also in direct contact with blood. It is formed by a monolayer of endothelial cells (4). The thickness of the intima gradually increases during life due to the process of low-grade injury and repair over time. Because of this, the intima layer gradually expands, and is composed of extracellular matrix proteins (etc. collagen and mucopolysaccharides) and migrating VSMC (3). The media is the largest component of the artery and is composed of concentrically arranged lamellar units (3). These enclose VSMC, collagen fibres, and a large number of proteoglycans. The number and thickness of the lamellar units grow with age. The adventitia is the outermost layer of the blood vessel (4). It is primarily

composed of fibroblast and loosely arranged connective tissue, vasa vasorum, including lymphatic vessels and low numbers of perivascular leukocytes (3).

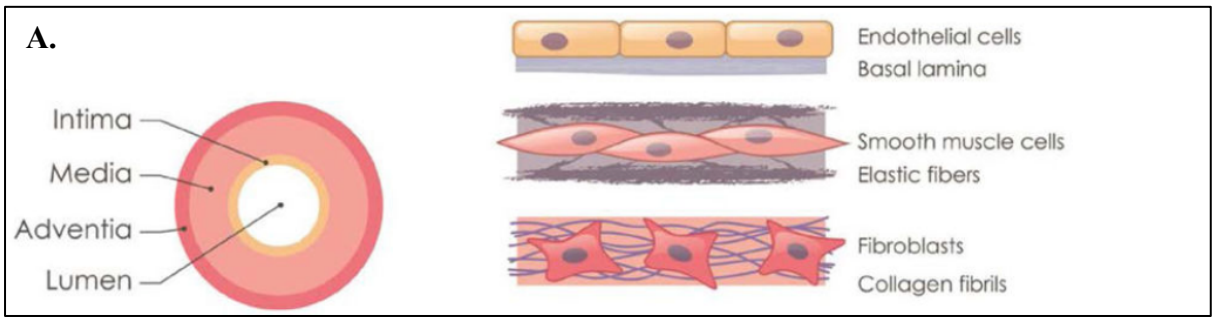

Figure 2. A: Schematic illustration of the three layers of the thoracic aorta. Illustration of the cellular and extracellular matrix components in each layer. Figure is modified from illustration from article written by Milewicz *et al*. (Doi:10.1161/ATVBAHA.118.310956) (5).

Adventitial cells can respond to external physiological stress and accordingly remodel the vascular wall (4). In this way, cells present in the adventitia contribute to the progression of different vascular diseases, such as atherosclerosis and hypertension (3). Adventitia is composed of multiple distinct cell populations, but the cell type most commonly associated with the adventitial layer is the fibroblast. These cells are responsible for the accumulation of abundant collagen fibrils around the vessels and have been shown to contribute to vascular remodelling (4). It has been observed that after vascular injury, fibroblasts secrete extracellular matrix (ECM) and inflammatory mediators leading to vascular stiffness and tissue disruption (4).

1.2. Aortic aneurysm

The unifying factor between many genetic disorders, affecting the aorta, is that they weaken the aortic wall predisposing the patient to fatal aortic aneurysms. Aneurysms are pathological dilations localized in any artery and vessel (6, 7). When the intima is damaged, blood can enter the wall of the blood vessel which can lead to formation of hematoma (7). Since the elasticity of the blood vessel wall weakens, whereby it can pouch out due to the impact of the constant blood pressure (7). The generally accepted definition of an aneurysm is a diameter of 1,5 times the normal. The pathological processes involved in the formation of the aneurysms include upregulation of proteolytic pathways, inflammation, arterial wall matrix degeneration and cell loss (6). When an aneurysm gradually expands, there is always a risk of rupture. In an untreated aneurysm, the aortic wall continues to weaken following progressive dilatation, and eventually ruptures. A ruptured aneurysm is linked to a mortality of 50-80% (8).

An aneurysm can develop in both the thoracic and abdominal aortic regions (8, 9) (Fig. 3). Thoracic aortic aneurysms (TAA) are around five times less common than abdominal aortic aneurysms (AAA) (6). Thoracic and abdominal aortic aneurysms are distinct disease entities and pathophysiology, and risk factors differ between them (6, 10). Differences between these disorders arise from differences in their wall structure, and the genetic variances underlying aneurysms in both regions. For example, the abdominal aorta is more prone to aneurysmal degeneration than the thoracic portion. AAA shares many risk factors with coronary artery disease, for example, atherosclerosis, smoking and male sex (10).

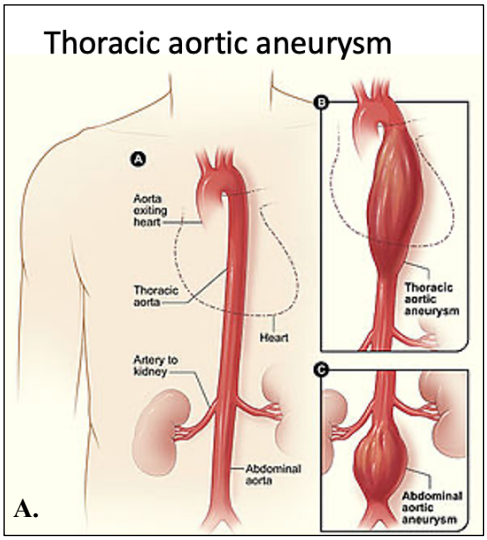

Figure 3. Aortic aneurysm. **A:** Thoracic aortic aneurysm (TAA) and Abdominal aortic aneurysm (AAA) illustrated. Figure modified from the illustration collected from webpage of British Heart Foundation (11).

TAA affects 1% of the general population, and it tends to enlarge an average of 0.14 cm per year (12). TAAs are usually asymptomatic until dissection or rupture, which are often fatal. Life expectancy can be improved if TAA is identified and treated with appropriate blood pressure control and surgical intervention (12). In TAA, genetic influences play an important role (10). Since the discovery of the familial nature of thoracic aortic aneurysm and dissection (TAAD) nearly 2 decades ago, at least 37 TAAD-causing genes have been identified to date. With this data, it has been estimated that 30% of the patients with familial non-syndromic TAAD harbor a pathogenic mutation in one of these genes (12).

TAA is demonstrated to be inherited in the autosomal dominant way by mendelian pedigrees, thus suggesting a considerable impact by single-gene mutations (10). TAAs are most seen in the ascending (40%) or descending (35%) portion of the thoracic aorta (Fig. 1, 3) (6). The inherent difference between these two is still not well known. However, it has been shown that

ascending TAA is genetically triggered whereas, in the case of descending TAA, this has not been demonstrated (10). Descending TAA is more often associated with atherosclerosis, hypertension and age than are ascending TAAs (10). This is also accurate with the absence of syndromic association (10).

1.3. Predisposing factor for thoracic aortic aneurysm

During their growth, thoracic aorta aneurysms (TAA) are asymptomatic, giving the treatment a poor prognosis. Mortality for the TAA ranges from 94% to 100% (13). Due to its location in the thorax, they are hard to diagnose. They are usually noticed incidentally in the context of other examinations like chest computed tomography (CT) (13). In the absence of a known genetic syndrome, it has hypothesized that genetic factors predispose an individual to aortic diseases (14). Genetic factors tend to have an influence on the familial aggregation of TAA with multiplex pedigrees (15). It has been indicated that 11% to 19% of patients with TAA have other affected family members, supporting the hypothesis (14).

Approximately 20% of TAAs are part of a syndrome that is often associated with single-gene mutations, including Marfan syndrome (MFS), Loeys-Dietz syndrome (LDS) and vascular Ehlers-Danlos syndrome (vEDS) (6). The importance of single gene mutations as a cause of an aneurysm decreases with the transition from the ascending to the descending and abdominal aorta (6). It is noted that especially genes influencing ECM proteins and microfibrils, the transforming growth factor-β (TGF-β) pathway and smooth muscle contraction appear to be very important in the development of TAA in humans (6). The early differentiation of aortic SMCs is dependent on TGF-β and microfibrils. These mechanisms are considered to have a contribution to TAAs observed in Loeys-Dietz syndrome and Marfan Syndrome (6).

Syndromic disorders, including MFS and LDS, has been associated with bicuspid aortic valve (BAV), congenital heart disease, which has been associated with a monogenic thoracic aortic aneurysm (16, 17). BAV is typically sporadic, but in ≈ 10% of the cases it has also been recognized in first-degree relatives (16). In a normal aortic valve, there are three cusps, in a bicuspid valve there are only two cusps, or in rare cases only one (17). BAV can cause narrowing of the aortic valve, backward flow of blood or enlarged aorta (aortopathy) (17).

1.4. Marfan syndrome

Marfan Syndrome (MFS) is a severe hereditary connective tissue disorder with multiple clinical manifestations (18). The characteristic histological manifestations are fragmentation, disorganization, and loss of elastic fibres. These involve skeletal and ocular structures, blood vessels, and lungs. MFS furthermore includes cardiovascular system abnormalities characterized by progressive aortic root enlargement and ascending aortic aneurysm (18). Aortic aneurysm leading to aortic dissection and rupture is the event that contributes to premature mortality (19).

MFS has a prevalence of ≈ 1 in 3000 to 5000 individuals (20, 21). It is the most recognised syndromic disorder causing TAA and thus best studied from genetic syndromes which are predisposing to TAA (22). MFS is caused by an autosomal dominant mutation in the *FBN1* (fibrillin-1) gene on chromosome 15 (18, 20, 21, 23). This gene codes a large scaffolding glycoprotein, one of three fibrillin subtypes, which is a necessary constituent of the extracellular matrix (19). As a result of mutation, fibrillin-1 is either dysfunctional or less abundant.

In healthy tissue, the interstitial space is full of microfibrils which form the connective tissue. The main component of microfibrils is a glycoprotein called fibrillin. Fibrillin is crucial for elastin deposition, to the formation of elastic fibres and laminae (24). It is also an important extracellular regulator of TGF-β activity (24). Fibrillin regulates tissue growth by removing or sequestering TGF-β, which, in turn, stimulates tissue growth. If fibrillin-1 is dysfunctional or less abundant, extracellular matrix containes fewer functioning microfibrils in, which causes less tissue integrity and elasticity. Additionally, TGF-β does not get effectively sequestered, leading to excessive tissue growth due to excessive TGF-β signalling (24).

More than 803 mutations of *FBN1* have been associated with the presence of aneurysms (24, 25). MFS predisposes to aorta dilations and cystic medial necrosis. Both conditions weaken the aorta, making it susceptible to aneurysms, dissection, or rupture. One of the fatal complications of MFS is the risk of developing TAA (19, 21). Ascending aortic aneurysm and any complications related to it are the primary cause of death before successful preventative therapies (21). Therefore, survival is mainly determined by aortic complications in MFS patients of whom progressive aortic root enlargement is the most common complication (19,

21). The rupture of aortic aneurysms is responsible for over 90 % of the mortality of patients with MFS.

1.5. Loeys-Dietz syndrome

Even though the MFS is the most prominent syndrome predisposing the TAA, there are other genetic syndromes with similar arterial phenotypes, including Loeys-Dietz syndrome (LDS) whose prevalence has been underestimated (22). LDS is a highly penetrant autosomal dominant disorder characterized by multisystemic involvement. The genetic cause is heterogeneous and includes mutations in *TGBR1/2, SMAD2/3,* or *TGFB2/3* gene (22, 26, 27). All these genes are coding for components of the TGF-β signalling pathway (22, 26, 27). In aortic tissue, these mutations cause loss and disruption of elastic fibres. This compromises the regular stretch and robustness of the tissue and accumulates collagen in the media or middle part of the aortic wall. Despite the loss of function associated with these mutations, the aortic tissues of patients show evidence of increased TGF- β signalling (26). Natural history is significant for early aggressive aortic root aneurysms and aortic dissection at the smaller aortic diameter and arterial aneurysms (28). This is true throughout the arterial tree.

1.6. Current therapies to treat aneurysm in syndromic patients

The current treatment of the MFS and LDS aims to delay aortic dilation progression to avoid aortic complications. Beta-blockers are the standard treatment for preventing this. Management of aortic dilation also includes regular aortic imaging to evaluate the process of aortic dilation. If aortic dilation has reached a defined threshold, it will be surgically repaired (20, 21).

Life expectancy in MFS and LDS has improved considerably due to the prophylactic surgical removal of the formed aortic aneurysm (21). This procedure has been applied more aggressively in the past decades, which has minimized sudden death due to ascending aortic rupture. Surgery is often performed in MFS children/adolescents. When treating the LDS, early surgical intervention is usally needed at the childhood (29). While aortic surgery is effective, it is a high-risk procedure. After surgery, the disease continues in other parts of the aorta, where aortic dissections in the thoracic descending aorta often occur before the surgical standards have been met (29).

Knowledge gained from the treatment of MFS patients have also been used in many treatments strategies for LDS patients (29). The current therapeutic strategy to treat MFS is thoracic

reparatory surgery combined with one of two approaches; One to reduce abrupt ventricular ejection and the second to reduce TGF-β hypersignalling (21, 30). However, results from clinical trials comparing the effectiveness of both treatment approaches have been conflicting (21, 30). Therefore, preventive open thoracic aorta surgery and endovascular repair remain the only effective strategies currently available to treat aortic-root dilatation in MFS. Advances in pharmacological and surgical therapies have resulted in a longer life expectancy for MFS and LDS patients (20, 31). Unfortunately, the number of MFS patients requiring secondary interventions as a consequence of other vascular complications even after successful aortic root surgery has substantially increased (32). For this reason, novel drugs to prevent, stop or revert the aortopathy are urgently needed.

1.7. The endoplasmic reticulum stress and the unfolding protein response (UPR)

The possible role of ER stress in the development of aortic aneurysms has been previously studied (8, 33). The ER is an extensive membranous network containing cisternae and microtubules (34, 35). This membranous network branches from the nuclear envelope to the cell surface and is present in all eukaryotic cells (35, 36). ER has a central role in the biosynthesis, folding, assembly and modification of soluble and membrane proteins (34, 36). The ER also acts as a storage of calcium and responds to a number of stimuli, such as growth factors and a state of redox (36).

Most importantly, ER has a role in sensing cellular stress. Endoplasmic reticulum stress (ER stress) is a condition in which there is an imbalance between the protein-folding load and the capacity of ER. Imbalance leads to the accumulation of misfolded or unfolded proteins in the ER lumen (36). ER stress can be triggered by a physiological state that increases the demand for protein folding, or stimuli that disrupt the reactions by which proteins fold (36). Pathophysiological conditions that can disturb ER homeostasis include e.g., stroke, hypertension, and mutations which can impair protein folding (37, 38). Increased protein traffic through the ER compartments caused by gene mutations and altered posttranslational modifications both can cause protein aggregation in the ER lumen (34). The aggregation of proteins is a consequence of the high concentration of partially folded and unfolded proteins (34). ER mediates a specific set of intracellular signalling pathways in response to the accumulation of unfolded or misfolded proteins. These pathways are known as the unfolded protein response (UPR) (34, 36).

ER stress results from the accumulation of misfolded proteins often caused by mutated genes. Momentary activation of UPR may restore ER homeostasis by reprogramming gene expression to reduce ER load and increase protein folding capacity (39). When ER stress occurs, the UPR is triggered, activating three ER transmembrane sensors that initiate adaptive responses for maintaining cellular homeostasis (34, 40). The main UPR signaling cascades are initiated by three ER-localized protein sensors: inositol-requiring 1α (IRE1α), double-stranded RNA-dependent protein kinase (PKR)-like ER kinase (PERK), and activating transcription factor 6 (ATF6) (Fig. 4) (36).

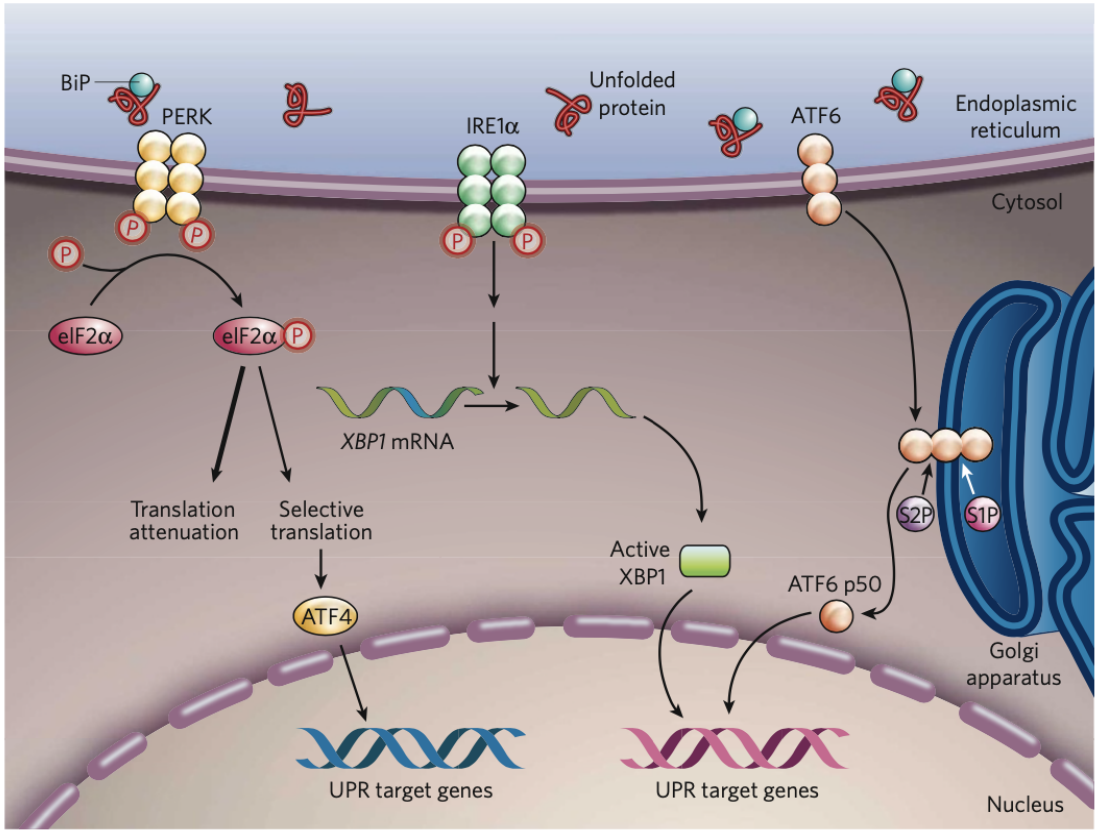

Figure 4. The mammalian UPR pathways. PERK, IRE1α and ATF6 sensor pathway during ER stress. Illustration is from article written by Zhang *et al*. (DOI: 10.1038/nature07203) (36).

In non-stressed conditions, all ER-stress sensors are kept in an inactive state by abundant ER chaperone BiP (34, 36). In the presence of ER stress, the BiP binds to unfolded or misfolded proteins leading to the release and activation of the ER-stress sensors (Fig.4) (34, 36). The most rapid response to ER stress is the release of the BiP from the PERK which leads to the homodimerization and transphosphorylation of the PERK (34, 36). This allows PERK to phosphorylate the α-subunit of eukaryotic translation-initiation factor 2α (eIF2α) (34, 36). This chain reaction activates the attenuations of the translations, which prevent the influx of

additional new protein into an ER lumen (Fig.4) (34, 36). Phosphorylation of the eIF2α also leads to translation of the ATF4 that induce expression of the UPR target genes involved in the oxidative stress response, and ER-stress-induced apoptosis, such as the C/EBP homologous protein or CHOP (Fig. 4) (34, 36).

In response to ER stress, pathways activated by ATF6 and IRE1α sensors function mainly in parallel. Autophosphorylation of the IRE1α activates its ribonuclease (RNase) activity which results in translation of the X-box binding protein (XBP1) isoform (34, 36). At the same time, ATF6 is released from BiP and translocated to the Golgi apparatus and there it is cleaved by the Proteases site-1 protease (S1P) and Proteases site-2 protease (S2P) (36). As a result of this process, a functional fragment of ATF6 is released into the cytosol from where it migrates the nucleus and activates transcription (Fig.4) (36). These two pathways induce transcription of the genes encoding ER chaperones, enzymes that promote protein folding, maturation, secretion, and ER-associated protein degradation or ERAD (36).

If the UPR-mediated efforts to restore correct protein-folding and homeostasis to the cell fail, apoptosis is activated (34, 36). Apoptosis caused by ER stress is mainly mediated by CHOP. CHOP induces the expression of numerous pro-apoptotic factors, which promotes protein synthesis and oxidative stress in already stressed cells (36). Chronic ER stress is a widespread causal mechanism of disease, including vascular disease (39).

1.7.1. ER stress is linked to mitochondrial dysfunction

ER and mitochondrial networks have an essential role determine cell fate under stress conditions and hence have a role in maintaining cellular homeostasis (35). Chronic ER stress and activation of UPR through endogenous or exogenous insults may cause impaired calcium and redox homeostasis and oxidative stress via protein overload, thereby affecting vital mitochondrial functions. ER and mitochondria are closely associated through structural and functional communication (35, 41) Harmful cross-talk between both organelles boosts mitochondrial dysfunction, generation of the reactive oxygen species (ROS) and apoptosis (34, 42). ROS generation plays a pivotal role in cardiovascular disease, especially mitochondrial ROS production, which could act as a unifying mechanism that links central pathways contributing to vascular dysfunction. Another significant source of vascular ROS is the nicotinamide adenine dinucleotide phosphate-oxidase (NADPH oxidase) family. Among other mediators, shear stress and ER stress upregulates NADPH oxidase (43). Mitochondria is a target of ROS produced by NADPH oxidase, which leads to more mitochondrial ROS

generation. If oxidative stress exceeds mitochondrial anti-oxidant capacity, mitophagy occurs to disrupt the damaged mitochondria and maintain cellular homeostasis (44).

Calcium released from the ER increases the production of mitochondrial ROS, and their toxic accumulation within ER and mitochondria disturbs organelle function. Continuous ER stress is known to stimulate inflammatory responses, potentially through UPR pathways. ER malfunction can be additionally increased by mitochodrial dysfunction and ROS formation due to inflammation. This causes a vicious cycle. Mitochondrial dysfunction causes changes in cell behaviour, exhaustion and eventually cell death which eventually contributes to in the development of aneurysm disease (45, 46).

Mitochondrial and ER stress are critically involved in the physiopathology of cardiovascular diseases. Persistent ER stress activation and its deleterious cross-talk with mitochondria initiate oxidative stress, mitochondrial dysfunction, and promote inflammatory pathways, which in turn contribute to the pathophysiology of aortic aneurysms (33, 47). The possible role of ER stress in the development of aneurysm formation in AAA patients and in MFS patients has been previously described (47, 48).

MFS is a representative model of aorta aneurysms in which oxidative stress is a relevant factor in pathogenesis. Continuous expression of mutated genes in MFS patients also results in a chronic inflammatory condition that gradually alters the structure of the vessel wall and leads to aortic dilation. Aortic aneurysms in MFS, and LDS agglutinate aspects in which ER stress may actively act as a pathological trigger leading to the expansion of cardiovascular damage. Since ER stress is a chronic event that maintains an inflammatory state, it will lead to cell apoptosis and tissue regeneration in a highly pro-oxidative environment. Therefore, further studies are needed to explore the implication of ER stress and its relationship with oxidative stress in arterial pathogenesis occurring in MFS and other related diseases including LDS.

1.8. Aim of the study

This study aims to identify new therapeutic targets among those related to the endoplasmic reticulum (ER) and mitochondrial stress to handle aortic aneurysms in syndromic patients. To achieve this objective, differentially expressed genes (DEGs) will be identified by RNA sequencing analysis in aneurysmal aortas from syndromic patients in comparison with aneurysmal aortas from non-syndromic patients (BAV and genetic) and with healthy aortas.

Using bioinformatic analysis, the most significant DEGs were selected and analyzed. The selected targets will be validated by gene and protein expression studies.

Additionally, this study aims to determine whether levels of circulating molecules related to ER stress, shear stress and inflammation are good potential biomarkers for the progression of the aneurysm in patients, by quantifying serum levels and tissue levels of ER-stress related markers as potential biomarkers for aortopathy prognosis. Finally, the study illustrated medial degenerations (MD) in TAA with different histological staining's.

2. Methodology

2.1. Human samples

The study population consisted of 43 patients. Samples were obtained during elective or emergency aortic root surgery for TAA dissection. Patient clinical data were retrieved while maintaining anonymity. Only patients of legal age were included. The Functional Unit for Aorta Pathologies of the Cardiology Service at the hospital provided the human aortic aneurysm samples collected from MFS and LDS patients and from non-syndromic patients (patients diagnosed with bicuspid aorta (BAV) or those patients who are classified as genetic due to a family history of aneurysm) undergoing corrective surgery of aortic aneurysm. Non-syndromic patients were classified into two groups: those diagnosed with BAV, or those who had a genetic mutation related to aneurysm formation and a family history of aneurysm but who were not classified under any syndrome. Baseline characteristics of the patients are shown in Table 1. Approval to use the discarded human tissue was given by the Ethics and Clinical Research Committee of the Hospital de la Santa Creu I Sant Pau (HSCSP, Barcelona), Ref. IIBSP-MAR-2019-08, and all the collected samples form part of the collection C.0005273 registered by the PI, Dr. María Galán, in the Instituto de Salud Carlos III system.

The aortas used as healthy controls (HC) were obtained anonymously and provided by the Barcelona Tissue Bank from multiorgan transplant donors. Research has been carried out following the Declaration of Helsinki. The patients' and control subjects' participation in this study was based upon the informed consent of patients or legal representatives. Tissue samples were collected and stored at -80 ºC for subsequent RNA and protein studies. Part of the tissues was immediately fixed in paraformaldehyde, kept at room temperature for 48 hours, and embedded in paraffin. Leftover serum samples (n= 32) of routine analysis were obtained from patients with TAA diagnosed by the Cardiology Service at the Hospital de la Santa Creu I Sant Pau.

ER stress activation was studied in aneurysmal aortic tissue from syndromic patients undergoing corrective surgery compared with healthy aortas from heart donors as well as with aneurysmal aortas from non-syndromic patients.

Table 1. Patients' baseline characteristics.

Patient number	Age	Notes
Syndromic patients		
- TAA6	- 42	- Mutation in *MYH11* gene
- TAA12	- 49	- Marfan syndrome
- TAA24	- 65	- Marfan syndrome
- TAA26	- 49	- Loeys-Dietz syndrome
- TAA28	- 26	- Marfan syndrome
- TAA32	- 58	- *Turner syndrome (TS)*
- TAA33	- 40	- Marfan syndrome
- TAA44	- 32	- Loeys-Dietz syndrome
Genetic patients		
- TAA2	- 53	
- TAA3	- 59	
- TAA41	- 48	
- TAA45	- 45	
- TAA50	- 57	
- TAA55		
- TAA60	- 60	
- TAA65	- 73	
- TAA70	- 43	
Bicuspid patients		
- TAA9	- 53	
- TAA11	- 63	
- TAA25	- 60	
- TAA27	- 43	
- TAA30	- 35	
- TAA31	- 68	
- TAA34	- 36	
- TAA42	- 28	
- TAA46	- 46	
- TAA47	- 60	
- TAA52	- 58	
- TAA58	- 42	
- TAA61	- 48	
- TAA69	- 70	
- TAA71	- 51	

- TAA75	- 45
- TAA81	- 50
- TAA82	- 58
- TAA83	- 62
Healthy donors	
- DO1	- 48
- DO2	- 54
- DO3	- 54
- DO4	- 53
- DO5	- 63
- DO6	- 53
- DO7	- 57

2.2. Total mRNA and protein isolation

Total mRNA and protein were isolated for the downstream studies. Isolation was conducted to 36 aneurysmatic tissue samples which are representative of the distinct pathological conditions (syndromic: n = 8, bicuspid: n = 19, genetic: n = 9), and to the healthy tissue samples (n = 7). The RNeasy Fibrous Mini Kit (Qiagen) was used to isolate total RNA from aorta samples. The isolation was done by following the manufacturer's instructions. About 30 mg of mashed aorta tissue from each sample was first homogenized in 300 µL of Buffer RLT containing β-mercaptoethanol (β-ME) using a TissueRuptor® (Qiagen). 585 µL RNase-free water and 15 µL proteinase K were added to the sample. After mixing by inverting several times, the whole mixture was incubated at 55 °C for 10 -15 minutes in a heating block, for proteinase K digestion. Once the samples were ready, they were centrifuged at 10 000 x g for 3 minutes at 15-25 °C, the supernatant was transferred to new tubes and 0,5 volumes of 96 % ethanol was added and mixed to the cleared lysate. 700 µL of each sample were transferred to the RNeasy Mini column (in a 2 ml collection tube) and centrifuged for 1 min at 8 000 x g at 15-25 °C, the flow-through was discarded. This step was repeated until all the lysate was filtered.

Once finished, 350 µL of Buffer RW1 was added to each RNeasy Mini spin column and they were centrifuged at 15-25 °C for 1 min at 8 000 x g, discarding the flow-through at the end. After this step, 10 µL of DNase I stock solution was mixed with 70 µL Buffer RDD, and 80 µL of the DNase I incubation mix was added directly to the RNeasy Mini spin columns membranes, followed by a 10-minute incubation at room temperature (RT).

After the incubation, 350 µL of Buffer RW1 was added to each RNeasy Mini spin column and

they were centrifuged at 8 000 x g for 1 min at 15-25 °C, the flow-through was discarded. 500 µL of Buffer RPE was added to each RNeasy Mini spin column, and the same centrifugation was performed. Flow-through was discarded. 500 µL of Buffer RPE was added again to each RNeasy Mini spin column. This time the samples were centrifuged for 2 minutes at 8 000 x g at 15-25 °C.

Once finished, the RNeasy Mini spin columns were placed into new 2 mL collection tubes and the old collection tubes with the flow-through were discarded. The new 2 mL tubes were centrifuged for 1 minute at 10 000 x g. Finally, RNeasy Mini spin columns were transferred into new 1,5 mL tubes and 40 µL of RNase-free water was added. Centrifugation was performed at 8 000 x g for 1 minute. RNA was quantified by a NanoDrop 1000 Spectrophotometer (Thermo Scientific). The quantity of RNA in each sample can be seen in the supplementary Table 1.

2.3. RNA sequencing analysis

To study upregulated and downregulated genes in different patient groups, a whole genome analysis was performed using RNA sequencing (RNA-seq). Total RNA, extracted from 30 aneurysmatic tissue samples which are representative of the distinct pathological conditions (syndromic: n = 8, bicuspid: n = 11, genetic: n = 5, and healthy donors (HC): n = 5) were analyzed for quality using BioAnalyzer, and for whole-genome transcriptome using RNA-seq at the Genomics / Transcriptomics Core of the Bank of Blood and Tissues of Barcelona (BST, Barcelona). Total RNA was used as starting material to synthesize cDNA libraries using the Illumina Stranded mRNA Prep kit based on the poly-A selection method, according to the manufacturer's protocol (Illumina, San Diego, CA, USA). Libraries were run simultaneously on an Illumina NextSeq 500 sequencing system by the NextSeq 500/550 High Output reagent kit v2.5 of 150 cycles (2x74 bp paired end) (Illumina).

Paired sequence files in FASTQ format were analyzed on the BaseSpace Sequence Hub platform with the Dragen RNA Pipeline v3.7.5 (Illumina). The reference genome used was UCSC hg19. Differential expression analyses were performed with the Dragen Differential Expression application (Illumina). The compared subsets of samples were bicuspid and healthy donor samples (AAT1), syndromic and healthy donor samples (AAT2), and genetic and healthy donor samples (AAT3). Significantly differentially expressed genes (DEGs) were defined as those with adjusted P-values of <0.05.

2.4. Gene enrichment analysis

To understand the molecular mechanisms underlying genome regulations, quantitative analyses of gene expression are conducted (49). Genome-wide gene expression studies test thousands of genetic variants across the genome to understand the molecular mechanisms underlying phenotypes of interest, such as a specific trait of human disease. To achieve this, changes in the expression of a single gene are typically analyzed for enrichment of the functional gene set. (50). These gene sets can represent molecular functions and biological processes defined by the Gene Ontology (GO), pathway databases such as KEGG and Reactome, or experimentally-derived gene sets such as those available in the molecular signatures database (MSigDB) (50). The two commonly used enrichment methods are overrepresentation analysis (ORA) and gene set enrichment analysis (GSEA). ORA is used for testing whether the gene set contains disproportionally many genes of significant expression changes. Conversely, GSEA is used for testing whether the genes in the gene set accumulate at the top or bottom of the full gene vector, ordered by direction and magnitude of expression change (50).

In this study, GESA were carried out using the WEB-based gene set analysis toolkit (WebGestalt) 2019 (http://www.webgestalt.org/). Specifically, DEGs were ranked by log2 fold change. Each run was conducted with 1 000 permutations, and a false discovery rate (FDR) in which a threshold of 0.05 was used. Specifically, the functional enrichment analyses were performed in Reactome and Gene Ontology (GO) databases, where categories with a size of fewer than five genes and greater than 2 000 genes were excluded. For GO, non-redundant terms of Biological Process, Cellular Component and Molecular Function groups were used.

2.5. Quantitative real-time polymerase chain reaction

Quantitative real-time chain reaction (quantitative RT-PCR) was run to validate the RNA-seq result regarding a chosen candidate genes and known ER stress and mitochodrial biogenesis markers . DNase I-treated total RNA (1 µg) was reverse transcribed into cDNA using the High-Capacity cDNA Archive Kit (Applied Biosystems, Foster City, CA, U.S.A.) with random hexamers. The master mix was prepared to contain 2 µl dNTPs, 1 µl reverse transcription enzyme, 2 µl buffer 10x and 2 µl random primers 10x. The total volume of the master mix was multiplied by the number of samples. For each sample, RT-PCR mix was added to 500 ng of RNA. RT-PCR was carried out using the following conditions: Two cycles of 10 min at 25 °C, 30 min at 37°C, 30 min at 37 °C, 5 min at 85 °C, and kept on 4 °C. Finally, to the total volume of RT-PCR reaction, ddH2O was added to dilute the samples ten times.

Quantification of mRNA levels was performed by real-time PCR by using an ABI Prism 7900HT sequence detection system (Applied Biosystems) and probes provided by Applied Biosystems for humans. The used TaqMan Gene Expression Assays probes and primers are shown in Table 2.

Table 2. Probes/Primers used to validate mRNA expression.

Gene	Probes and Primers, TaqMan Gene Expression Assays (2X), Assay ID
Galanin And GMAP Prepropeptide (*GAL*)	Hs00544355_m1
Mesothelin (*MSLN*)	Hs00245879_m1
Aquaporin 9 (*AQP9*)	Hs01033361_m1
C-C Motif Chemokine Ligand 7 (*CCL7*)	Hs00171147_m1
Pro-Platelet Basic Protein (*PPBP*)	Hs00234077_m1
Interleukin 11 (*IL11*)	Hs01055414_m1
SLAM Family Member 7 (*SLAMF7*)	Hs00904275_m1
Mucin 16 (*MUC16*)	Hs01065175_m1
Ficolin 1 (*FCN1*)	Hs00975735_m1
Kallikrein Related Peptidase 11 (*KLK11*)	Hs00374672_g1
Uroplakin 1B (*UPK1B*)	Hs01041715_ m1
Oxidized Low Density Lipoprotein Receptor 1 (*OLR1*)	Hs01552593_m1
Secreted Phosphoprotein 1 (*SPP1*)	Hs80959010_m1
Glyceraldehyde-3-phosphate dehydrogenase (*GAPDH*)	Hs02758991_g1
DNA Damage Inducible Transcript 3 (*DDIT3*)	Hs99999172_m1
X-Box Binding Protein 1(*XBP1*)	Hs00231936_m1
Activating Transcription Factor 6 (*ATF6*)	Hs00232586_m1
Sirtuin 1 (*SIRT1*)	Hs01009006_m1
Cysteine Rich with EGF Like Domains 2 (*CRELD2*)	Hs00360923_g1
SEL1L Adaptor Subunit of ERAD E3 Ubiquitin Ligase (*SEL1L*)	Hs01071406_m1
Mitochondrially Encoded Cytochrome C Oxidase III (*MT-CO3*)	Hs02596866_g1
Mesencephalic Astrocyte Derived Neurotrophic Factor (*MANF*)	Hs00180640_m1

With the TaqMan Gene Expression Master Mix quantitative RT-PCR was carried out using the following conditions: 2 min at 50°C, 10 min at 95°C followed by 40 cycles of 15 s at 95°C and 1 min at 60°C. With the TagMan 2X, Universal PCR Master Mix quantitative RT-PCR was carried out using the following conditions: 2 min at 95°C followed by 40 cycles of 19 s at 95°C and 30 s at 60°C. Relative mRNA levels were determined using the $2^{-\Delta\Delta Ct}$ method.

2.6. Enzyme-linked immunosorbent assay

To determine circulating protein levels of the chosen candidate genes and ER stress markers from serum samples, Enzyme-linked immunosorbent assay (ELISA) was performed. Previously, validated MSLN and FCN1 were selected since they were known to be soluble and circulating proteins. The circulating levels of the cytokine S100A8 and the growth differentiation factor 15 (GDF-15) in aneurysm patients were determined, since they have been shown to have potential as novel biomarkers in cardiovascular diseases (49, 50). OMENTIN 1 (Intelectin 1, ITLN1) was analyzed since it has known to have cardiovascular protective effects, and its decrease can predict coronary artery disease (51). To study ER stress markers in syndromic patients, ER stress-associated cytokines (TNFα, IL-1β, IFNγ, IL-6, IGF-1, MCP-1, Leptin and TGFβ-1) were quantified in aneurysmal tissue lysates (HC: n= 6, syndromic: n=6). The ER stress ELISA Strips kit was performed to measure circulating ER stress-associated cytokines (EA-1141, Signosis) according to manufacturer´s instructions. Soluble proteins, S100A8 (CSB- E11833h-96T, Cusabio Biotech Co, LTD, China), OMENTIN 1 (CSB-E09745h-96T, Cusabio Biotech Co, LTD, China), MSLN (CSB-E13382h-96T, Cusabio Biotech Co, LTD, China), FCN1 (ab213777, Abcam) and GDF15 (DGD150, R&D Systems) were measured in serum from TAA patients (syndromic: n = 4, bicuspid: n = 11, genetic: n = 7) using commercially available ELISA kits in accordance with the manufacturer's instructions.

Briefly, we followed the steps as described in every protocol as specified in the book instructions of every ELISA kit. First, all the reagents were prepared according to every ELISA kit manufacturer´s instructions. The standard curves were prepared by producing a stock solution with a concentration of 4 000 pg/ml for MSLN, 100 pg/ml for OMENTIN-1, and 80 ng/ml for A100A8. The stock solution was used to produce a 2-fold dilution series. The Lyophilized recombinant Human FCN1/M-Ficolin standard (2 x 50 ng) was prepared by producing a stock solution with a concentration of 50 ng/mL. For GDF15, the standard was diluted to generate a stock solution with a concentration of 15 000 pg/ml. For MSLN and S100A8 serum samples were 5-fold diluted. For OMENTIN-1 serum samples were 200-fold diluted. For FCN1 serum samples were 2-fold diluted whereas for GDF15 serum samples were 4-fold diluted.

After preparations, the standard and serum samples were added to the wells. Then, the primary antibody was added to bind to the antigen during 2 h of incubation. Afterwards, each well was washed three times with wash buffer to remove the unbound antibodies, followed by adding detection antibody, secondary antibody, and the plate was incubated for 1 h followed by a wash

step and a final incubation with the substrate solution. The final incubation was necessary to protect from light. Finally, the stop solution was added to stop the enzymatic reaction and the absorbance reading at 450 nm was performed within the next 15 min using a microplate reader.

2.7. Histology analysis

Histological analysis was performed in the paraffined tissue sections to study the morphological features of the tissue and visualize vascular remodeling. Tissue specimens were formalin-fixed and paraffin-embedded. The histological characterization of the human aortic samples was carried out by Sirius red (SR), MOVAT pentachrome and Haematoxylin-Eosin (HE) stainings, while the elastic fibre integrity was assessed by orcein staining using a commercial kit (Casa Álvarez, Madrid, Spain).

Histological staining was performed into paraffin sections (5 μm) of human aortas. In each staining, method samples were first deparaffined by washing with xylol 2 x 7 min. Samples were then rehydrated by gradually decreasing alcohol percentage from 100° to 70° and finally soaked in distilled water for 5 min. After this, sections were stained with the chosen method. For HE, the staining samples were stained in Hematoxylin Mayer for 5 min and Eosin for 30 sec. Between staining's, samples were washed in distilled water. For SR stain, samples were immersed in a picro-sirius red solution for one hour following three 3 min washes in acidic water. Orcein staining was performed by following the kit manufacturer´s instructions (Casa Álvarez, Spain. Ref. O-1045). Sections were kept in a horizontal position in a humidity chamber. Reagents were added in the order indicated and incubation was performed as directed. After staining procedures, the samples were dehydrated by washing the samples in 100° alcohol 3 x 2min and in xylol 2 x 3 min. At the end, samples were mounted in a mounting medium.

MOVAT staining's were performed at the pathology department of the Sant Pau Hospital. Imaging of the stained sections and the capture of pictures were performed using an OLYMPUS BX51TF microscope.

2.8. Statistical analysis

GraphPad Prism 4.0 software (GraphPad, U.S.A.) was used for statistical analysis. Data were expressed as a standard error of mean (SEM) and values of $P \leq 0.05$ were considered significant. In cases of abnormal data distribution, differences between two groups were assessed using Student's t test (two-tailed) and one-way analysis of variance (ANOVA), and the Bonferroni test

for more than two groups. When normality failed, we used the Mann–Whitney rank sum test to compare two groups and Kruskal–Wallis one-way analysis of variance on ranks for multiple comparisons (Dunn's method).

3. Results

3.1. Patient Characteristics

The study included three different patient groups and a control group containing a total of 36 TAA patients with aortic aneurysms and 7 healthy patients (Table 1). The syndrome group included patients diagnosed with Marfan syndrome or Loeys-Diets syndrome, who underwent corrective surgery. The non-syndromic patients were divided into bicuspid patients and genetic patients. Genetic patients included individuals who are classified as genetic due to a family history of aneurysm. Heart donors with healthy aortas formed the control group.

3.2. Identification of Transcripts associated with TAA

To identify genes and pathways associated with TAA patients, a mRNA-Seq whole-transcriptome analysis was performed in a total of 30 RNA samples. Next generation sequencing was performed to a mean sequencing depth of 27 million reads (18-33 million). The percentage of mapped reads ranges from 88.2 to 99.6%.

DEGs were evaluated between different combinations of subsets of samples. Results showed both significantly upregulated and downregulated DEGs (adjusted P-values of <0.05). In bicuspid *versus* donor samples comparison (AAT1), a total of 569 significant DEGs were detected. Among them, 483 were upregulated and 86 were downregulated. The comparison between syndromic and donor samples (AAT2) revealed a total of 1460 significant DEGs were detected. Among them, 774 were upregulated and 686 were downregulated. The analysis of genetic *versus* donor samples (AAT3), found a total of 1450 significant DEGs (830 were upregulated and 620 were downregulated). These results are illustrated in the volcano blots in Fig. 5: **A-C**. According to the results from the RNA-seq, overlap between the differently expressed gene sets in the AAT2 and AAT3 analysis was noted. Genes expressed in the AAT1 analysis, for the most part, did not overlap with the other two analysis sets.

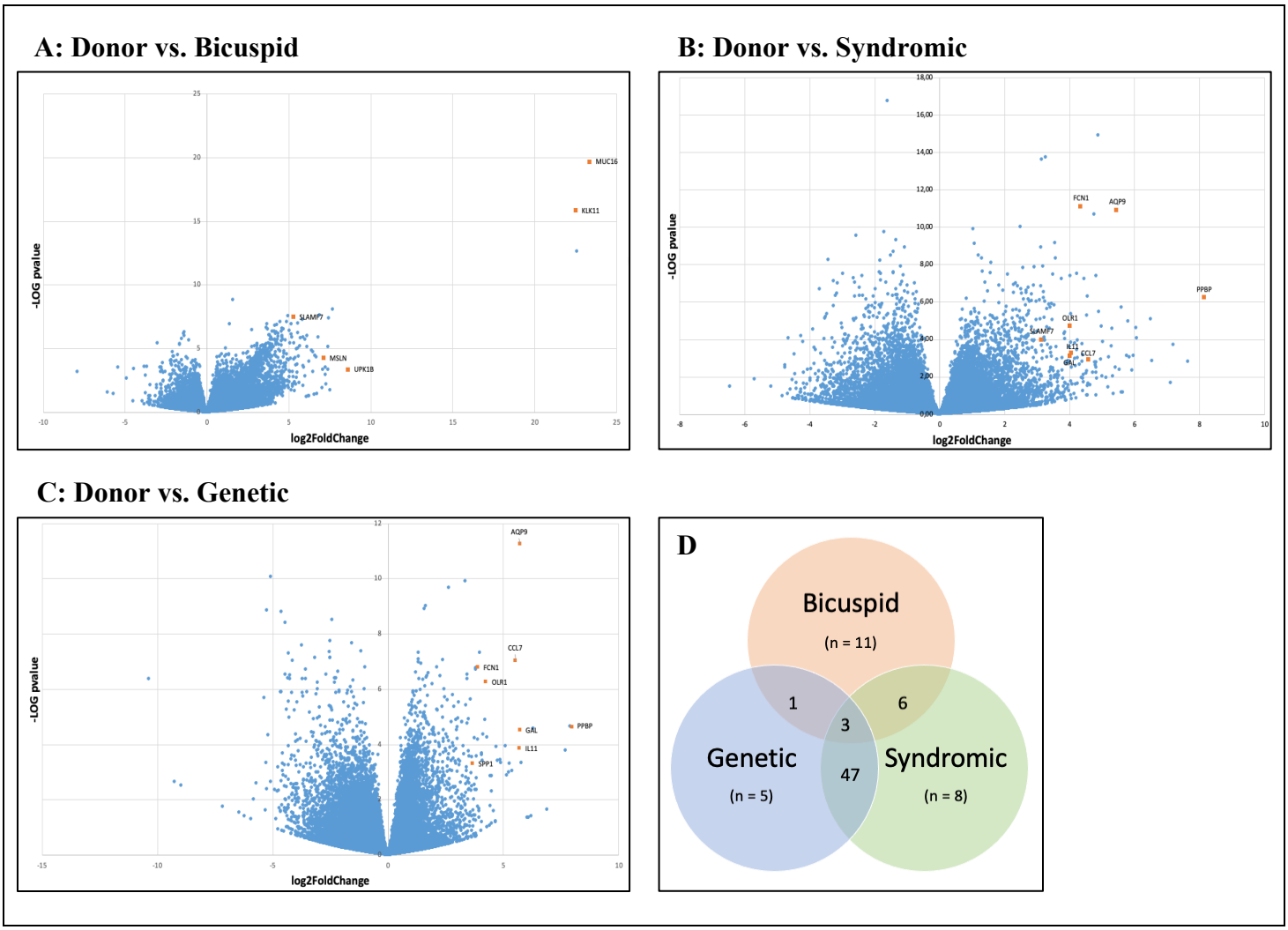

Figure 5. DEGs represented by dots obtained by RNA sequencing. **A:** Volcano plot showing DEGs of RNA-seq from AAT1 comparison. Chosen candidate genes for further analyses are marked as orange dots. **B:** Volcano plot showing DEGs of RNA-seq from AAT2 comparison. Chosen candidate genes for further analyses are marked as orange dots. **C:** Volcano plot showing DEGs of RNA-seq from AAT3 comparison. Chosen candidate genes for further analyses are marked as orange dots. Log2FoldChange is shown in x-axis and -LOG P-value is shown in y-axis. **D:** Number of shared genes among the top-50 most upregulated genes among the different patient groups.

From RNA-seq data, the 50 most upregulated genes from each patient group were taken into closer consideration. Data extracted from RNA-seq analysis of these genes are presented in Table S2-S4. The upregulated DEGs, in each patient group, were compared with the other groups to elucidate whether the different patient groups exhibited any of the DEGs exclusively modulated in their particular group and those genes which were similarly upregulated among groups. The number of the shared DEGs are shown in Fig. 5: **D**. The top-50 upregulated genes in AAT1, AAT2, and AAT3 analysis were searched in the literature by using PubMed.*gov* (https://pubmed.ncbi.nlm.nih.gov), for any previous association with aortic aneurysm disease. Based on the results of RNA-seq and data from previous studies, thirteen candidate genes were selected for further analysis (Table 3). Candidate genes were among the top-50 upregulated

genes and were previously mentioned in studies as a possible biomarker of cardiac disease. The chosen genes [mucin16 (*MUC16*), kallikrein11 (*KLK11*), uroplakin-1B (*UPK1B*), and mesothelin (*MSLN*)] were only differentially expressed in bicuspid *versus* healthy donor. Pro-Platelet Basic Protein (*PPBP*), Aquaporin9 (*AQP9*), C-C Motif Chemokine Ligand 7 (*CCL7*), Ficolin1 (*FCN1*), Galanin peptides (*GAL*), Opioid Related Nociceptin Receptor one (*ORL1*), Interleukin11 (*IL11*) and Secreted Phosphoprotein 1 (*SPP1*) were differentially expressed in both syndromic *versus* healthy donor and genetic *versus* healthy donor comparisons. Gene SLAM Family Membrane 7 (*SLAMF7*) was differentially expressed in the three groups comperad with healthy aortas, but in the genetic group it did not reach the statistic significance. Some of the selected genes had been previously desribed in literature in the context of cardiac disease, but most of them have not been associated with aneurysms.

Table 3. Fold change of mRNA levels corresponding to selected significantly differentially expressed genes (DEGs). *MUC16, KLK11, UPK1B, MSLN* genes were only upregulated in bicuspid patients (AAT1). *PPBP, AQP9, CCL7, IL11, GAL, OLR1,* and *SPP1* genes were both upregulated in syndromic and genetic patients (AAT2 and AAT3). *SLAMF7* gene was upregulated in samples from bicuspid, syndromic and genetic patients. DEGs were defined as those with adjusted P-values of <0.05.

Patient group: AAT1 - Bicuspid vs. Donors (Healthy)						
List order	**Fold Change**	**-LOG P value**	**gene ID**	**Gene:**	**log2Fold Change**	**P value**
1	10825001,85	19,6712731	ENSG00000181143.11	MUC16	23,367863	2,1317E-20
3	5968138,858	15,8248607	ENSG00000167757.9	KLK11	22,508849	1,49672E-16
4	391,4926937	3,35471048	ENSG00000114638.3	UPK1B	8,6128415	0,000441865
11	139,330693	4,2463764	ENSG00000102854.10	MSLN	7,1223692	5,67053E-05
37	38,69878521	7,47791487	ENSG00000026751.12	SLAMF7	5,2742163	3,32725E-08
Patient group: AAT2 - Syndrome vs. Donors (Healthy)						
1	281,1493133	6,25939316	ENSG00000163736.3	PPBP	8,1351927	5,50309E-07
13	43,32088802	10,9244863	ENSG00000103569.5	AQP9	5,4369909	1,18991E-11
23	23,82010799	2,92296754	ENSG00000108688.7	CCL7	4,5741080	0,001194077
31	20,07014904	11,0931400	ENSG00000085265.6	FCN1	4,3269794	8,06975E-12
40	16,5644977	3,28668300	ENSG00000095752.2	IL11	4,0500225	0,000516793
43	16,10871847	3,10898609	ENSG00000069482.6	GAL	4,0097698	0,000778061
44	16,05509243	4,73293660	ENSG00000173391.4	OLR1	4,0049590	1,84954E-05
45	10,6325888	5,69167029	ENSG00000118785.9	SPP1	3,4104209	2,0339E-06
81	8,693421387	3,98752282	ENSG00000026751.12	SLAMF7	3,1199240	0,000102915
Patient group: AAT3 - Genetic vs. Donors (Healthy)						
1	253,2306822	4,61132795	ENSG00000163736.3	PPBP	7,9843084	2,44721E-05
5	52,69705748	11,2562442	ENSG00000103569.5	AQP9	5,7196505	5,54314E-12

6	52,64518862	4,50522839	ENSG00000069482.6	GAL	5,7182297	3,12444E-05
7	52,16546846	3,84745878	ENSG00000095752.2	IL11	5,7050232	0,000142083
8	46,13126668	7,02059025	ENSG00000108688.7	CCL7	5,5276730	9,53696E-08
16	19,04164941	6,25262948	ENSG00000173391.4	OLR1	4,2510865	5,58947E-07
24	14,80905424	6,78809481	ENSG00000085265.6	FCN1	3,8884076	1,62894E-07
29	12,79656317	3,31018017	ENSG00000118785.9	SPP1	3,6776844	0,000489576
641	2,359946045	0,83355876	ENSG00000026751.12	SLAMF7	1,2387538	0,146703758

Additionally, DEGs encoding for ER stress and mitochondrial biogenesis markers were searched for. RNA-seq results showed that some of these markers were differentially expressed in syndromic patient (AAT2), and in the genetic patient (AAT3) groups. However, none of them were statistically or differentially expressed in the bicuspid patient (AAT1) group according to RNA-seq results. DEGs encoding for ER stress and mitochondrial biogenesis markers were not included among the top-50.

Table 4. Fold change of mRNA levels corresponding to the ER stress and mitochondrial biogenesis (*SIRT1* and *MT-CO3*) markers when compared to healthy donors. DEGs were defined as those with adjusted P-values of <0.05.

Patient group: AAT1 - Bicuspid vs. Donors (Healthy)					
Fold Change	**-LOG P value**	**gene ID**	**Gene:**	**log2FoldChange**	**P value**
1,51044426	0,876572435	ENSG00000096717.7	SIRT1	0,5949729	0,13287019
1,35326033	0,80577379	ENSG00000172071.14	EIF2AK3	0,4364394	0,15639621
1,245785805	0,161071843	ENSG00000175197.6	DDIT3	0,3170560	0,69012563
1,2413128	0,45127571	ENSG00000108064.11	TFAM	0,3118667	0,35377268
1,160343213	0,236813597	ENSG00000071537.9	SEL1L	0,2145515	0,57967745
1,133079167	0,342782621	ENSG00000184164.10	CRELD2	0,1802486	0,45416889
0,893287753	0,257757662	ENSG00000118217.5	ATF6	-0,1628031	0,55238559
0,757734038	1,488553786	ENSG00000145050.11	MANF	-0,4002365	0,0324673
0,575124155	0,90510005	ENSG00000198938.2	MT-CO3	-0,7980546	0,12442279
Patient group: AAT2 - Syndrome vs. Donors (Healthy)					
1,912018583	2,040985619	ENSG00000100219.12	XBP1	0,9350965	0,00909943
1,85465727	2,35094592	ENSG00000108064.11	TFAM	0,8911526	0,00445712
1,79710439	2,8793574	ENSG00000172071.14	EIF2AK3	0,8456742	0,00132021
1,583855047	1,709620963	ENSG00000071537.9	SEL1L	0,6634403	0,01951547
1,495272565	1,634577897	ENSG00000118217.5	ATF6	0,5804084	0,02319648
1,388989086	0,773231768	ENSG00000145050.11	MANF	0,4740352	0,16856532
1,387136389	1,28910396	ENSG00000096717.7	SIRT1	0,4721096	0,05139206
1,182090376	0,383303058	ENSG00000184164.10	CRELD2	0,2413403	0,41371088

0,807555444	0,193241158	ENSG00000175197.6	DDIT3	-0,3083667	0,64085362
0,243729515	5,250179442	ENSG00000198938.2	MT-CO3	-2,0366471	5,6211E-06
Patient group: AAT3 - Genetic vs. Donors (Healthy)					
2,04625088	4,20604904	ENSG00000172071.14	EIF2AK3	1,0329830	6,22E-05
1,660871321	1,880893667	ENSG00000071537.9	SEL1L	0,7319403	0,01315547
1,538821153	1,552687181	ENSG00000100219.12	XBP1	0,6218255	0,02800998
1,44326246	1,19291845	ENSG00000118217.5	ATF6	0,5293336	0,064133
1,24204413	0,716274973	ENSG00000096717.7	SIRT1	0,3127164	0,19218745
1,213830116	0,743956487	ENSG00000145050.11	MANF	0,2795665	0,18031984
1,148004186	0,365387112	ENSG00000184164.10	CRELD2	0,1991279	0,43113461
0,582108378	0,866665819	ENSG00000175197.6	DDIT3	-0,7806403	0,1359359
0,292292065	2,667315369	ENSG00000198938.2	MT-CO3	-1,7745174	0,00215122

3.3. Validation of the candidate genes by mRNA analysis

The results from the RNA-seq were validated by assessing the mRNA levels of the thirteen candidate genes through quantitative RT-PCR using specific taqman probes. Additionally, gene expression assays of six ER stress markers and two mitochondrial biogenesis indicators were runed. Results shown in fig. 6 and fig. 7 were normalized to the expression of the housekeeping gene *GAPDH*.

The validation was consistent with RNA-seq data for all the genes which were differentially expressed in bicuspid patients. The genes *MUC16, KLK11, MSLN*, and *UPK1B* whose expression was found significantly regulated by RNA-seq (Table 3) were also significantly upregulated by quantitative RT-PCR (Fig.6: **A-D**). Regarding genes differentially expressed in syndromic and genetic patients (Table 3), validation was successful for the *CCL7, GAL, PPBP* and *OLR1* gene expression (Fig. 6: **F-H, K**). In addition, validation of *IL11* and *FCN1* gene expression was successful in syndromic patients. These genes were significantly differentially expressed by RNA-seq (Table 3) and were significantly upregulated by quantitative RT-PCR (Fig.6: **J, M**). *PPBP, AQP9* and *FCN1* were not found to be differently expressed in bicuspid patients by RNA-seq, but they were found to be significantly upregulated in this group by quantitative RT-PCR (Fig. 6: **F, I, M**). *FCN1, IL11, AQP9* and *SPP1* were significantly differently expressed by RNA-seq in genetic patients (Table 3), but it could not be validated by quantitative RT-PCR because it was not statistically significant due to the low number of patient samples included in this group (Fig. 6: **M, I, J, L**). Finally, the *SLAMF7* gene, which was significantly differently expressed by RNA-seq in syndromic and bicuspid patient groups

(Table 3), was not significantly upregulated by quantitative RT-PCR in the bicuspid group (Fig. 6: **E**).

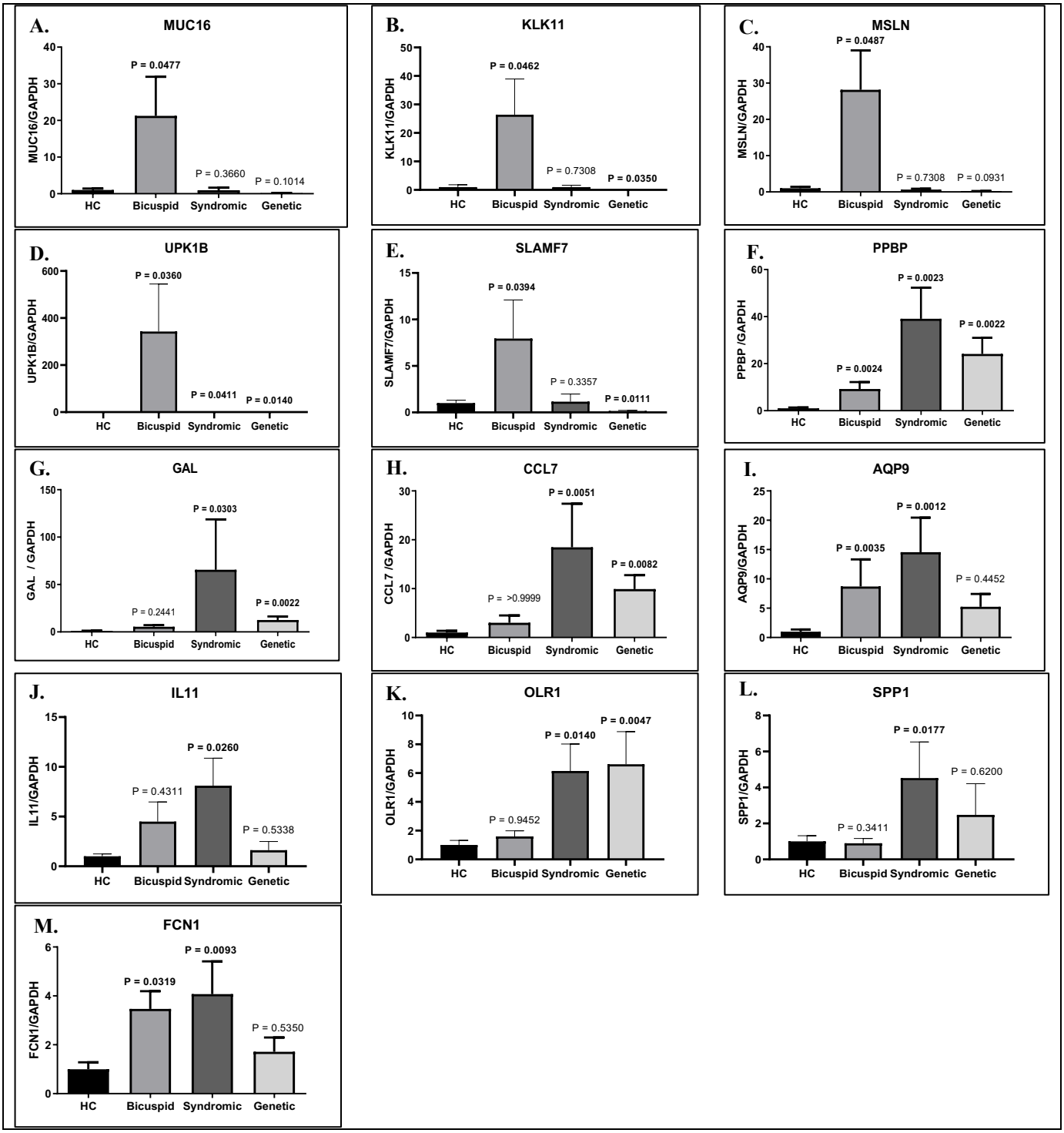

Figure 6. Quantification of the mRNA levels of *MUC16* (**A**), *KLK11* (**B**), *MSLN* (**C**), *UPK1B* (**D**), *SLAMF7* (**E**), *PPBP* (**F**)*, GAL* (**G**), *CCL7* (**H**)*, AQP9* (**I**), *IL11* (**J**), *OLR1* (**K**), SPP*1* (**L**) and *FCN1* (**M**) in aortas from patients (bicuspid, syndromic and genetic) and healthy controls (HC). Data is normalized to *GAPDH* expression. Histograms show values expressed as mean ± SEM. Values of P≤ 0.05 were considered significant.

Data corresponding to the quantification of mRNA levels of ER stress markers and mitochondrial biogenesis indicators in the genetic patient group were not included due to the low number of samples (n=5) and the high variability of the obtained results. According to the RNA-seq results, *CRELD2* was not differentially expressed in any group of patients (Table 4); however, quantitative RT-PCR analysis in bicuspid and syndromic patients, evidenced that it was significantly upregulated (Fig. 7: **A**), being the most upregulated ER stress marker in the bicuspid group. Similar results were observed for *ATF6* and *SEL1L* mRNA levels (Fig. 7: **B, E**). Among the studied ER stress markers, The RNA-seq analysis showed that *XBP1* was the most upregulated gene in the syndromic patient group (Table 4), and this result was subsequently confirmed by quantitative RT-PCR analysis, as shown in fig. 6: **F**. Regarding *MANF* mRNA levels in bicuspid and syndromic patients (Table 4), data matched with RNA-seq results (Fig. 7: **C**).

According to RNA-seq results, *MT-CO3* was significantly downregulated in syndromic and genetic patient groups, but not in the bicuspid group (Table 4). However, these results were not corroborated. On the contrary, *MT-CO3* mRNA levels were found to be significantly increased in bicuspid patient (Fig. 7: **H**). *SIRT1* and *DDIT3* were not significantly regulated in any of the patient groups (Table 4), and this was confirmed by quantitative RT-PCR (Fig. 7: **D, G**).

Overall, quantitative RT-PCR analysis only partly confirmed the RNA-seq results. For bicuspid patients' we confirmed the regulation of *MUC16, KLK11, MSLN, UPK1B* and *MANF*. In syndromic patients', quantitative RT-PCR corroborated data corresponding to *CCL7, IL11, FCN1, GAL, OLR1, MANF* and *XBP1*. And regarding genetic patients′, the validation confirmed only results for *CCL7, GAL* and *OLR1*. Validation was unsuccessful for ER stress markers and mitochondrial biogenesis indicators in genetic patients.

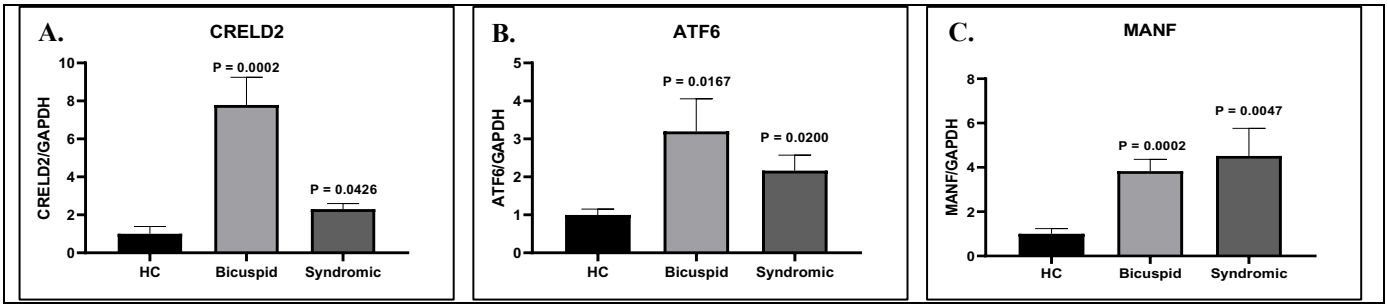

F.

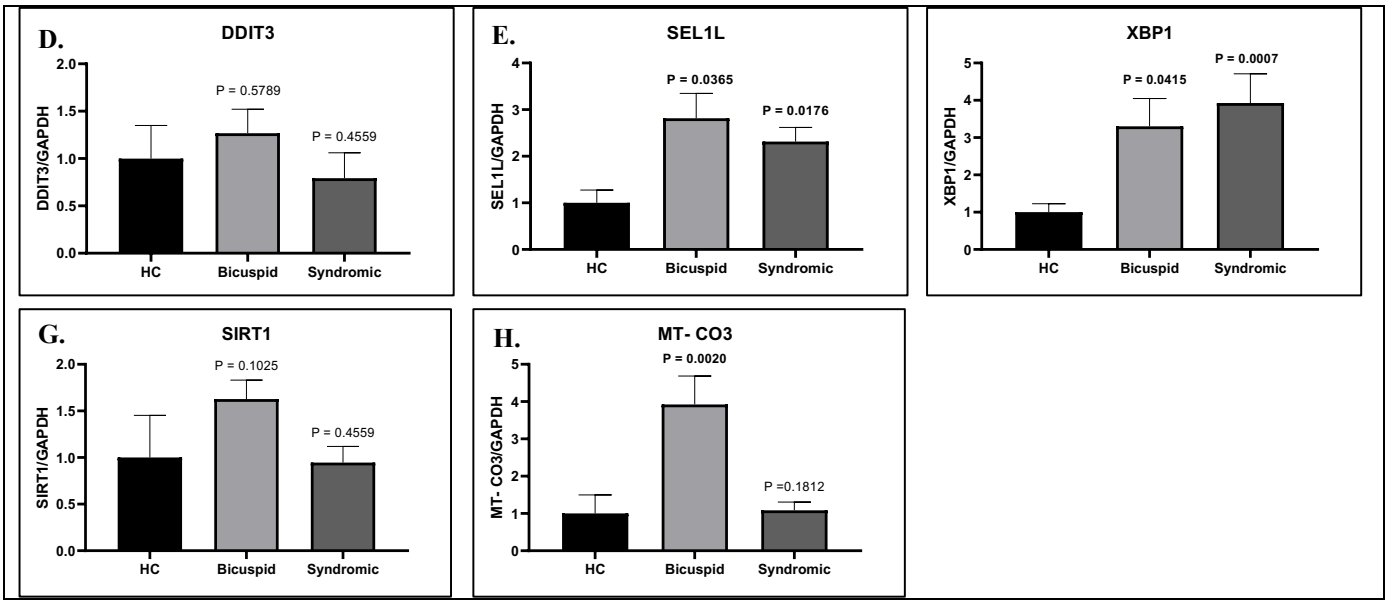

Figure 7. Quantification of the mRNA levels of *CRELD2* (**A**), *ATF6* (**B**), *MANF* (**C**), *DDIT3* (**D**), *SEL1L* (**E**), *XBP1* (**F**), *SIRT1* (**G**) and *MT-CO3* (**H**) in aortas from patients (bicuspid and syndromic) and healthy controls (HC). Data is normalized to the expression of *GAPDH.* Histograms show values expressed as mean ± SEM. Values of P≤ 0.05 were considered significant.

3.4. Validation of targeted genes by Enzyme-linked immunosorbent assay

Next, we aimed to quantify some chosen protein encoded by the top-50 DEGs by enzyme-linked immunosorbent assay (ELISA) in the serum/protein tissue lysates of the three groups of patients. MSLN, FCN1, S100A8, Intelectin 1 (ITLN1) and ER stress-associated molecules and cytokines such as GDF-15, TNFα, IL-1β, IFNγ, IL6, IGF1, MCP1, Leptin and TGFβ-1 were quantified.

The levels of circulating markers in serum samples from the three groups of patients did not agree with their aortic detected by RNA-seq analysis. The serum levels of MSNL, ITLN1 and S100A8 were similarly increased in all patient groups (Fig. 8: **A, B, D**). The quantity of the FCN1 soluble protein was increased in bicuspid and genetic serum samples, but in syndromic serum samples it was found to be slightly decreased (Fig. 8: **C**). Regarding the GDF15 levels, they were decreased in serum of syndromic patient whereas in serum of genetic patients, circulating GDF15 levels were increased in comparison to bicuspid and syndromic patients (Fig. 8: **E**). Regarding the quantitative profiling of eight ER stress-associated cytokines measured in aneurysm tissue lysates of syndromic patients compared to healthy controls, a significant increase in IL6 cytokine levels was detected. Cytokine IL6 showed the highest increase of all eight cytokines analyzed (Fig.8: **F**).

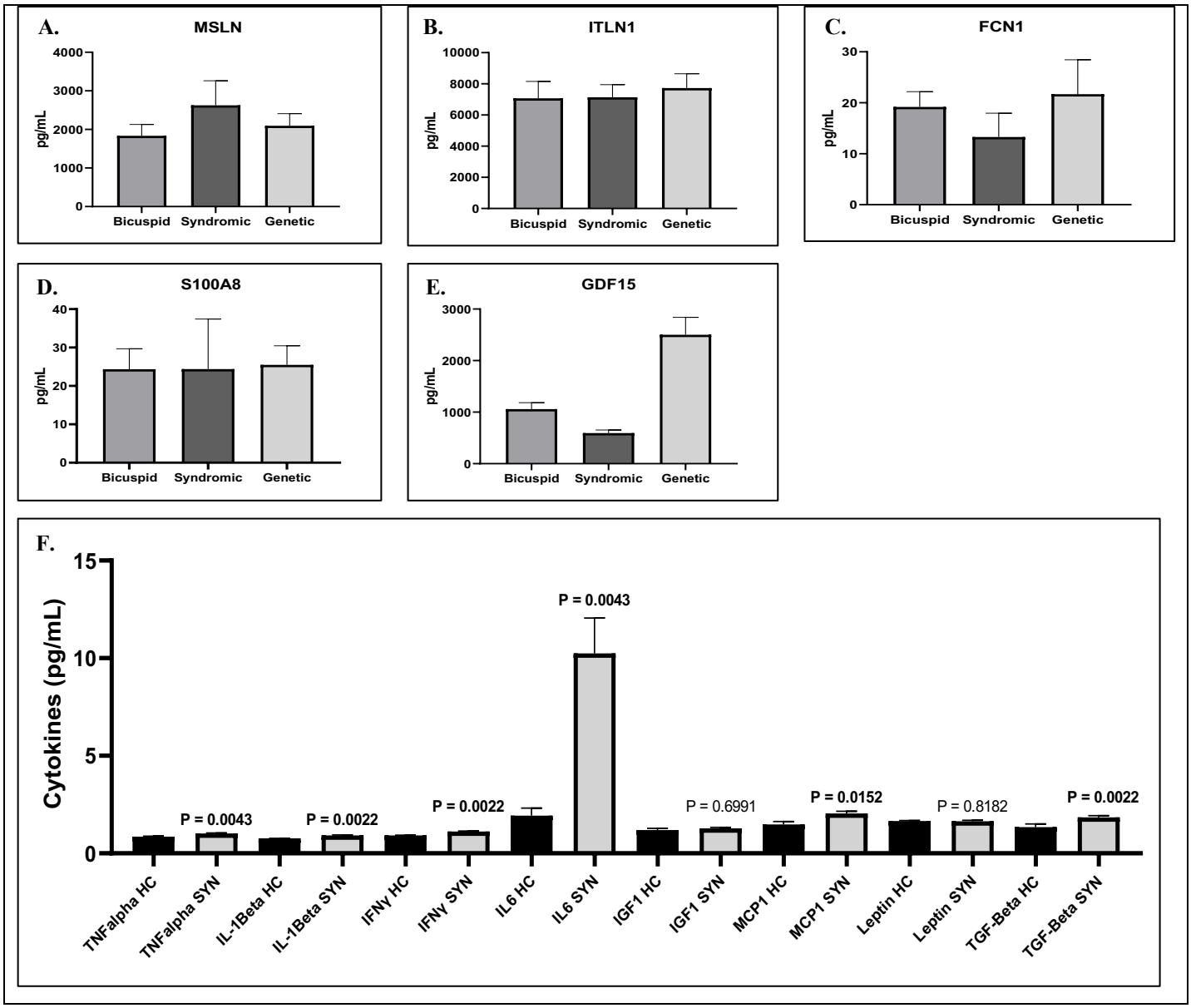

Figure 8. Levels of some circulating biomarkers encoded by DEGs and quantitative profile of eight ER stress-associated cytokines analysed by ELISA. **A:** Protein levels of MSLN. **B:** Protein levels of ITLN1. **C:** Protein levels of FCN1. **D:** Protein levels of S100A8. **E:** Protein levels of GDF15. **F:** Protein levels of TNFα, IL-1β, IFNγ, IL6, IGF1, MCP1, Leptin and TGFβ-1 cytokines. ELISA analysis for MSLN, ITLN1, FCN1, S100A8 and GDF15 were performed in serum samples from all groups of patients (bicuspid, syndromic and genetic). ELISA analysis for eight ER stress-associated cytokines were performed in serum samples from syndromic patients *versus* healthy controls (HC). Histograms show values expressed as mean ± SEM. Values of P≤ 0.05 were considered significant.

3.5. Enriched categories from Gene Ontology and Reactome in different TAA patient groups

The functional enrichment analyses showed several significant results (FDR≤0.05). 92 GO Biological Process categories were significantly enriched in bicuspid *versus* healthy controls (AAT1, Fig. 9: **A**). Focusing on GO Cellular Component we found 12 significantly enriched gene sets, while 2 of them were downregulated in these patients (Fig. 9: **B**). In addition, 19 GO Molecular Function categories were found enriched from terms of GO Molecular Function

(Fig. 9: **C**), and 22 enriched categories were identified from the Reactome pathways database (Fig. 9: **D**). For syndromic *versus* healthy controls comparison (AAT2), 60 positive and 12 negative related categories were identified as enriched categories from the Reactome database (Fig. 11: **A**), and from terms of GO Biological Process, 144 positive and 6 negative related categories were significantly enriched (Fig. 11: **B**). From terms of GO Molecular Function, 17 positive and 2 negative related categories were identified as enriched (Fig. 11: **C**) and 26 positive and 5 negative related categories were enriched from terms of GO Cellular Component (Fig. 11: **D**). Finally, for genetic *versus* healthy controls comparison (AAT3), 13 positive related categories were identified as enriched from terms of GO Molecular Function (Fig. 13: **A**), 15 positive and 4 negative related categories were enriched from terms of GO Cellular Component (Fig. 13: **B**), and 65 positive and 9 negative related categories were identified as enriched categories from the Reactome database (Fig. 13: **C**). Also, 77 positive and 1 negative related category were significantly enriched from terms of GO Biological Process (Fig. 13: **D**).

From the top enriched categories of each comparison group, those related to biological processes and pathomolecular mechanisms involved in aneurysm and / or vascular remodeling, were selected and further analyzed. Likewise, other enriched categories associated with ER stress or TAA formation were taken into further considerations. The enrichment categories of the mRNA-Seq whole-transcriptome analysis were studied more closely by using the © STRING CONSORTIUM 2022 (https://string-db.org/). From each chosen category, proteins involved in pathways of interest are highlighted with different colors as shown in the fig. 10, fig.12 and fig.14.

In the analysis of the AAT1 comparison, the “homeostasis of a number of cells” category (GO Biological Process) was enriched, and it was selected for further analysis (Fig. 10: **A**). From this category, we highlighted HIF1A (marked with arrow), which is involved in vascular remodeling and has an important role in cardiovascular development and cellular response to systemic oxygen level (52). The ER-stress related cytokine, IL6, was also involved in this category (marked with arrow). The gene set “Chaperone complex” of the GO Cellular Component sub-oncology (Fig. 10: **B**) was downregulated. The “Chaperone complex” gene set was chosen since it is heavily involved with protein folding and unfolding and closely related to ER function. In turn, the “Ficolin-1-rich granule” class (Fig. 10: **C**) was selected. This gene set includes FCN1, together with other enriched proteins involved in extracellular matrix

regulation such as MMP9 (marked with arrow) and other mediators involved in inflammatory processes (ALOX5, CD300A) (marked with arrows). From the category of GO Molecular Function, we found that the "serine hydrolase activity" pathway is enriched (Fig.10: **D**) in bicuspid patients. Note that FCN1, several MMPs and other proteins involved in inflammation were included in the cluster (marked with arrows).

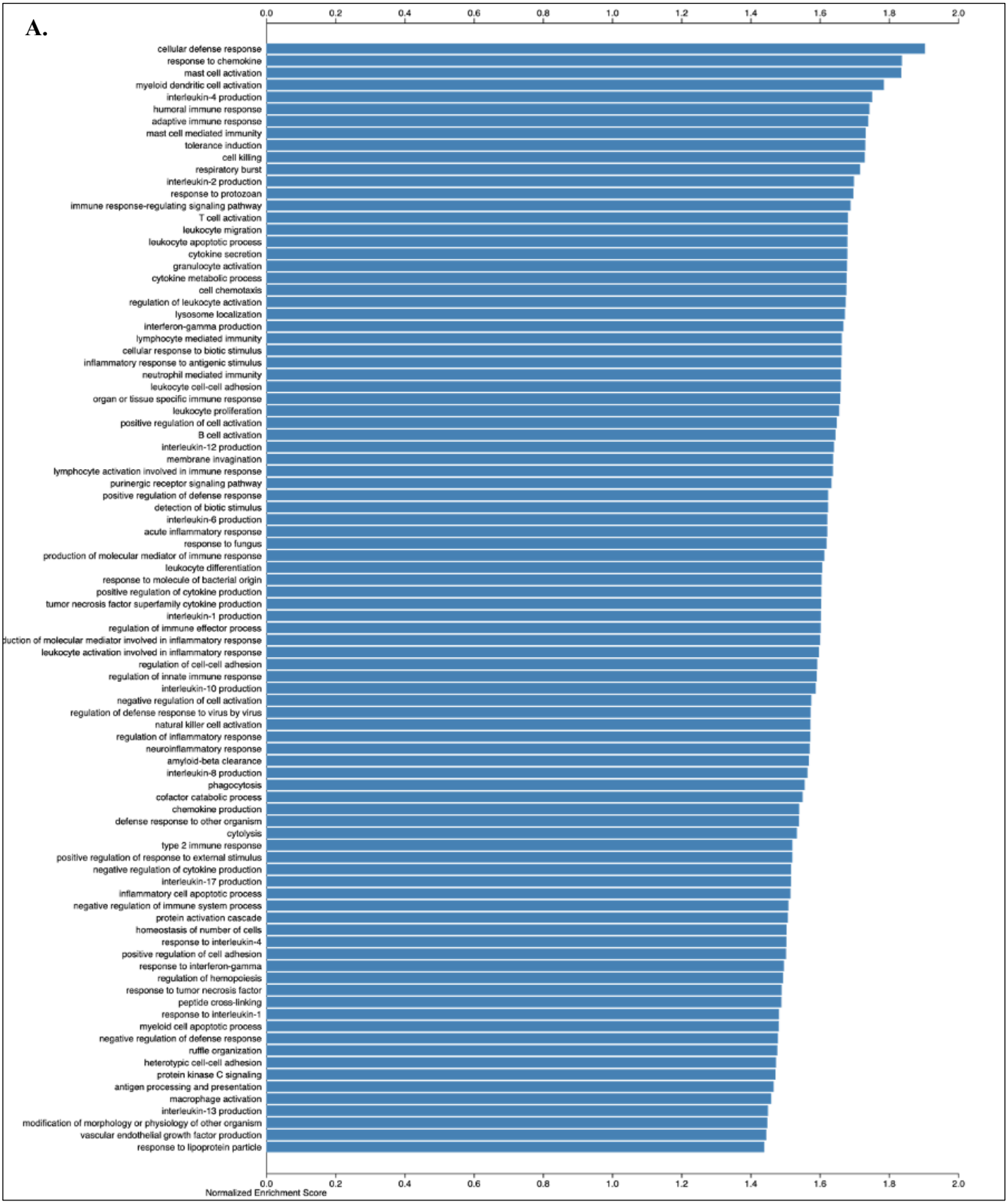

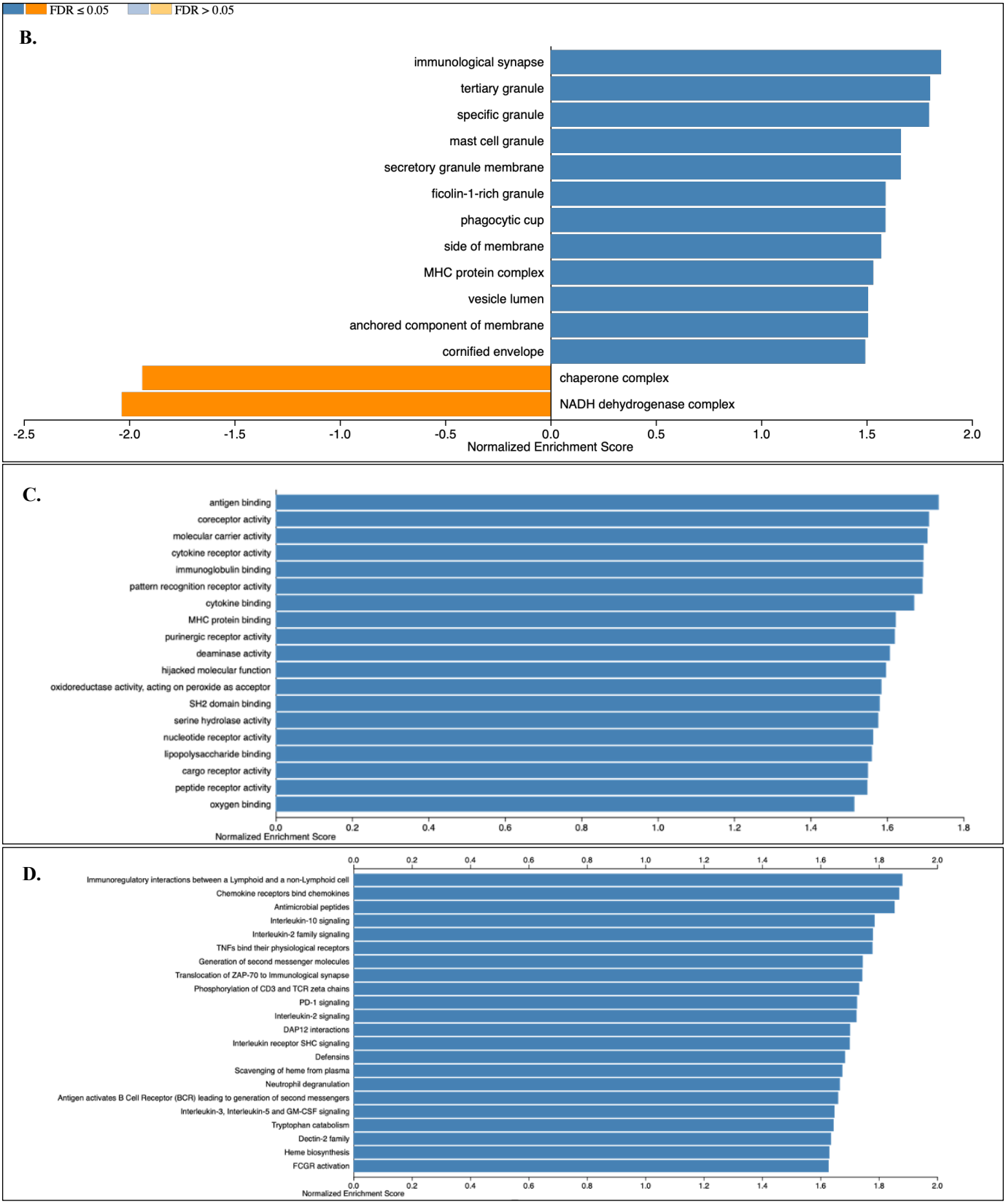

Figure 9. GSEA analysis from the Bicuspid *versus* Healthy controls comparison. Normalized Enrichment Score is shown in x-axis. **A**: GO Biological Process. **B:** GO Cellular Component. **C:** GO Molecular Function. **D:** Reactome pathway. FDR≤0.05.

A. GO:0048872 homeostasis of number of cells

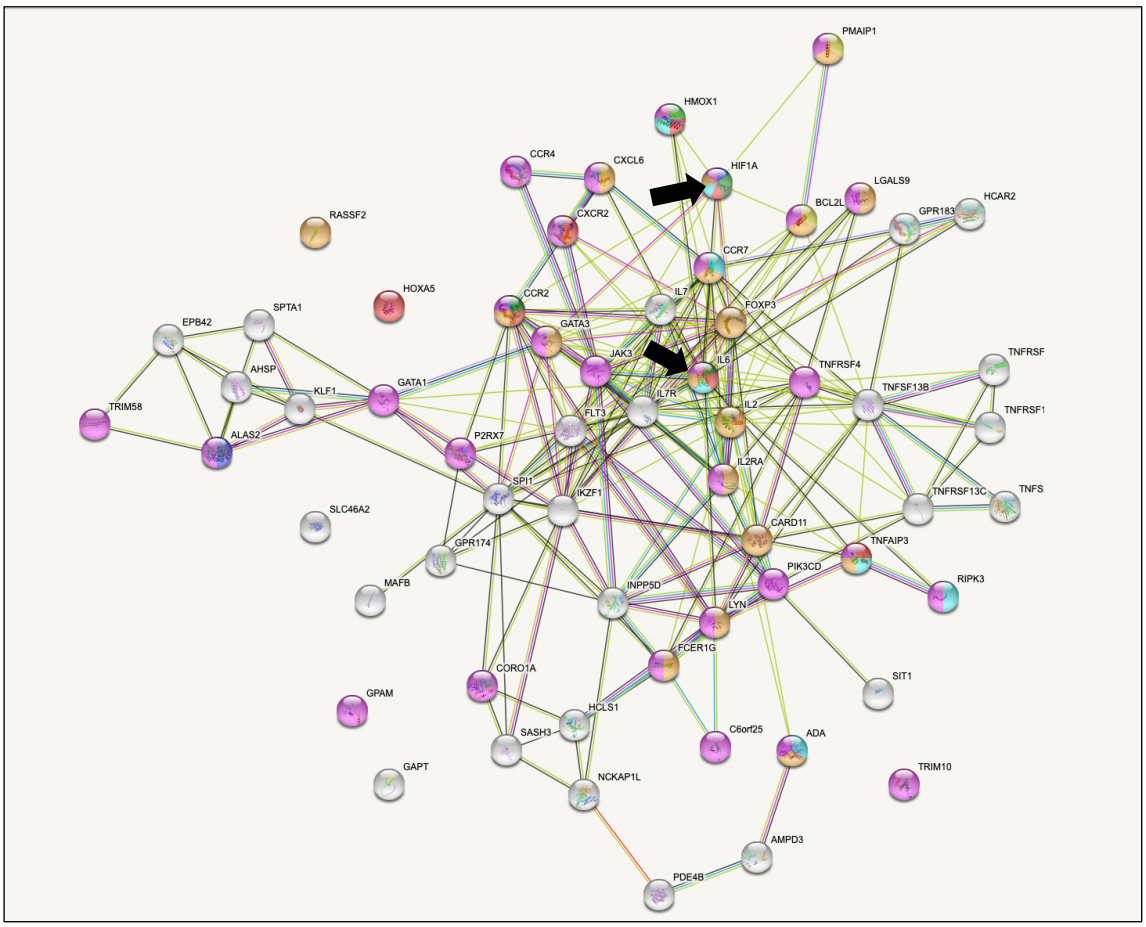

B. GO:0101031 chaperone complex

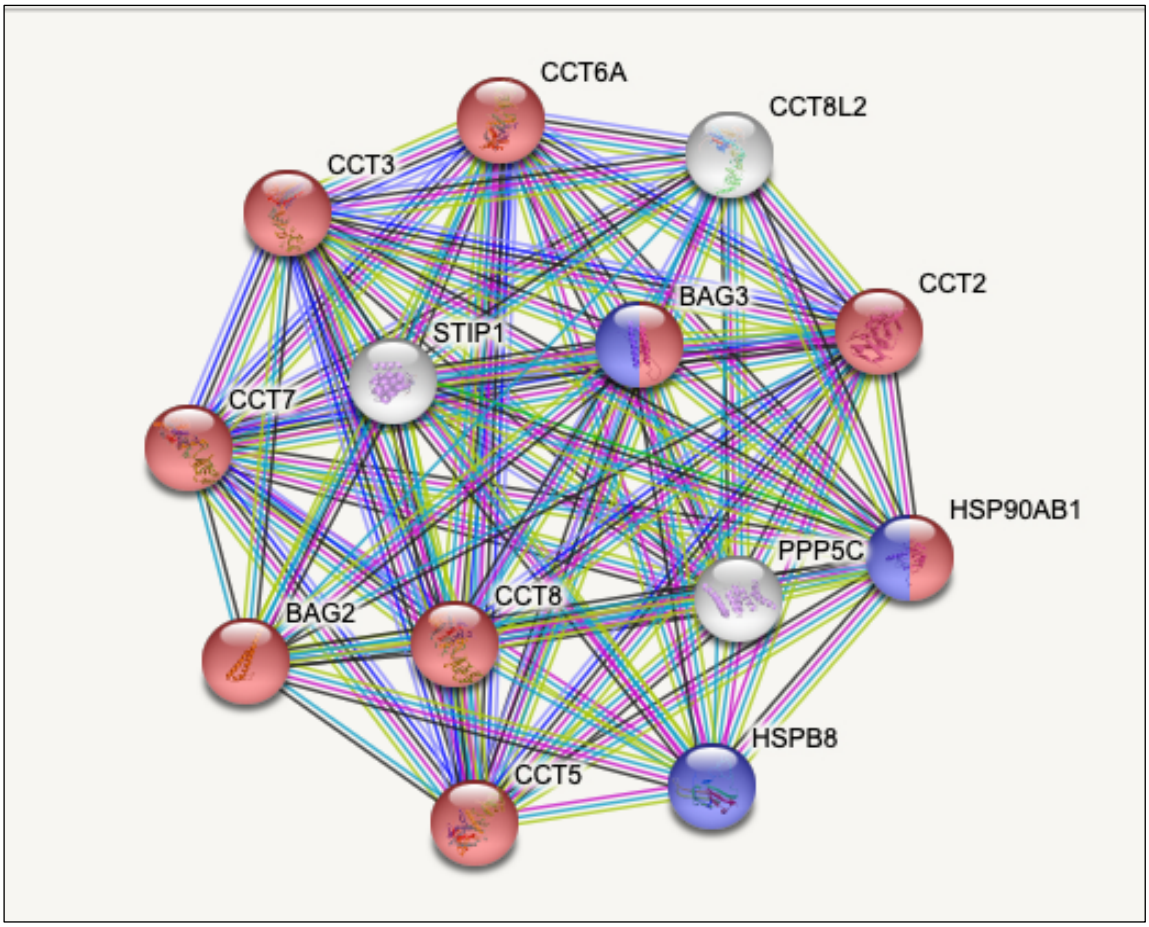

C. GO:0101002 ficolin-1-rich granule

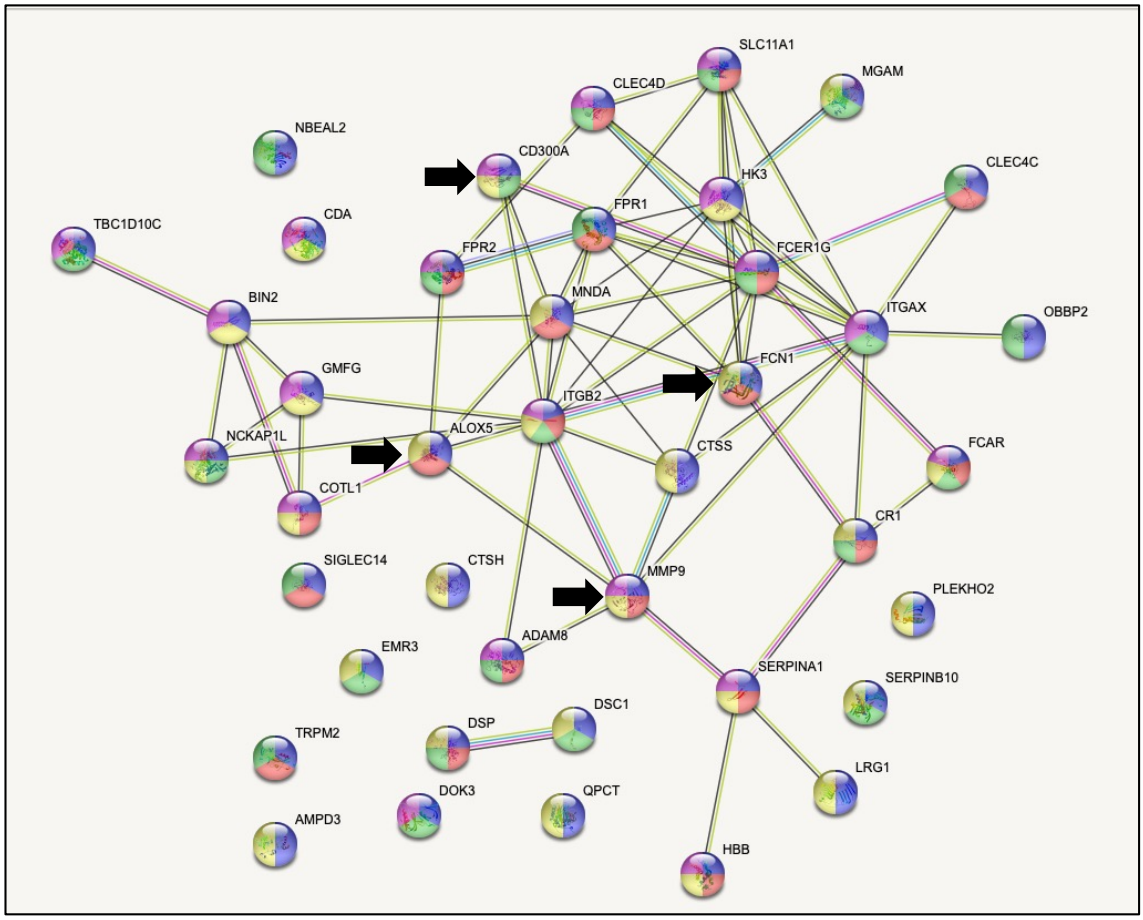

D. GO:0017171 serine hydrolase activity

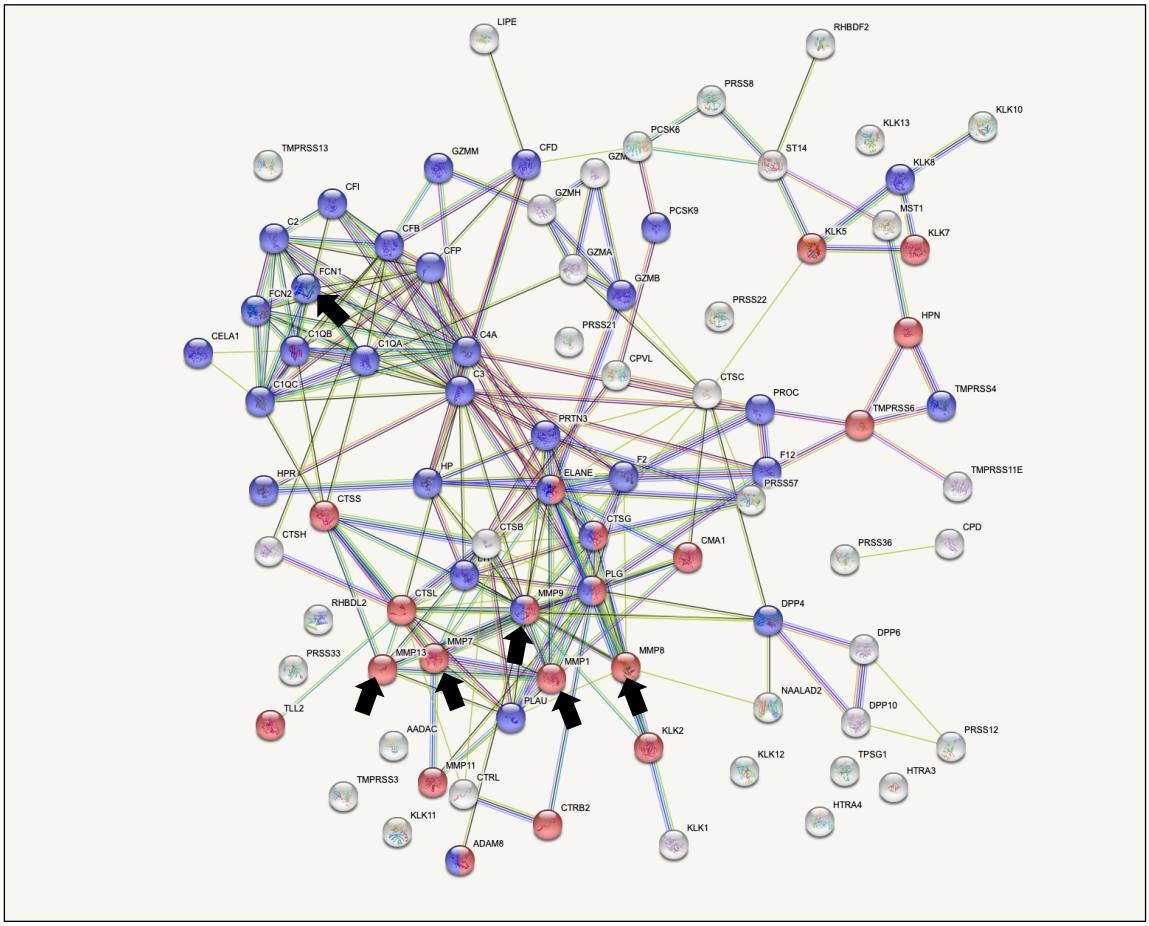

Figure 10. Clusters of enriched categories in the aorta of bicuspid patients *versus* healthy controls comparison assay represented by © STRING CONSORTIUM 2022. **A**: **GO:0048872 homeostasis of number of cells;** Red: GO:0045765 Regulation of angiogenesis, Dark blue: GO:0032364 Oxygen homeostasis, Light green: GO:0043619 Regulation of transcription from RNA polymerase ii promoter in response to oxidative stress, Yellow: GO:1902237 Positive regulation of endoplasmic reticulum stress-induced intrinsic apoptotic signaling pathway, Pink: GO:0006950 Response to stress, Dark green: GO:0010574 Regulation of vascular endothelial growth factor production, Light blue: GO:0006979 Response to oxidative stress, Brown; GO:0080134 Regulation of response to stress. IL6 and HIF1A proteins are marked with arrows. **B: GO:0101031 chaperone complex**; Red: GO:0006457 Protein folding, Blue GO:0006986 Response to unfolded protein. **C: GO:0101002 ficolin-1-rich granule**; Blue: GO:0043312 Neutrophil degranulation, Yellow: GO:0005576 Extracellular region, Green: GO:0101003 ficolin-1-rich granule membrane, Red: GO:0006950 Response to stress, Pink: BTO:0000089 Blood. FCN1, MMP9, ALOX5 and CD3001 proteins are marked with arrows. **D: GO:0017171 serine hydrolase activity**; Red: GO:0022617 Extracellular matrix disassembly, Blue: GO:0006950 Response to stress. FCN and KLK11 proteins and MMPs are marked with arrows.

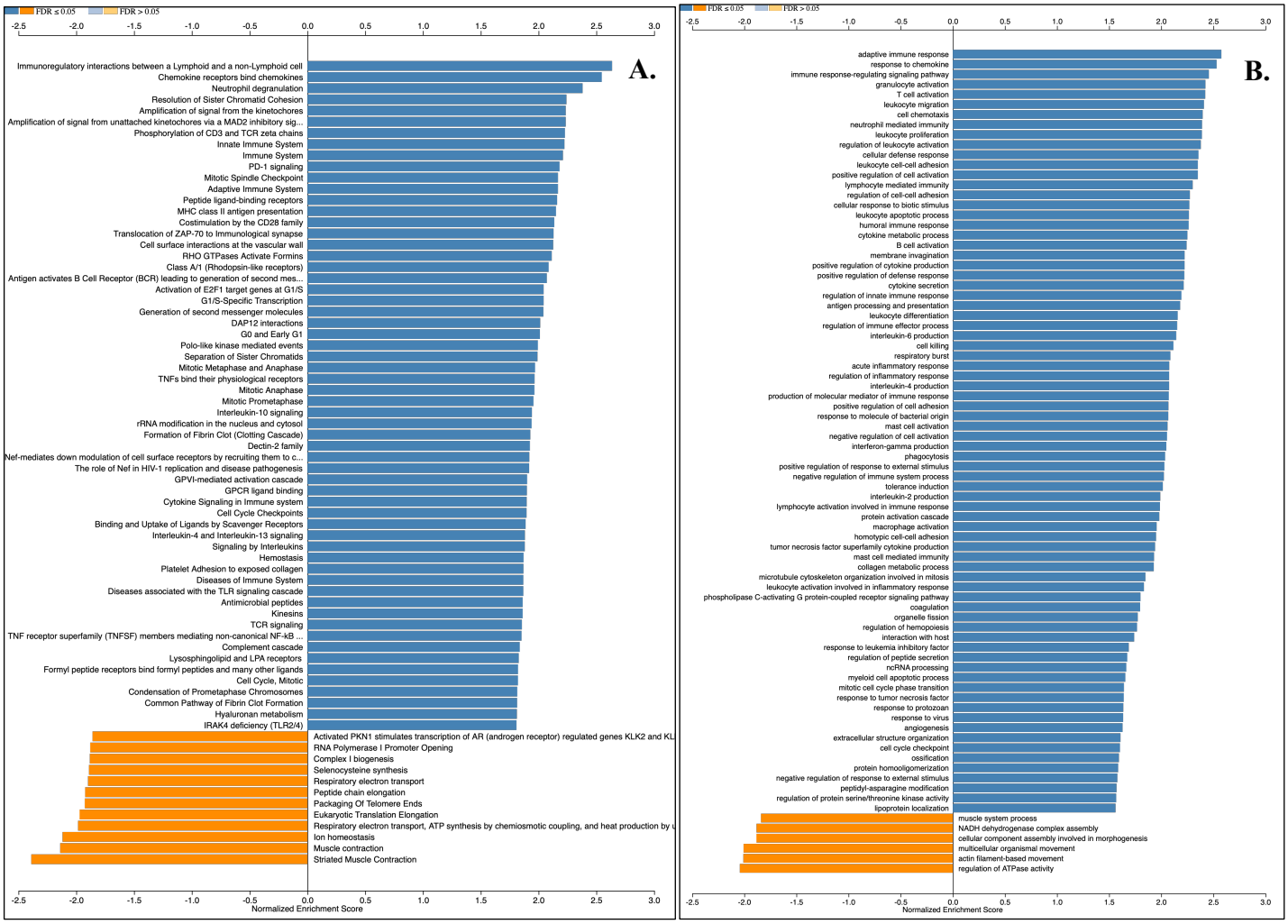

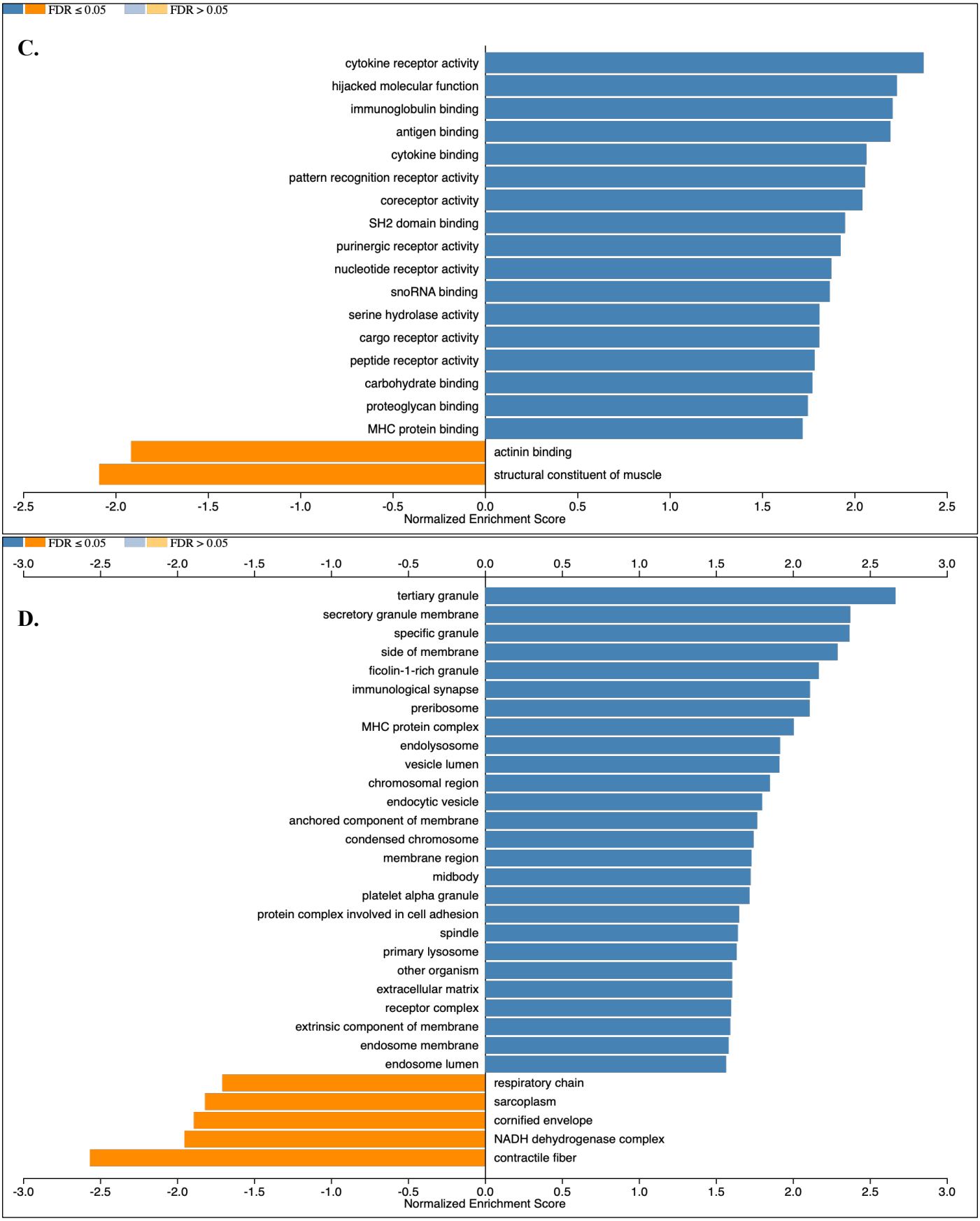

Figure 11. GSEA analysis after syndromic *versus* healthy controls comparison. Normalized Enrichment Score is shown in x-axis. **A**: Reactome pathways. **B**: GO Biological Processes. **C**: GO Molecular Function. **D**: GO Cellular Component. FDR≤0.05.

After GSEA analysis performed with DEGs identified by the AAT2 comparison, the following enriched categories were selected from the GO Biological Process database: “extracellular structure organization” (Fig. 12: **A**), “angiogenesis” (Fig. 12: **B**), and “regulation of vasculature development” (Fig. 12: **C**). All these categories contained proteins of interest (marked with arrows) due to their link with vascular remodeling. The cluster “extracellular structure organization” contained multiple collagens and MMPs strongly connected to each other. This category contained SPP1, FBN1 and NOX1 proteins. NOX1 is a member of the NADPH oxidase family of enzymes responsible for the generating of superoxidase and plays a critical role in the pathogenesis of cardiovascular diseases ranging from atherosclerosis to hypertension, restenosis and ischemia/reperfusion injury (53). NOX1 was also found in the “angiogenesis” category as well as, ER stress-related markers (XBP1 and IL6), and HIF1A protein. The cluster “Regulation of vasculature development” category contained these same ER-stress markers and HIF1A protein. Further, “Hemostasis” (Fig. 12: **D**) was an enriched category selected from the Reactome Pathway database, and “extracellular matrix” (Fig. 12: **E**) was an enriched category selected from the GO Cellular Component database. Both categories included proteins of interest (marked with arrows). For example, in the cluster of “Hemostasis” were enriched proteins such as PPBP and OLR1. In this category, serpin family member proteins and kinesin superfamily proteins were heavily involved. The “Extracellular matrix” category contained enriched proteins such as FCN1 together with the ER-stress related proteins GDF15 and S100A8. Again, this category also contained multiple MMPs and collagens.

A. GO:0043062 Extracellular structure organization

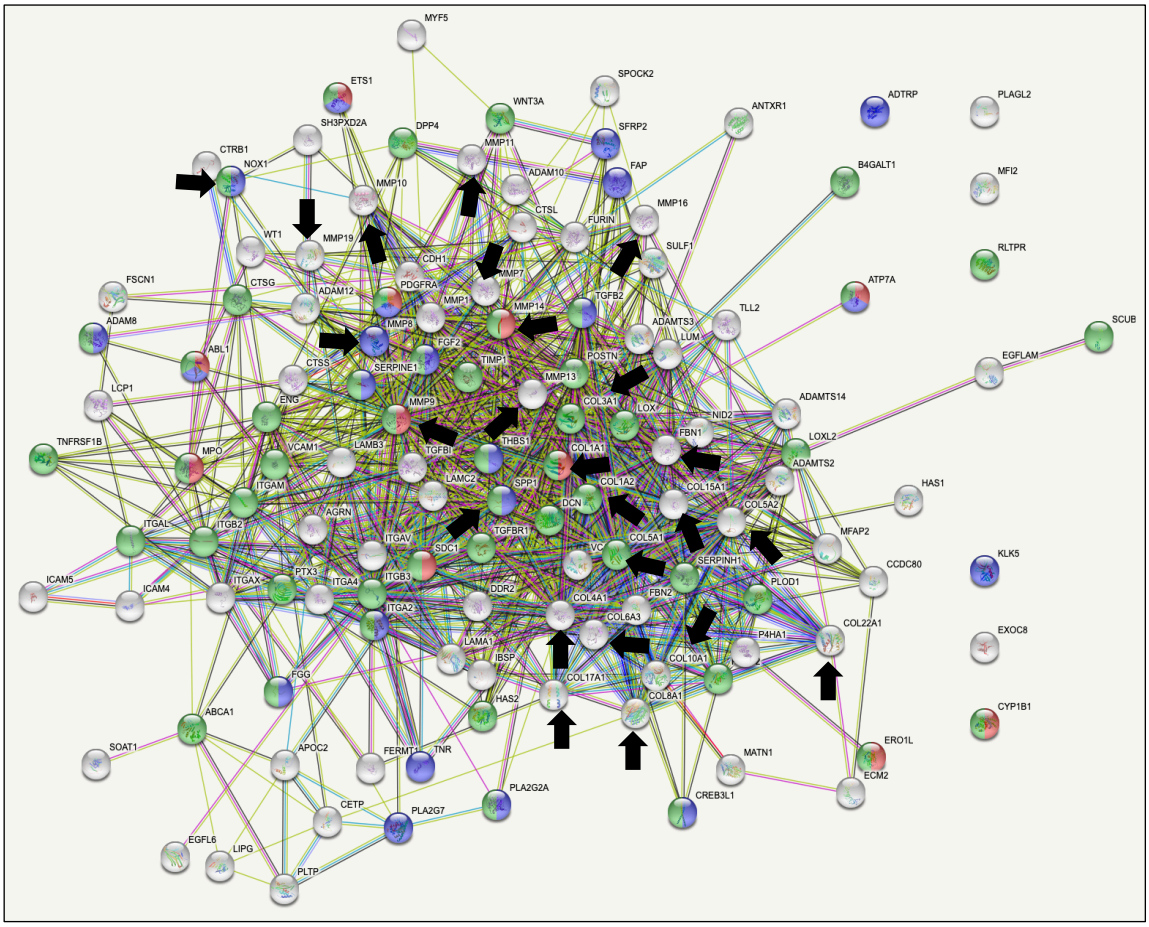

B. GO:0001525 Angiogenesis

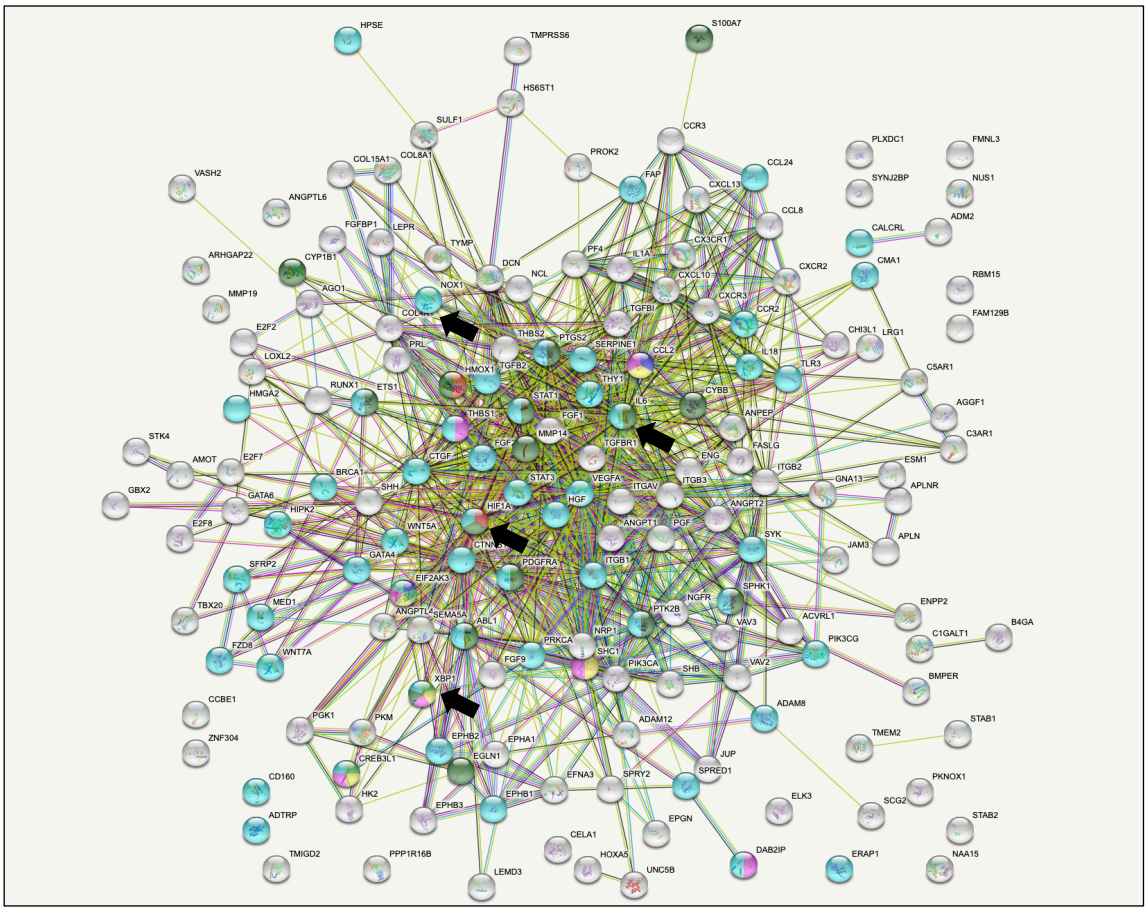

C. GO:1901342 regulation of vasculature development

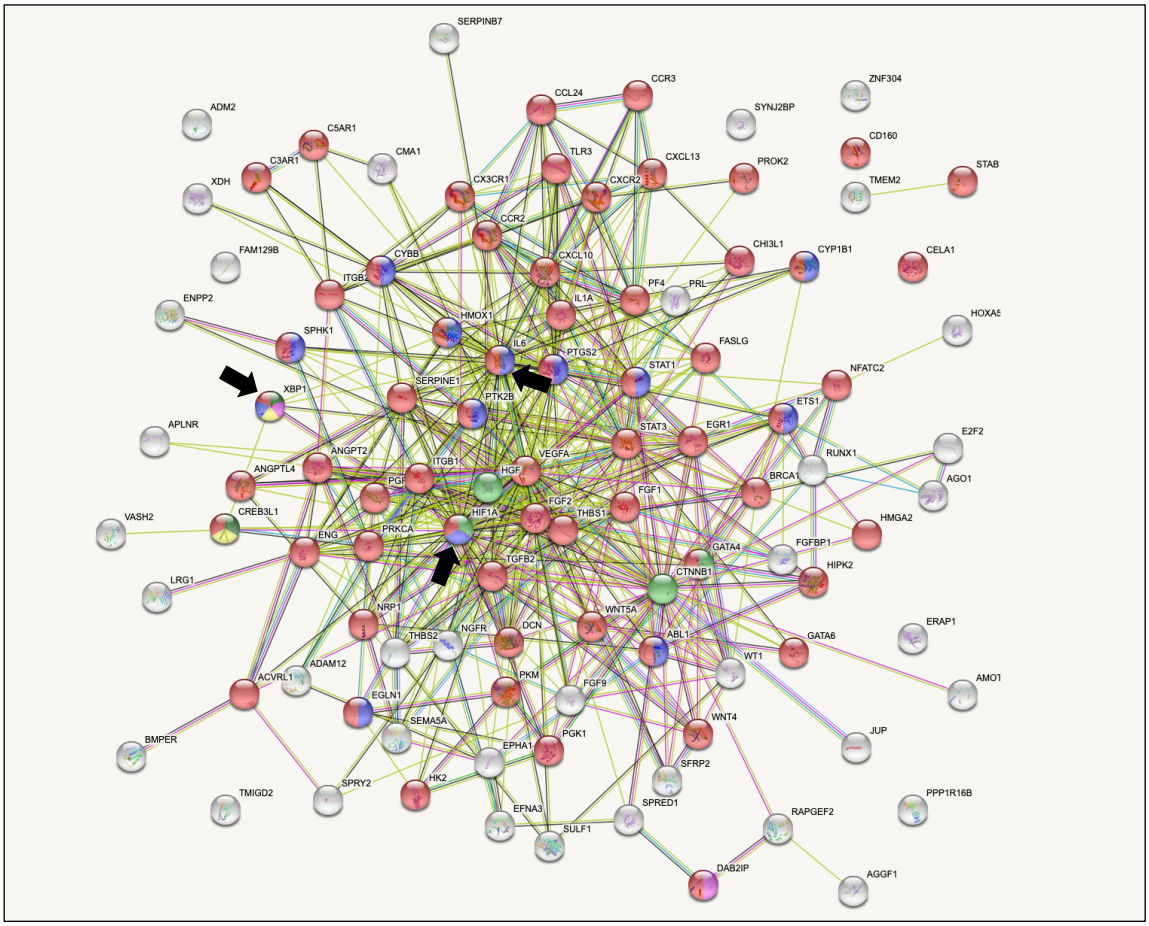

D. R-HSA-109582 Hemostasis

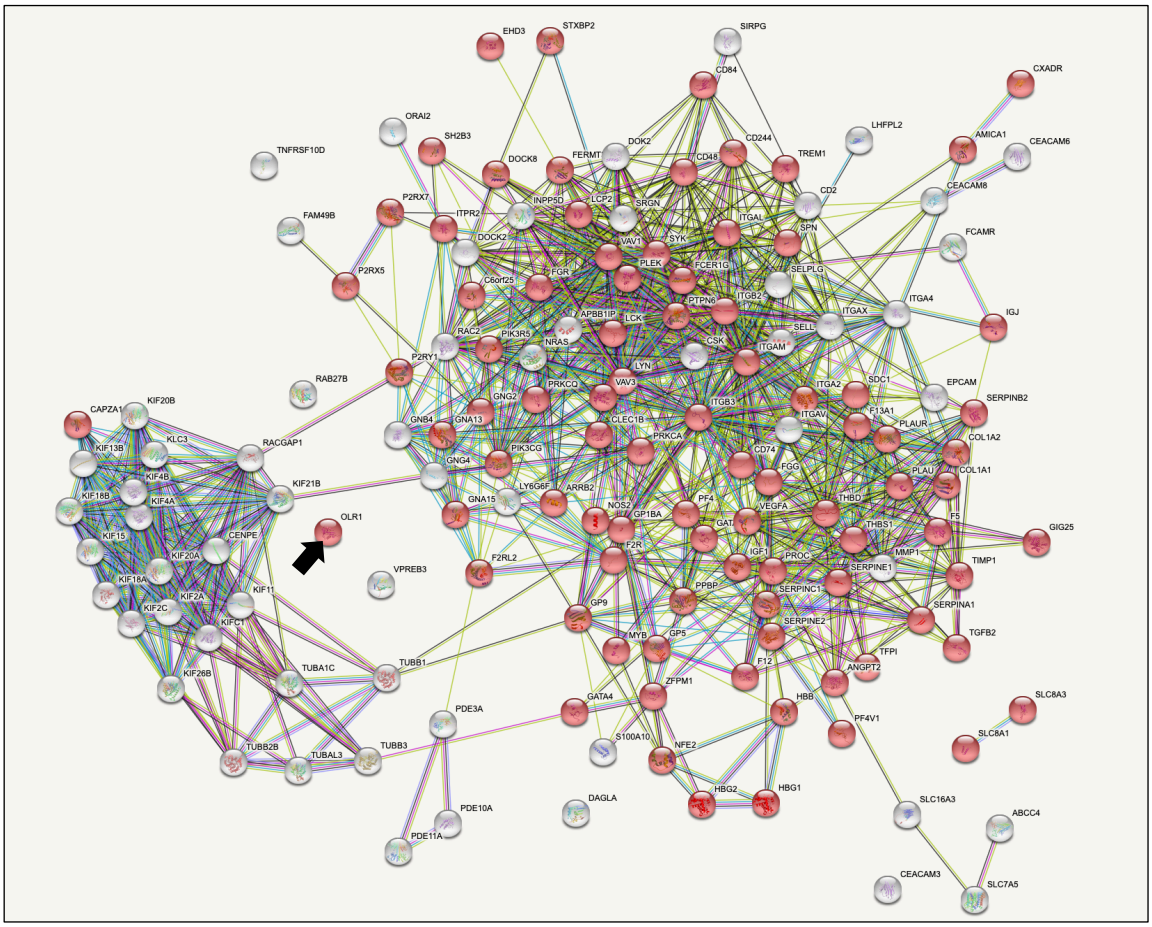

E. GO:0031012 Extracellular matrix

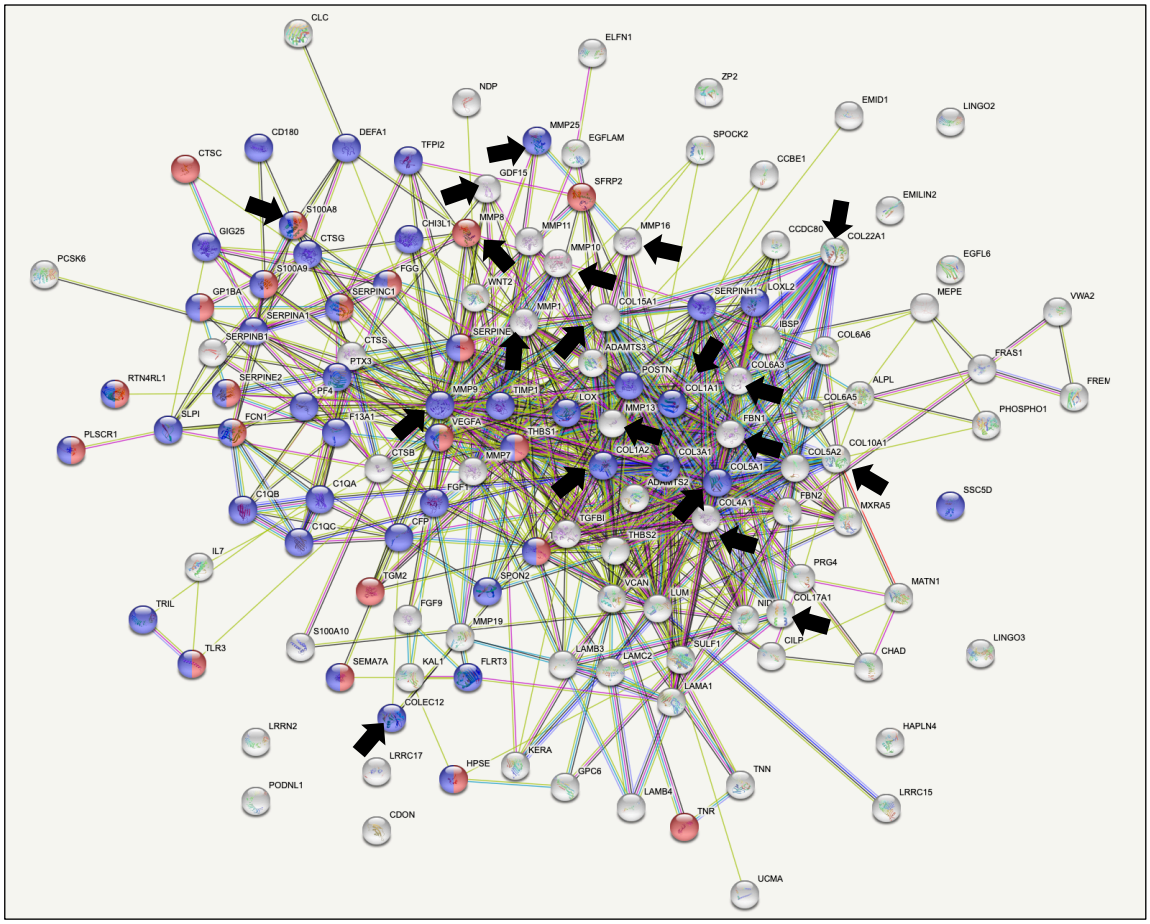

Figure 12. Clusters of enriched categories corresponding to the comparison between syndromic *versus* healthy controls represented by © STRING CONSORTIUM 2022. **A**: **GO:0043062 Extracellular structure organization**; Red: GO:0006979 Response to oxidative stress, Blue: GO:0080134 Regulation of response to stress, Green: GO:0006950 Response to stress. Multiple collagens and MMPs and SPP1, FBN1 and NOX1 proteins are marked with arrows. **B: GO:0001525 Angiogenesis**; Red: GO:0043619 Regulation of transcription from RNA polymerase ii promoter in response to oxidative stress, Dark blue: GO:0036499 PERK-mediated unfolded protein response, Light green: GO:1902235 Regulation of endoplasmic reticulum stress-induced intrinsic apoptotic signaling pathway, Yellow: GO:0030968 Endoplasmic reticulum unfolded protein response, Pink: GO:0006986 Response to unfolded protein, Dark green: GO:0006979 Response to oxidative stress, : GO:0080134 Regulation of response to stress. IL6, NOX1, HIF1A and XBP1 proteins are marked with arrows. **C: GO:1901342 regulation of vasculature development;** Red: GO:0006950 Response to stress, Dark blue: GO:0006979 Response to oxidative stress, Light green: GO:1903202 Negative regulation of oxidative stress-induced cell death, Yellow: GO:1902236 negative regulation of endoplasmic reticulum stress-induced intrinsic apoptotic signaling pathway, Pink: GO:1900103 Positive regulation of endoplasmic reticulum unfolded protein response. Dark green: GO:1990440 Positive regulation of transcription from RNA polymerase ii promoter in response to endoplasmic reticulum stress. IL6, HIF1A and XBP1 proteins are marked with arrows. **D: R-HSA-109582 Hemostasis;** Red: GO:0006950 Response to stress. PPBP and ORL1 proteins are marked with arrows. **E: GO:0031012 Extracellular matrix**; Blue: GO:0080134 Regulation of response to stress, Red: GO:0006950 Response to stress. FCN1, GDF15, S100A8 proteins and multiple MMPs and collagens are marked with arrows.

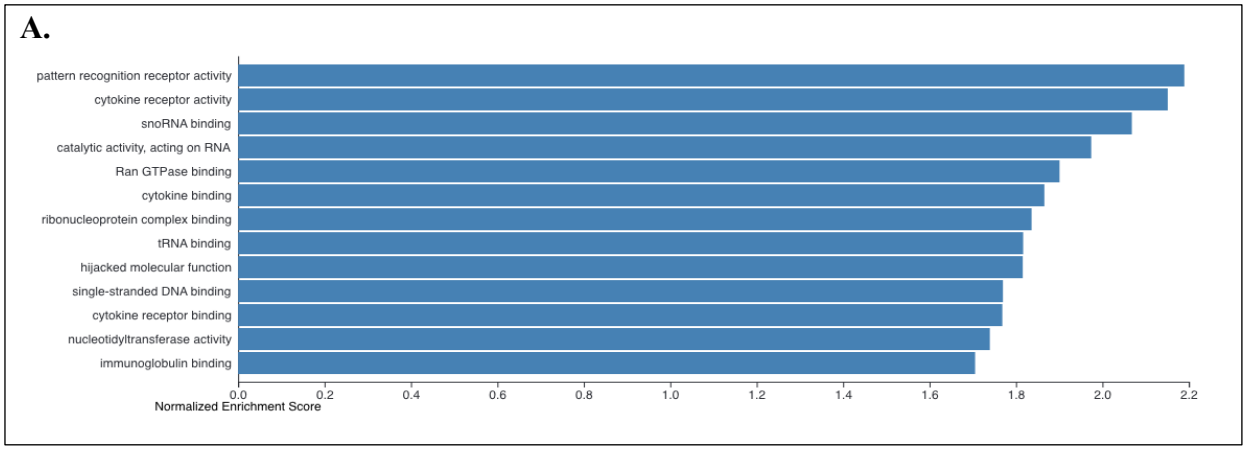
A.
pattern recognition receptor activity
cytokine receptor activity
snoRNA binding
catalytic activity, acting on RNA
Ran GTPase binding
cytokine binding
ribonucleoprotein complex binding
tRNA binding
hijacked molecular function
single-stranded DNA binding
cytokine receptor binding
nucleotidyltransferase activity
immunoglobulin binding
0.0 0.2 0.4 0.6 0.8 1.0 1.2 1.4 1.6 1.8 2.0 2.2
Normalized Enrichment Score

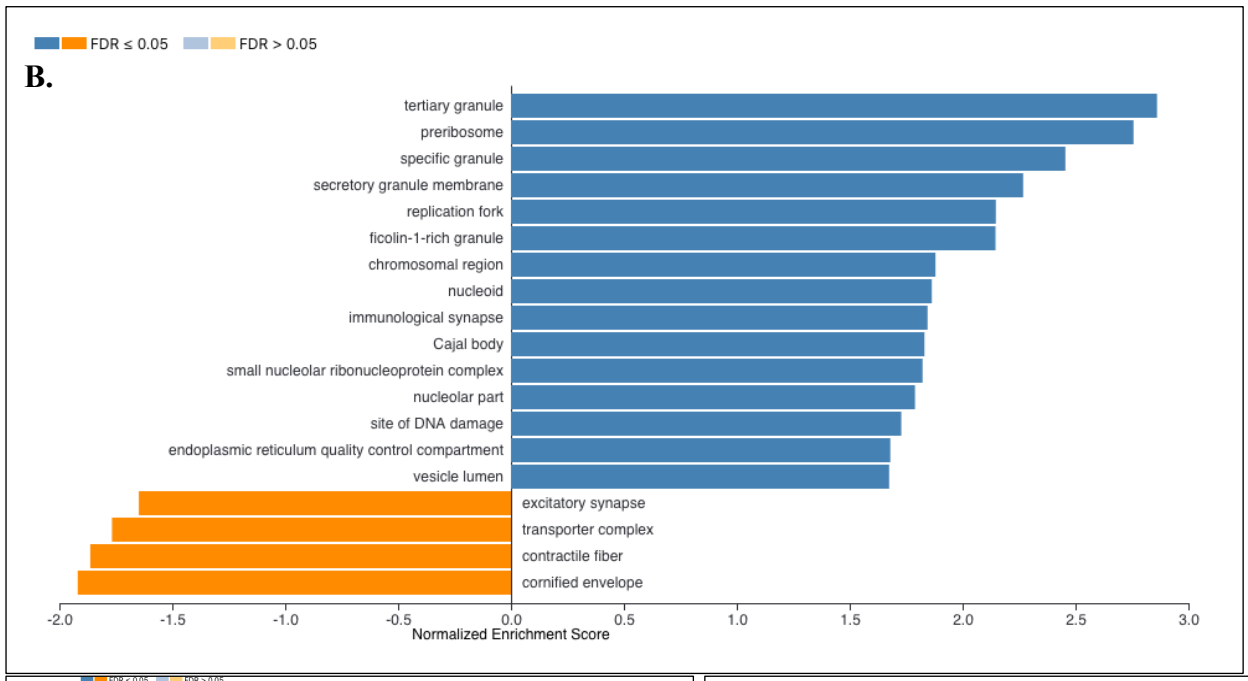
FDR ≤ 0.05
FDR > 0.05
B.
tertiary granule
preribosome
specific granule
secretory granule membrane
replication fork
ficolin-1-rich granule
chromosomal region
nucleoid
immunological synapse
Cajal body
small nucleolar ribonucleoprotein complex
nucleolar part
site of DNA damage
endoplasmic reticulum quality control compartment
vesicle lumen
excitatory synapse
transporter complex
contractile fiber
cornified envelope
-2.0 -1.5 -1.0 -0.5 0.0 0.5 1.0 1.5 2.0 2.5 3.0
Normalized Enrichment Score

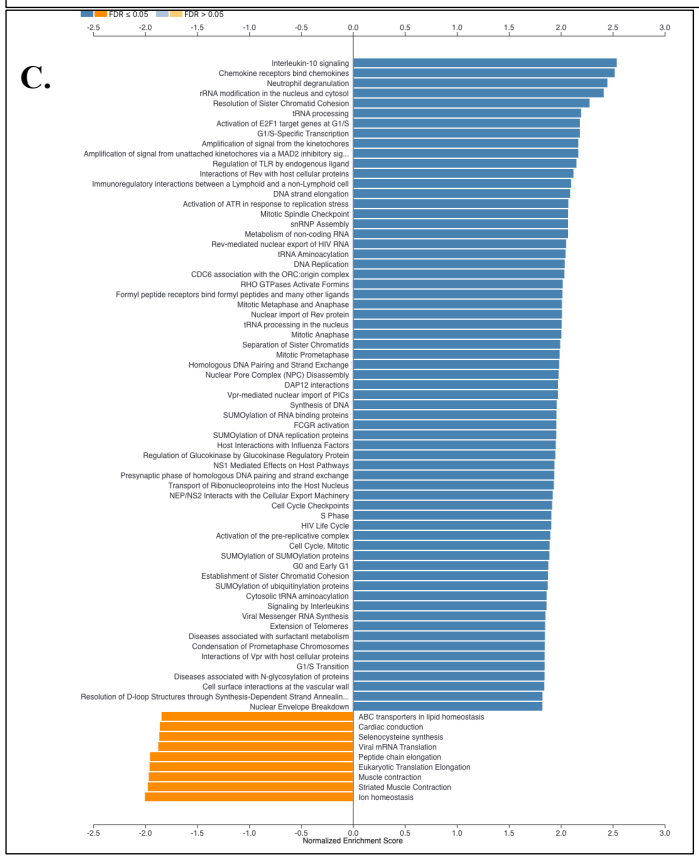
C.
Normalized Enrichment Score

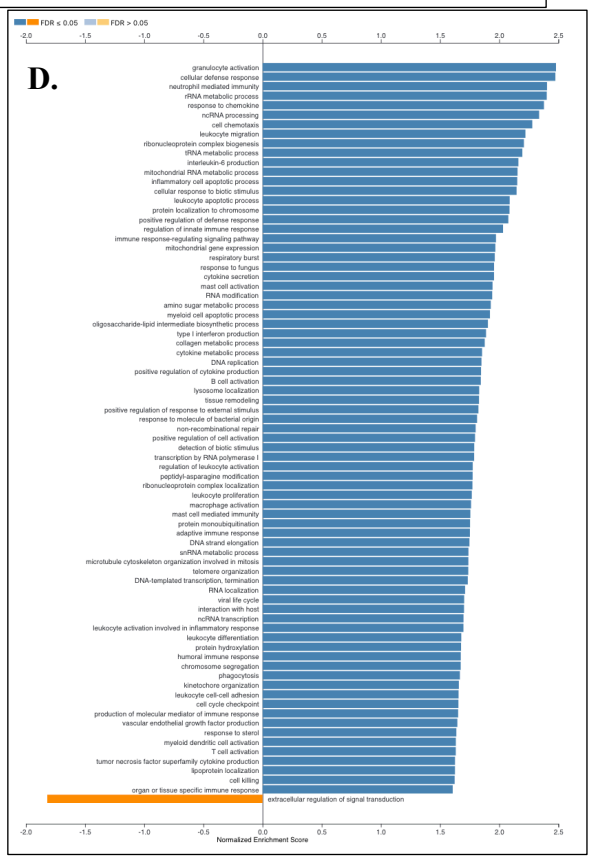
D.
Normalized Enrichment Score

Figure 13. GSEA analysis after genetic *versus* healthy controls comparison. Normalized Enrichment Score is shown in x-axis. **A**: GO Molecular Function. **B:** GO Cellular Component **C:** Reactome pathway. **D:** GO Biological Processes. FDR≤0.05.

GSEA analysis performed with data from the AAT3 comparison revealed the enrichment of genes involved in the clusters (GO Biological Process): "mitochondrial gene expression" (Fig. 14: **A**) and "tissue remodeling" (Fig. 14: **B**). The first category contained proteins involved in mitochondrial biogenesis and the second included proteins involved in inflammatory processes and tissue remodeling (IL1A, IL7, IL6, LIF; SPP1, HIF1A and MMP14) (marked with arrows). Additionally, we identify the cluster "Cell surface interactions at the vascular wall" (Fig.14: **C**) from the Reactome database as an enriched category in the aorta from genetic patients and identified OLR1 (marked with arrow) as an enriched in these subjects. Further, the focus was also at the enriched category "Neutrophil degranulation" (Fig.14: **D**), which was among the top three enriched categories from the Reactome Pathway database and contained several proteins of interest (PPBP, OLR1, FCN1 and S100A8) (marked with arrows).

A. GO:0140053 Mitochondrial gene expression

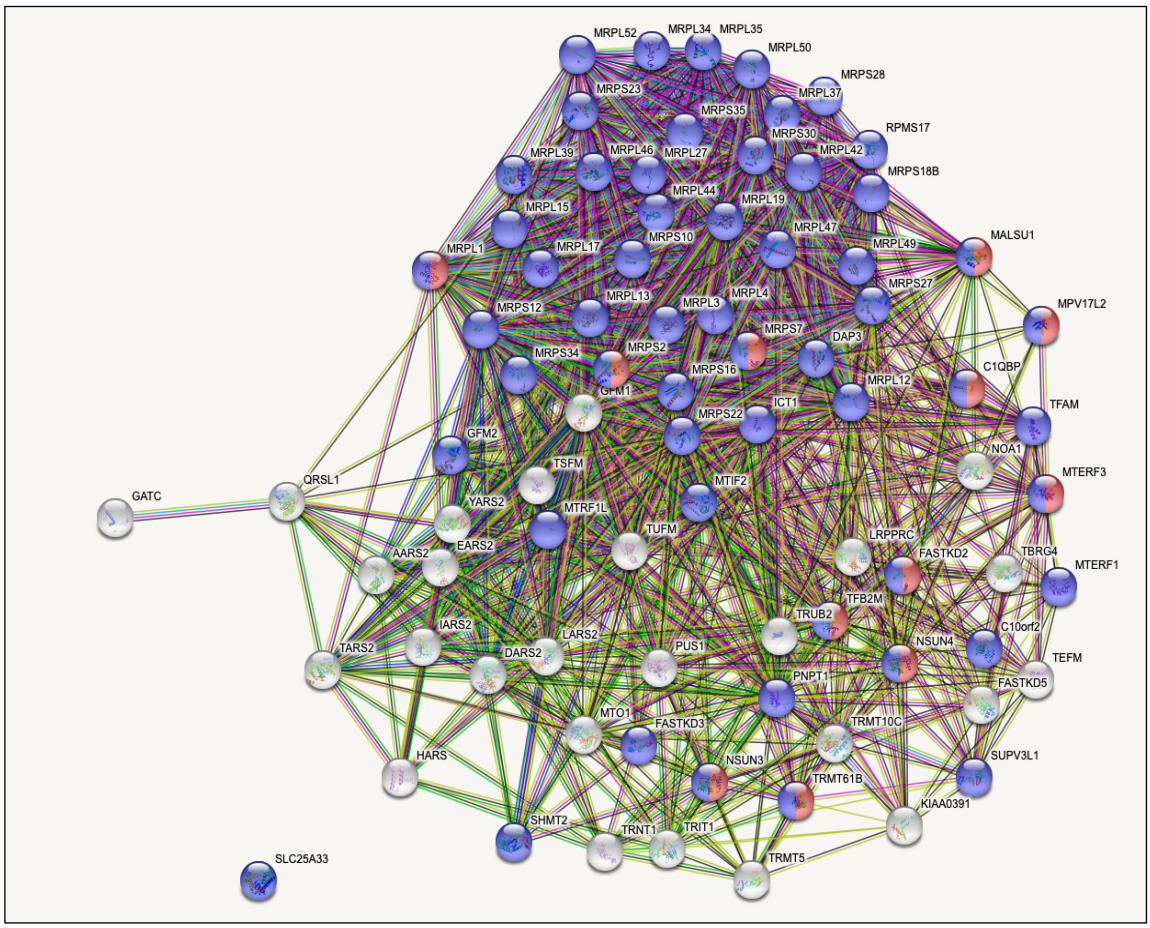

B. GO:0048771 Tissue remodeling

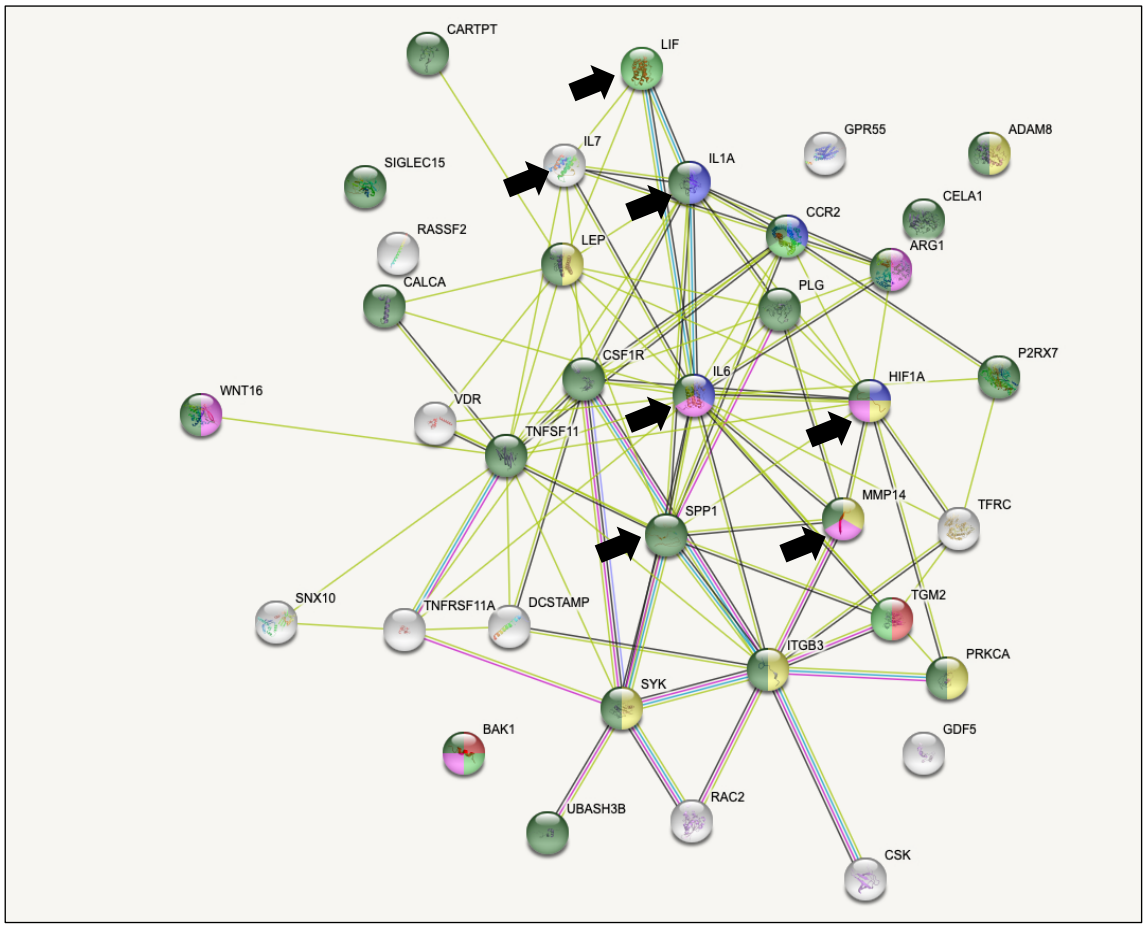

C. R-HSA-202733 Cell surface interactions at the vascular wall

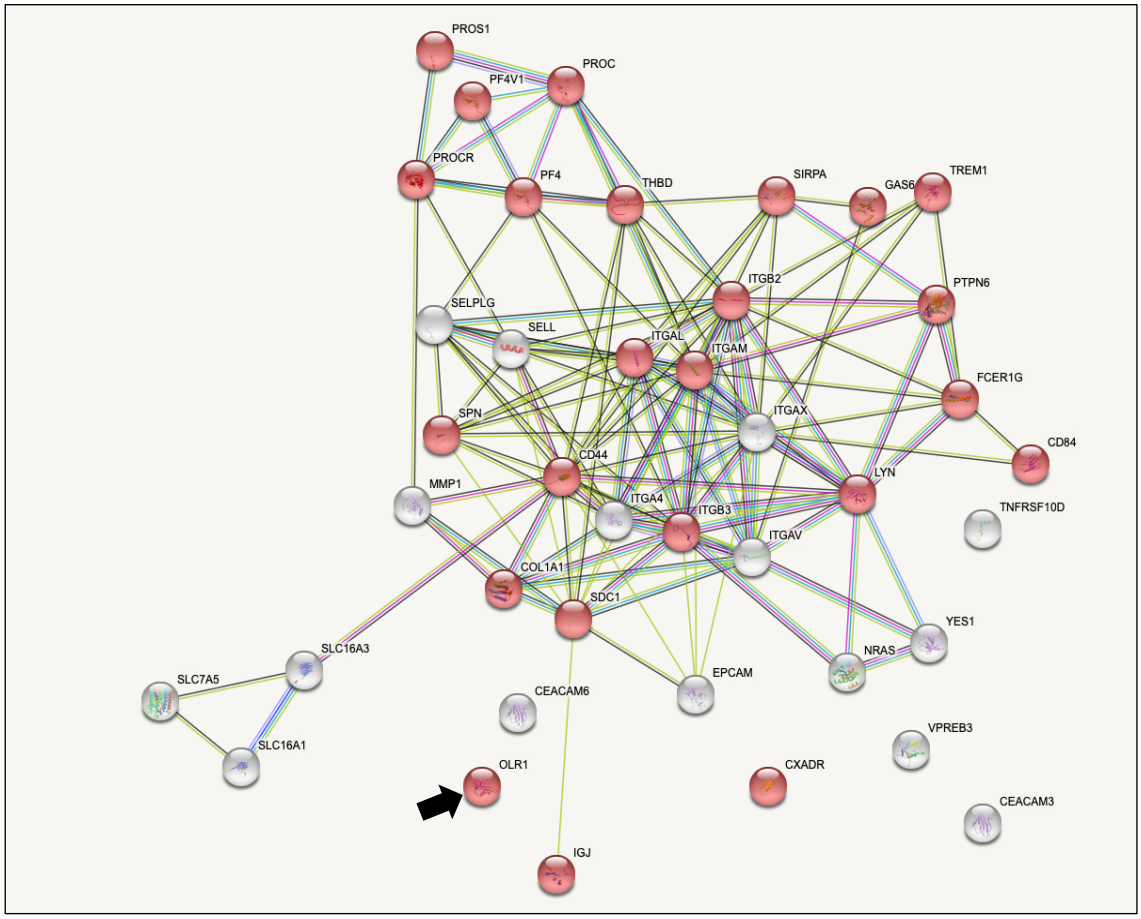

D. R-HSA-6798695 Neutrophil degranulation

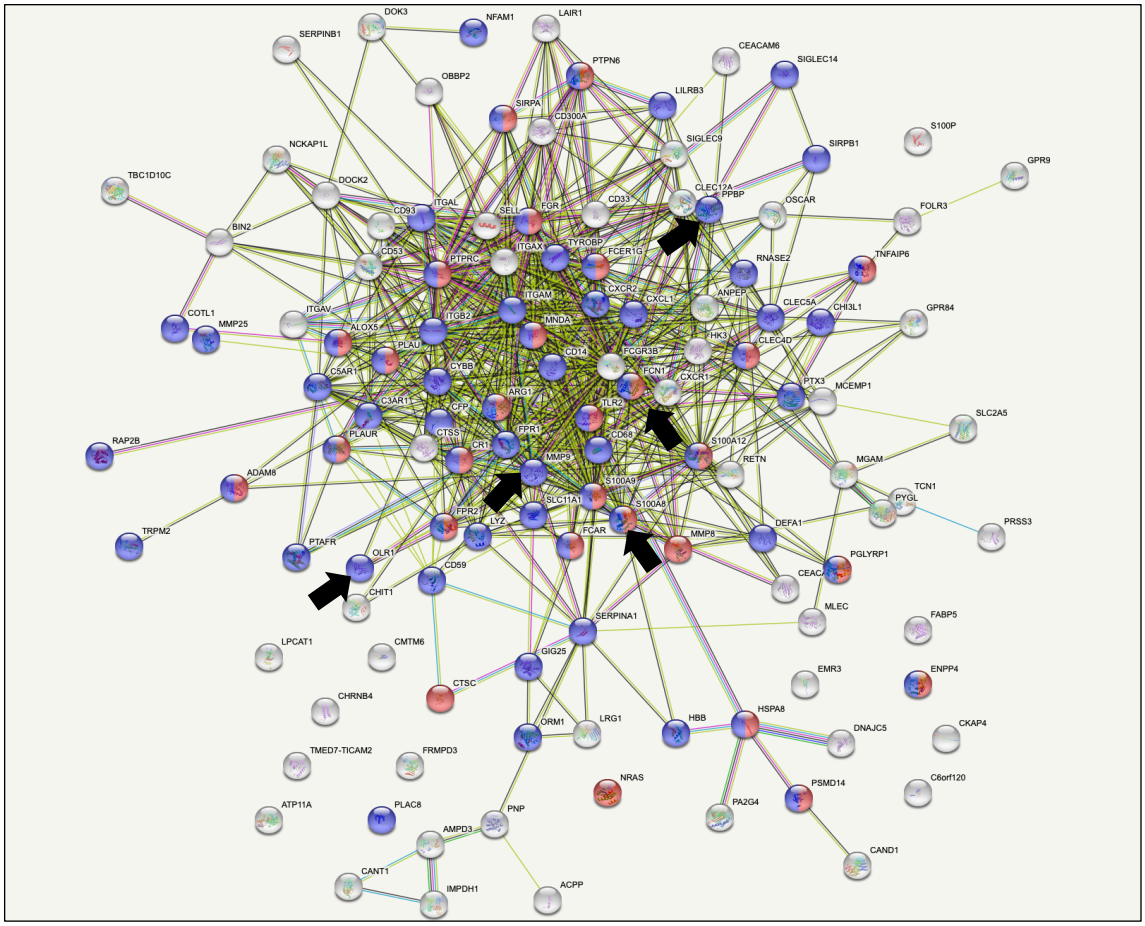

Figure 14. Clusters of enriched categories on Genetic versus Healthy controls assay represented by © STRING CONSORTIUM 2022.**A: GO:0140053 Mitochondrial gene expression**; Red: GO:0042254 Ribosome biogenesis, Blue: GO:0071840 Cellular component organization or biogenesis. **B: GO:0048771 Tissue remodeling**; Red: GO:0032471 Negative regulation of endoplasmic reticulum calcium ion concentration, Blue: GO:0010574 Regulation of vascular endothelial growth factor production, Light green: GO:0001974 Blood vessel remodelling, Yellow: GO:0001525 Angiogenesis, Pink: GO:0006979 Response to oxidative stress, Dark green: GO:0006950 Response to stress. IL1A, IL7, IL6, LIF, SPP1, HIF1A and MMP14 proteins are marked with arrows. **C: R-HSA-202733 Cell surface interactions at the vascular wall;** Red: GO:0006950 Response to stress. OLR1 protein is marked with arrow. **D: R-HSA-6798695 Neutrophil degranulation;** Red: GO:0080134 Regulation of response to stress, Blue: GO:0006950 Response to stress. PPBP, OLR1, FCN1 and S100A8 proteins are marked with arrows.

3.6. Histopathology of the Vascular Wall

The staining of the paraffin sections of TAA fixed tissue was performed to study potential differences in medial degenerations (MD) of the aortic vascular wall among patient groups. Degenerative changes or damage in the medium layer are due to sums of individual histopathological degenerative lesions (3). We aimed to identify individual histopathologic degenerative lesions by considering the following features: elastic fibre fragmentation and/or loss (EFFEL), elastic fibre thinning (EFTO), elastic fibre disorganization (EFD), smooth muscle cell nuclei loss (SMCNL), laminar medial collapse (LMS), smooth muscle cell

disorganization (SMCD), medial fibrosis (MF) and mucoid extracellular matrix accumulation (MEMA). MEMA can be divided into two phenomena: intralamellar (MEMA-I) and translamellar (MEMA-T). In MEMA-I, the increase in mucoid ECM does not alter the arrangement of the lamellar units unlike in MEMA-T (3). Every one of these features affects lamellar units in cellular and extracellular space (3).

Medial degeneration was the most systematic histopathological feature found in ascending TAA (54). Ascending TAA is caused most commonly by the breaking down of the tissue of the aortic wall and/or elastic fibre fragmentation (3). It is known that genetic syndromes lead to degenerative changes that are mainly MEMA and EFFEL (54).

Haematoxylin eosin (HE) staining showed EFFEL in the aortic wall of all patient groups (Fig. 15: **A-J**). HE stains showed alterations in the arrangement of the lamellar units by MEMA-T in the aortic wall in patients with MFS (Fig. 15: **A, B**). Medial degeneration caused by MEMA-T is frequently seen in MFS patients (54, 55). Regardless, this can also be seen in the aortic wall of the bicuspid patients (Fig. 15: **C, D**). In contrast, increased MEMA-I is seen in the aneurismal wall of genetic patients (Fig. 15: **G, H, I**). In genetic patients, also SMCD can be observed in the aneurismal wall (Fig. 15: **I**, indicated with an arrows). Fibre thinning and SMCNL in patches (Fig. 15: **F**, indicated with an arrow) is also seen in the aneurysmal wall of bicuspid patients (Fig. 15: **C, D**).

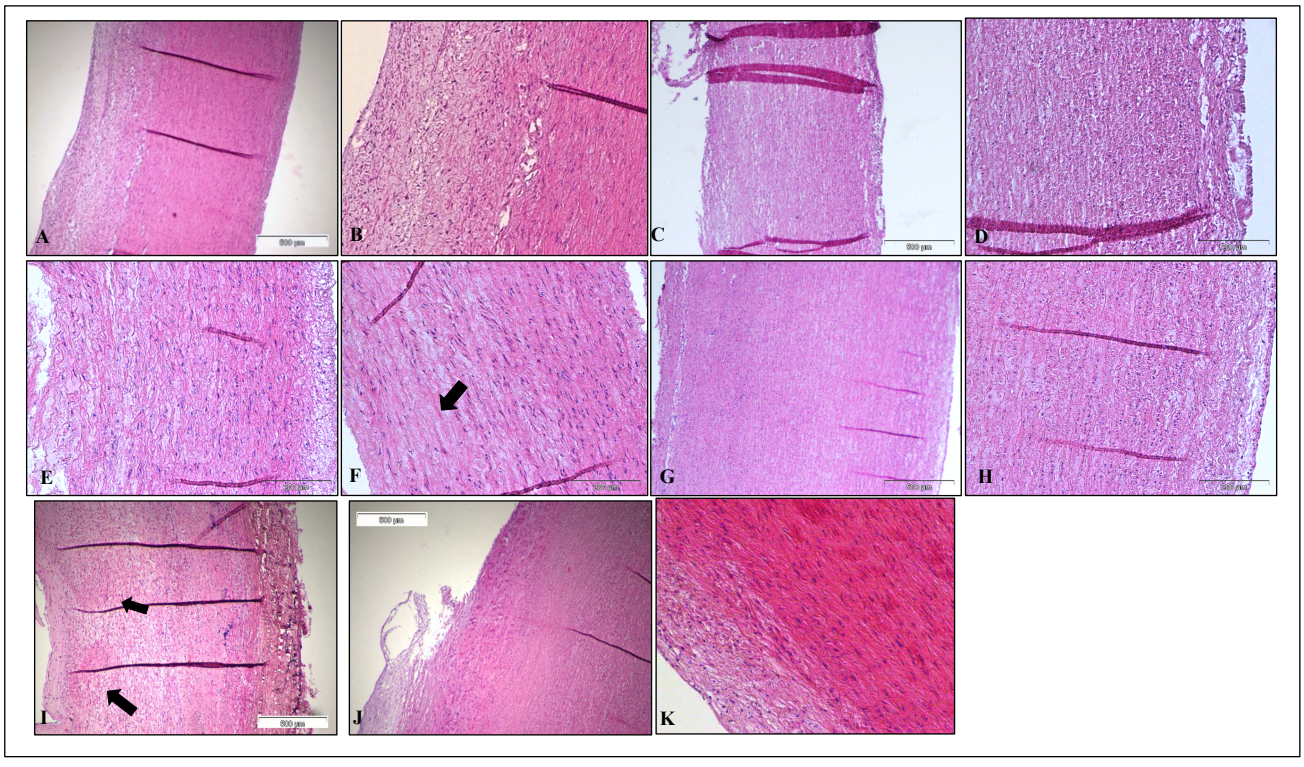

Figure 15. Aortic paraffin sections were stained with Haematoxylin Eosin (HE) to visualize differences in medial degenerations (MD) of the aortic vascular wall between patient with different aortopathies. Representative images are shown. Magnification (**A, C, E, G, I, J**) 4x and (**B, D, F, H, J**) 10x were used to capture the images. **A-B** images are from the same histological section of a syndromic patient with different microscope objectives (MFS). **C-D & E-F:** images taken from the same histological section of 2 representative samples from bicuspid patients with different microscope objectives. Arrow in image **F** is indicating SMCNL patches. **G-H** representative images are from the same histological section of a genetic patient taken under different microscope objectives. Representative image **I** is from a genetic patient. Arrows in image **I** are indicating SMCD. **J-K** representative pictures taken with different microscope objectives from the same histological section of healthy ascending aortas from donors. Bars: 500µm at the 4x images and 200µm at the 10x images.

Orcein staining revealed elastic fibre thinning (EFT) in genetic (Fig. 16: **E, F**) and syndromic patients (Figure 15: **A, B**). Elastic fibre fragmentation/loss as well as ruptures was observed in the aneurysmal wall of MFS (Fig. 16: **A, B**) and bicuspid patients (Fig. 16: **C, D**), in which also severe MEME-T was evidenced (Fig. 16: **C, D**). In the TAA of bicuspid patient's laminar medial collapse was observed (Fig. 16: **E,** indicated with arrow).

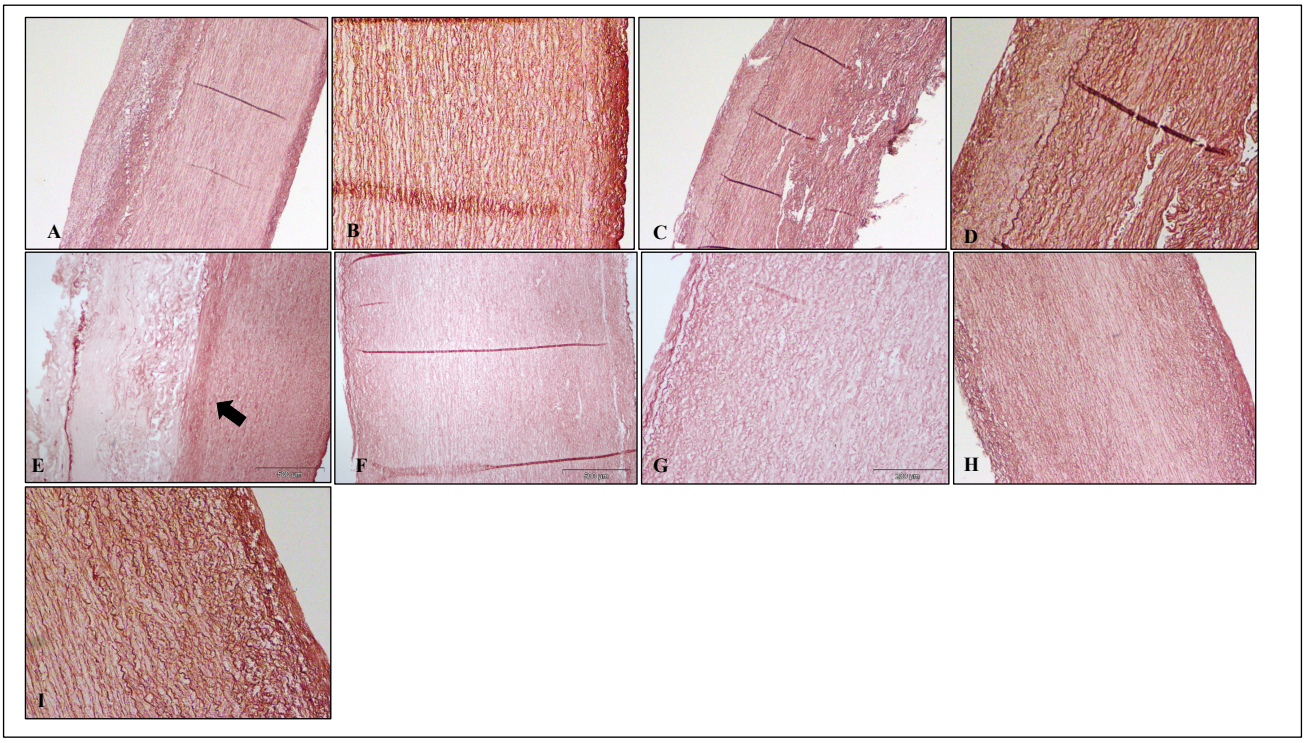

Figure 16. Aortic paraffin sections were stained with orcein to analyze differences in medial degenerations (MD) of the aortic vascular wall between patient with different aortopathies. Representative images are shown. Magnification (**A, C, E, F, H, J**) 4x and (**B, D, G, I**) 10x were used to capture the images. **A-B** images are from the same histological section of a syndromic patient with different microscope objectives (MFS). **C-D** representative images are from the same histological section of the bicuspid patient with different microscope objectives. Representative image **E** is from bicuspid patient in which laminar medial collapse is indicated with arrow. **F-G** representative images are from the same histological section of a genetic patient with different microscope objectives. **H-I** representative pictures taken with different microscope objectives from the same histological section of healthy aortas from donors. Bars: 500µm at the 4x images and 200µm at the 10x images.

Sirius Red (SR) showed disrupted collagen fibres in the aneurysmal wall of syndromic patients with MFS (Fig. 17: **A, B, C**). In bicuspid patients, an increase in translamellar collagen can be observed (Fig. 17: **E, F,** indicated with arrows). This is an increase in collagen which causes scar-like alterations in the arrangement of the lamellar units (3). In the aneurysmal wall of the other patient groups, an increase in the interlamellar collagen increase was also observed, which is noted as an expansion within the interlamellar space by collagen (Fig. 17: **A, B, C, G, H, J,** indicated with arrows). This collagen is disorganised and unstructured and forms cloudy spaces rather than wavy fibre bundles (3), in comparison with non-syndromic healthy aortas from donors, where collagen deposition was less and exhibited a normal distribution in the aortic wall (Fig. 17: **I, J**).

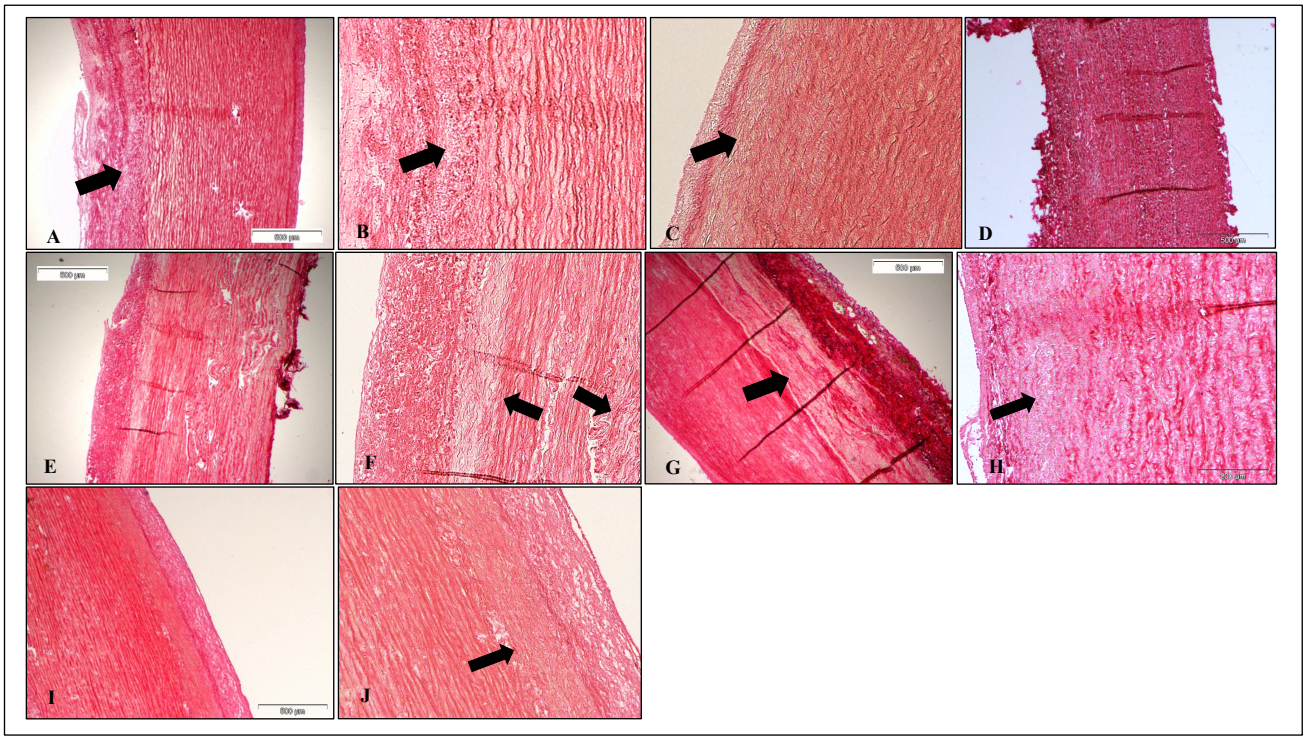

Figure 17. Aortic paraffin sections were stained with Sirius Red (SR) to determine differences in medial degenerations (MD) of the aortic vascular wall between different aortopathies. Representative images are shown. Magnification (**A, B, D, E, G, I**) 4x, (**B, C, F, H, J**) 10x were used to capture the images. **A-B** representative images are from the same histological section of a syndromic patient with different microscope objectives (MFS). Representative image **C** is from the histological section of a syndromic patient with MFS. Representative image **D** is from the histological section of the bicuspid patient. **E-F** representative images are from the same histological section of the bicuspid patient with different microscope objectives. In image **F,** an increase in translamellar collagen is indicated with arrows. **G-H** representative images are from the same histological section of a genetic patient with different microscope objectives. **I-J** representative pictures taken with different microscope objectives from the same histological section of healthy aortas from donors. In images **A-C, G-H, J**, an expansion within the interlamellar space by collagen is indicated with arrows. Bars: 500µm at the 4x images and 200µm at the 10x images.

In the histological section stained with MOVAT, lamellar units are highlighted with black lines of elastic laminae (3). Elastic fibre fragmentation can be observed in MFS (Fig. 18: **A, B**) and bicuspid patients (Fig. 18: **C, D, E**) as compared with healthy aorta from healthy controls (Fig. 18: **H, I**) by MOVAT staining. In genetic patients' laminar medial collapse can be observed (Fig. 18: **F**, indicated with an arrow). In genetic patients' loss of three-layer architecture is also noted and mucoid extracellular matrix accumulation is shown in blue (Fig. 18: **F, G**, indicated with an arrow).

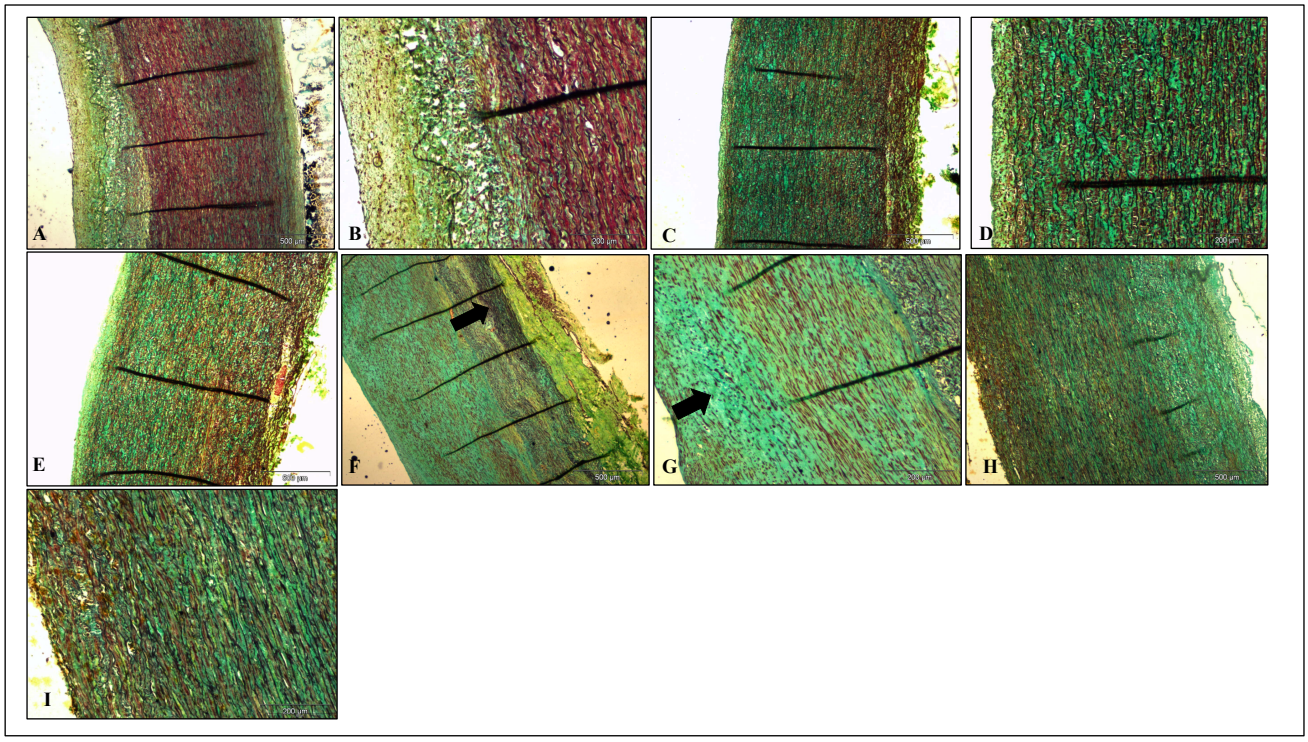

Figure 18. Aortic paraffin sections were stained with MOVAT to visualize differences in medial degenerations (MD) of the aortic vascular wall between patient with different aortopathies. Representative images are shown. Magnification (**A, C, E, F, H**) 4x, (**B, D, G, I**) 10x were used to capture the images. **A-B** representative images are from the same tissue section of a syndromic patient with different microscope objectives (MFS). **C-D** representative images are from the same histological section of the bicuspid patient with different microscope objectives. Representative image **E** is from the tissue section of the bicuspid patient. **F-G** representative images are from the same tissue section of a genetic patient with different microscope objectives. In image **F**, laminar medial collapse is indicated with arrow and in image G, mucoid extracellular matrix accumulation is indicated with arrow. **H-I** representative pictures taken with different microscope objectives from the same tissue section of healthy aortas from donors. Bars: 500µm at the 4x images and 200µm at the 10x images.

4. Discussion

This study aimed to identify new therapeutic targets, with special emphasis on those related to ER and mitochondrial stress, to improve the management of aortic aneurysms in syndromic patients. This was done by studying the expression profile and circulating protein levels of the chosen candidate genes in TAA patient samples based on RNA sequencing results. The DEGs were analyzed, and enriched GO categories and Reactome pathway clusters were determined. In addition, the histology of TAA tissue from the three groups of patients was compared with the ascending aorta tissue of healthy donors to establish differences among them in the context of TAA aortic wall degeneration.

4.1. Upregulated genes in syndromic patients had been previously described as potential biomarkers in other cardiac diseases

Based on the RNA-seq results, it was noticed that inflammation plays a critical role in TAA formation, which was expected based on previous studies regarding both AAA and TAA formation (56-58). Many of the top highly expressed DEGs were related to inflammation but others did not, and we selected some of them as potential targets to manage aneurysm disease. These target genes encode proteins that have been previously described as potential biomarkers for various cardiac diseases (58-74). Still, none of them, apart from *SPP1*, was noted to be a potential biomarker specifically for TAA

Among the target genes validated and showing significantly increased mRNA levels in patients diagnosed with a syndrome (*CCL7, IL11, PPBP, GAL, AQP9, SPP1, FCN1, SPP1* and *OLR1)*, only *SPP1* had previously been shown to affect the formation of TAA (58) *SPP1* has been demonstrated to affect TAA formation by enhancing vascular permeability and loss of wall integrity (58), making it an interesting candidate for future studies to handle TAA disease and supporting the suitability of our approach

Other selected candidate genes were described in the literature as potential biomarkers for various cardiac diseases; *AQP9* for myocardial infarction and septic shock (59, 60), *FCN1* for acute myocardial infarction (69), and *OLR1* for coronary artery disease (62), while *CCL7, PPBP* and *IL11*deserve special attention. In the aortic wall, macrophages cause oxidative stress (63), and CCL7 has previously been confirmed to contribute to AAA formation by promoting macrophage infiltration (63). In turn, macrophage infiltration is reported to induce the expression of PPBP, which has been noted to be increased in calcified aortic valves (64). In

response to aortic inflammation, macrophages promote the secretion of IL11, which is enhanced in the thoracic aorta and plasma of acute thoracic aortic dissection (TAD) (65). These associations make these proteins interesting candidates as targets for therapeutic purposes and as biomarkers with prognostic value.

4.2. There was a considerable overlap in DEGs between syndromic and genetic patients

When we compared RNA-seq results among the three groups, the overlap between syndromic and genetic patients was considerable, evidencing that the pathomolecular mechanisms underlying TAA formation were more alike between them with respect to syndromic and bicuspid patients.

The list of DEGs obtained by RNA-seq in the bicuspid patient group *versus* healthy donors (AAT1) was the most different when compared to AAT2 and AAT3. We observed a significantly increased expression of *MUC16, MSLN, KLK11, UPK1B* and *SLAMF7* only in bicuspid patients. Of these DEGs, *MSLN* was previously mentioned in studies of ER stress (66, 68). MSLN is a cell surface-bound protein, whose normal expression is restricted to the mesothelial cells, and it binds with high affinity to the surface mucin (MUC16) (70). *MSLN* has been widely studied in the context of cancer, and it has been linked with ER stress (72). Wang K *et al* described that silencing of the *MSLN* gene triggered a significant decrease in endoplasmic oxidoreductase-1 (Ero1) expression, one of the molecules involved in the ER-stress pathway and induced by UPR (72).

Other genes upregulated in the bicuspid patient group were described as potential biomarkers for various cardiac diseases but were not associated with TAA. *MUC16* encodes a large antigen carbohydrate 125 (CA125) which is a promising biomarker for heart failure (66). Overexpression of KLK11 promotes Ang II-induced increase in protein synthesis which is, for example, why KLK11 is considered to be involved in the regulation of cardiac hypertrophy (71). *UPK1B* has also been studied in the context of cardiac hypertrophy as well as in the context of cardiomyocytes (73). *SLAMF7* is a key regulator of carotid atherosclerosis by inhibiting vascular smooth muscle cell proliferation through several proinflammatory cytokines (74).

Based on the RNA-seq results, we were able to better understand the underlying pathomolecular mechanisms involved in TAA formation and find important differences in the gene expression and regulation between the groups of bicuspid and syndromic patients. Still, when searching for specific determination of TAA progression in syndrome patients, further analyses are needed to establish a clear distinction between the molecular mechanisms involved in TAA formation in syndromic and genetic patients.

4.3. Differences in the expression of ER stress and mitochondrial biogenesis markers among groups were assessed

The expression levels of DEGs related to ER stress and mitochondrial biogenesis markers were notably lower than those of the other selected candidate genes in all patient groups. Regarding the DEGs of ER stress markers studied by RNA-seq analysis, we noticed that some of the genes involved in the UPR were significantly enriched in syndromic patients and in genetic patients (AAT2 and AAT3) but not in bicuspid patients (AAT1). For instance, in syndromic and genetic patient groups, *EIF2AK3* was upregulated. *EIF2AK3* encodes PERK from upstream of UPR, which regulates ATF4 and CHOP pathways. However, when we validate these data by quantitative RT-PCR, we found that most ER stress markers were significantly upregulated in bicuspid patients as well as in syndromic patients. This suggests that ER stress is somehow involved in TAA development, but we could not distinguish clear differences between syndromic and bicuspid patients at all.

Regarding mitochondrial biogenesis markers, we observed a significant increase in the expression of *MT-CO3* only in bicuspid patients as compared to healthy controls and syndromic patients group. This result did not match with the data obtained by RNA-seq analysis, where *MT-CO3* was found to be decreased in bicuspid patients. *MT-CO3* was significantly decreased in syndromic and genetic patient groups indicating that mitochondrial biogenesis was impaired.

As a counterpart, in the RNA-seq analysis of the syndromic *versus* healthy donors, the *TFAM* gene was found to be upregulated which was not seen in genetic patients. TFAM has been shown to play a central role in the mtDNA stress-mediated inflammatory (75) and upregulation of *TFAM* might act as a protective counteract mechanism. In MFS patients, a decrease in TFAM (transcription factor A, mitochondrial) expression and mitochondrial respiration has been proved (46). TFAM is a DNA-binding protein that activates the transcription of the two major promoters of mitochondrial DNA (mtDNA) (76). Because of this, glycolytic metabolism

is increased to balance the decline in oxidative phosphorylation. This mitochondrial decline is a suggested driver and is a common hallmark of different hereditary TAAs (46). During aortic remodelling, mitochondrial metabolism is an important regulator of the VSMC phenotype (46). Both the metabolism and the phenotype of VSMCs depend on the signal coming from the extracellular matrix (46). Changes in the ECM composition during aneurysms development drive metabolic rewiring toward glycolysis in all the cell types present in the vascular wall (46). In VSMCs, TFAM defiance also promotes mitochondrial dysfunction, which induces aortic aneurysms (46).

4.4. No significant differences in the circulating levels of soluble proteins encoded by selected DEGs were assessed among study groups

In general, we could not observe differences among groups of patients in the circulating protein levels when quantified in serum samples by ELISA. Serum levels of MSLN and FCN1 were not consistent with the results obtained by gene expression studies (RNA-seq and quantitative RT-PCR assays). MSLN protein levels were similarly increased in all patient groups. This is somehow encouraging since MSLN has been previously linked with ER stress (72), making it an interesting candidate for further studies. FCN1 soluble protein levels were similar in bicuspid and genetic serum samples. For syndromic patients, FCN1 was found to be slightly decreased in serum samples, which is not in line with aortic gene expression results either.

We further measured ITLN1 and S100A8 serum levels and found that they were also increased in all groups. ITLN1 (also named OMENTIN-1) has an important role in chronic inflammation-related diseases that are driven by inflammation (51). Calprotectin S100A8 is a pro-inflammatory molecule that together with S100A9 is involved in several ischemia/reperfusion stress reactions, such as suppression of mitochondrial function (61).

In contrast, we found that circulating levels of GDF15 were significantly decreased in syndromic patients when compared to other study groups. GDF15 is a member of the TGFβ family whose expression is induced by oxidative stress. GDF15 is produced and secreted by endothelial cells, macrophages, VSMC, and cardiac myocytes in response to oxidative stress, pro-inflammatory stimuli or ischemia (77). It has been previously studied as a candidate biomarker in both myocardial fibrosis and inflammation in the context of coronary artery aneurysms in Kawasaki disease (78), but it has never been involved in TAAs development.

In the pathophysiology of some inflammatory arterial diseases, such as an aneurysm, different soluble molecules, including proinflammatory cytokines (TNFα, IL-1β, IL6 etc.), has been shown to trigger critical regulatory pathways (79). Of the ER stress-related cytokines, IL6, IL-1β, TNFα, IFNγ, MCP-1 and TGFβ-1 were most significantly increased in syndromic patients, IL6 levels being the highest. Of note, no changes in the protein levels of other ER stress-related cytokines such as IGF-1 and Leptin were observed in the aneurysmal tissue of syndromic patients.

An increase in MSLN, S100A8, and ITLN1 protein levels indicates that ER stress is somehow involved in TAA formation. The increase in ER-stress related cytokine levels in damaged tissue of syndromic patients is further confirming this and proves that inflammation plays an important role in TAA development in syndromic patients.

4.5. Pathways related to extracellular matrix were enriched in syndromic patients

Enriched pathways confirmed the existing perception that inflammation and apoptosis are important events occurring in TAA development. The enriched pathways we found in this study were mostly related to inflammation. Again, pathways enriched in bicuspid patients differed from syndromic and genetic patients, which were more overlapping with each other.

Enriched pathways related to extracellular matrix distinguished syndromic TAA patients from other patient groups, which is logical, since the fibrillin-1 expression is impaired in Marfan patients due to genetic mutations, while TGF-beta signalling is damaged in Loeys-Dietz patients, both affecting the deposition, maturation, and integrity of elastin fibres in the aortic wall. It has been widely described that disrupting the ECM, drives the development of aortic aneurysms (46). The enriched pathways related to mitochondria regulation distinguished genetic TAA patients from other patient groups and indicates that the homeostasis of mitochondria is somewhat disrupted. There is a bidirectional connection between the extracellular matrix (ECM) composition and the cellular metabolism with a critical implication in aortic tissue homeostasis. The function of the mitochondria in VSMCs is controlled by the extracellular matrix (ECM) (46).

In addition, pathways related to vascular tissue, like vascular development and vascular cell interaction, were enriched in both syndromic and genetic patients, while this was not observed in the bicuspid TAA group. VSMCs can shift their phenotype from a contractile to a synthetic

phenotype, a key mechanism in arterial remodeling. Indeed, this process generates pathological features such as an elevated proliferation rate and increased ECM accumulation (46). This favors medial degeneration in the aneurysm development resulting in increased aortic stiffness. Stiffness and alteration in the composition of the ECM in the vascular wall regulate mitochondrial metabolism (46).

4.6. Medial degeneration and thinning of the intima were observed in all study TAA patients

Systematic histological evaluation of aorta wall segments showed moderate to severe medial defects and thinning of the intima in all patient groups. An increase in collagen deposition was observed in all patient groups compared to healthy donors in which collagen deposition was normal. Collagen increase is a common phenomenon in ageing but also in those artery diseases where there is a loss of integrity of elastic fibres (3). An increase in collagen synthesis and deposition occurs as a compensatory mechanism aiming to maintain the structure of the vessel. Hereditary syndromes evidences a clear defect in elastic fibres formation due to mutations in extracellular matrix related genes including, fibrillin or elastin, among others (80). But oxidative stress can also damage elastin and other ECM components and trigger changes in the structure and function of these molecules. In this way, oxidative stress can favour the progression of various cardiovascular diseases (80). Thinning and/or fragmentation of elastic fibres was mainly observed in aortic aneurysms of bicuspid and syndromic patients.

Smooth muscle cell (SMC) disorganization or nuclei loss was observed in all patient groups. Normal ageing of the aorta decreases the number of medial SMCs, but most of these patients were young. It has been suggested that apoptosis would affect the degeneration and decrease the number of medial SMCs as well (3). In addition, mucoid extracellular matrix accumulation and a loss of three-layer architecture were observed in tissue samples of genetic patients. Altogether, these degenerative lesions cause medial wall deterioration and thinning of the intima, as a result of which the intima is unable to withstand the tearing forces caused by the blood which can lead to an intimal tear. Results derived from our histological analyses strengthen the existing perception that TAA associates with pre-existing aortic wall defects.

5. Conclusion

Based on our preliminary results, we were able to determine some potential therapeutic targets to manage aortic aneurysm formation not only in syndromic patients but also in bicuspid and genetic patients. However, due to the similarity of results obtained with syndromic and genetic patients comparison groups, more validation studies are required to clearly distinguish targeted genes between both groups. Further research to elucidate the link between ER stress and TAA development in patients diagnosed with Marfan or Loeys-Dietz syndromes is needed.

Based on the RNA-seq analysis, thirteen DEGs were selected. Only *SPP1* was previously described to influence TAA formation, and it was differentially expressed in syndromic patients. Results from quantitative RT-PCR analysis were supporting this by showing that *SPP1* mRNA levels were clearly upregulated in syndromic patients. In addition, the upregulated expression of candidate genes: *PPBP, GAL, CCL7, AQP9, OLR1, IL11* and *FCN1* was validated by quantitative RT-PCR in the syndromic patients' group. The DEGs of the above-mentioned genes were also significant in the AAT3 group by RNA-seq analysis. But the upregulation of their mRNA levels was only assessed for *GAL, CCL7* and *OLR1* and not for the rest of the genes suggesting that they are not good targets to handle aneurysms in genetic patients though they may be useful in the case of syndromic patients. Significant upregulation of *PPBP, AQP9* and *FCN1* was also observed in bicuspid patients even though when a differential expression of *PPBP, AQP9* and *FCN1* was not detected in the AAT1 group by RNA-seq. This indicates that these genes may be involved in the aneurysm formation in all the groups and cannot be considered specific targets for any group of patients.

In addition, based on RNA-seq and quantitative RT-PCR analysis, some markers associated with ER stress and mitochondrial dysfunction were enriched and upregulated in the syndromic patient group, indicating that ER stress is somehow involved in TAA development. Bioinformatic analysis indicated that in all TAA patients, some homeostasis-related pathways were enriched. Further, in syndromic patients, some pathways related to the endoplasmic reticulum were enriched, which can be explained in MFS and LDS patients due to genetic mutations. In genetic patients, some pathways related to mitochondria were enriched, indicating disrupted homeostasis of mitochondria. Based on ELISA analysis, the quantification

of cytokines related to ER stress further evidenced the implication of ER stress in TAA formation and additionally, proves that inflammation plays an important role in TAA formation in syndromic patients.

Histological staining strengthened the existing perception that TAA uniformly associates with pre-existing aortic wall defects. MD is the most systematic histopathological substrate found in TAA, which was observed in all TAA patient groups.

6. Limitations of the study

The numbers of patient samples in syndromic and genetic patient groups were low, above all in the group of genetic patients. The low sample size per group may lead to bias and because of this, it was not possible for us to give a definitive interpretation of the data.

In ELISA assays no healthy donor control (HC) group was included because we were aiming to compare MSLN, ITLN1, FCN1, and GDF15 levels among groups of patients. In the ELISA assay for ER-stress related cytokines, only tissue lysates of syndromic patients in comparison with tissue lysates from healthy controls were included since only 12 different samples could be used due to the nature of this assay.

7. References

1. Murillo H, Lane MJ, Punn R, Fleischmann D, Restrepo CS. Imaging of the aorta: embryology and anatomy. Semin Ultrasound CT MR. 2012;33(3):169-90.
2. White H, Bordes S, Borger J. Anatomy, Abdomen and Pelvis, Aorta. StatPearls [Internet]: Treasure Island (FL): StatPearls Publishing; 2022. Available from: https://www.ncbi.nlm.nih.gov/books/NBK537319/.
3. Halushka MK, Angelini A, Bartoloni G, Basso C, Batoroeva L, Bruneval P, et al. Consensus statement on surgical pathology of the aorta from the Society for Cardiovascular Pathology and the Association For European Cardiovascular Pathology: II. Noninflammatory degenerative diseases - nomenclature and diagnostic criteria. Cardiovasc Pathol. 2016;25(3):247-57.
4. Kuwabara JT, Tallquist MD. Tracking Adventitial Fibroblast Contribution to Disease: A Review of Current Methods to Identify Resident Fibroblasts. Arterioscler Thromb Vasc Biol 2017;37(9):1598–607.
5. Milewicz DM, Ramirez F. Therapies for Thoracic Aortic Aneurysms and Acute Aortic Dissections. Arterioscler Thromb Vasc Biol. 2019;39(2):126-36.
6. Norman PE, Powell JT. Site specificity of aneurysmal disease. Circulation. 2010;121(4):560-8.
7. Tingting T, Wenjing F, Qian Z, Hengquan W, Simin Z, Zhisheng J, et al. The TGF-beta pathway plays a key role in aortic aneurysms. Clin Chim Acta. 2020;501:222-8.
8. Kuivaniemi H, Ryer EJ, Elmore JR, Tromp G. Understanding the pathogenesis of abdominal aortic aneurysms. Expert Rev Cardiovasc Ther. 2015;13(9):975-87.
9. Filardo G, Powell JT, Martinez MA, Ballard DJ. Surgery for small asymptomatic abdominal aortic aneurysms. Cochrane Database Syst Rev. 2015(2):CD001835.
10. Isselbacher EM, Lino Cardenas CL, Lindsay ME. Hereditary Influence in Thoracic Aortic Aneurysm and Dissection. Circulation. 2016;133(24):2516-28.
11. Foundation BH. British Heart Foundation: British Heart Foundation; [cited 2022 13.5.2022]. Available from: https://www.bhf.org.uk/informationsupport/heart-matters-magazine/medical/all-about-aortic-aneurysm.
12. Faggion Vinholo T, Brownstein AJ, Ziganshin BA, Zafar MA, Kuivaniemi H, Body SC, et al. Genes Associated with Thoracic Aortic Aneurysm and Dissection: 2019 Update and Clinical Implications. Aorta (Stamford). 2019;7(4):99-107.
13. Gouveia EMR, Silva Duarte G, Lopes A, Alves M, Caldeira D, Fernandes EFR, et al. Incidence and Prevalence of Thoracic Aortic Aneurysms: A Systematic Review and Meta-analysis of Population-Based Studies. Semin Thorac Cardiovasc Surg. 2022;34(1):1-16.
14. Hasham SN, Lewin MR, Tran VT, Pannu H, Muilenburg A, Willing M, et al. Nonsyndromic genetic predisposition to aortic dissection. Ann Emerg Med. 2004;43(1):79-82.
15. Coady M, Davies R, Roberts M, al. e. Familial Patterns of Thoracic Aortic Aneurysms. Arch Surg. 1999;134(4):361–7.
16. Braverman AC, Roman MJ. Bicuspid Aortic Valve in Marfan Syndrome. Circ Cardiovasc Imaging. 2019;12(3):e008860.
17. Milleron O, Ropers J, Arnoult F, Bouleti C, Delorme G, Langeois M, et al. Clinical Significance of Aortic Root Modification Associated With Bicuspid Aortic Valve in Marfan Syndrome. Circ Cardiovasc Imaging. 2019;12(3):e008129.

18. Dietz HC, Cutting GR, al. e. Marfan Syndrome Caused by a Recurrent de novo Missense Mutation in the Fibrillin Gene. Nature; London. 1991;352(6333):337-9.
19. Canadas V, Vilacosta I, Bruna I, Fuster V. Marfan syndrome. Part 1: pathophysiology and diagnosis. Nat Rev Cardiol. 2010;7(5):256-65.
20. Teixido-Tura G, Forteza A, Rodriguez-Palomares J, Gonzalez Mirelis J, Gutierrez L, Sanchez V, et al. Losartan Versus Atenolol for Prevention of Aortic Dilation in Patients With Marfan Syndrome. J Am Coll Cardiol. 2018;72(14):1613-8.
21. Milewicz DM, Dietz HC, Miller DC. Treatment of aortic disease in patients with Marfan syndrome. Circulation. 2005;111(11):e150-7.
22. Meester JAN, Verstraeten A, Schepers D, Alaerts M, Van Laer L, Loeys BL. Differences in manifestations of Marfan syndrome, Ehlers-Danlos syndrome, and Loeys-Dietz syndrome. Ann Cardiothorac Surg. 2017;6(6):582-94.
23. Franken R, Teixido-Tura G, Brion M, Forteza A, Rodriguez-Palomares J, Gutierrez L, et al. Relationship between fibrillin-1 genotype and severity of cardiovascular involvement in Marfan syndrome. Heart. 2017;103(22):1795-9.
24. Neptune ER, Frischmeyer PA, Arking DE, Myers L, Bunton TE, Gayraud B, et al. Dysregulation of TGF-beta activation contributes to pathogenesis in Marfan syndrome. Nat Genet. 2003;33(3):407-11.
25. Bernstein HS, Moore P, Stanger P, Silverman NH. The levoatriocardinal vein: Morphology and echocardiographic identification of the pulmonary—systemic connection. J Am Coll Cardiol. 1995;26(4):995-1001.
26. Van Laer L, Dietz H, Loeys B. Progress in Heritable Soft Connective Tissue Diseases - Loeys-Dietz syndrome: Springer, Dordrecht; 2014.
27. Schepers D, Tortora G, Morisaki H, MacCarrick G, Lindsay M, Liang D, et al. A mutation update on the LDS-associated genes TGFB2/3 and SMAD2/3. Hum Mutat. 2018;39(5):621-34.
28. Takeda N, Yagi H, Hara H, Fujiwara T, Fujita D, Nawata K, et al. Pathophysiology and Management of Cardiovascular Manifestations in Marfan and Loeys–Dietz Syndromes. Int Heart J. 2016;57(3):271-7.
29. Halper J. Progress in Heritable Soft Connective Tissue Diseases. 2 ed: Springer International Publishing; 2014. XIII, 343 p.
30. Yacoub M, Radford M. COMPARE and Pediatric Heart Network Investigator trials: Losartan finally validated in humans with Marfan, but much work remains! Glob Cardiol Sci Pract. 2014;2014(4):371-8.
31. Pyeritz RE, Loeys B. The 8th international research symposium on the Marfan syndrome and related conditions. Am J Med Genet A. 2012;158A(1):42-9.
32. Girdauskas E, Kuntze T, Borger MA, Falk V, Mohr FW. Distal aortic reinterventions after root surgery in Marfan patients. Ann Thorac Surg. 2008;86(6):1815-9.
33. Navas-Madronal M, Rodriguez C, Kassan M, Fite J, Escudero JR, Canes L, et al. Enhanced endoplasmic reticulum and mitochondrial stress in abdominal aortic aneurysm. Clin Sci (Lond). 2019;133(13):1421-38.
34. Malhotra JD, Kaufman RJ. Endoplasmic reticulum stress and oxidative stress: a vicious cycle or a double-edged sword? Antioxid Redox Signal. 2007;9(12):2277-93.
35. Giorgi C, De Stefani D, Bononi A, Rizzuto R, Pinton P. Structural and functional link between the mitochondrial network and the endoplasmic reticulum. Int J Biochem Cell Biol. 2009;41(10):1817-27.
36. Zhang K, Kaufman RJ. From endoplasmic-reticulum stress to the inflammatory response. Nature. 2008;454(7203):455-62.

37. Belmadani S, Matrougui K. Broken heart: A matter of the endoplasmic reticulum stress bad management? World J Cardiol. 2019;11(6):159-70.
38. Zhang C, Syed TW, Liu R, Yu J. Role of Endoplasmic Reticulum Stress, Autophagy, and Inflammation in Cardiovascular Disease. Front Cardiovasc Med. 2017;4:29.
39. Hetz C, Zhang K, Kaufman RJ. Mechanisms, regulation and functions of the unfolded protein response. Nat Rev Mol Cell Biol. 2020;21(8):421-38.
40. Walter P, Ron D. The Unfolded Protein Response: From Stress Pathway to Homeostatic Regulation. Science. 2011;334(6059):1081-6.
41. Timmins JM, Ozcan L, Seimon TA, Li G, Malagelada C, Backs J, et al. Calcium/calmodulin-dependent protein kinase II links ER stress with Fas and mitochondrial apoptosis pathways. J Clin Invest. 2009;119(10):2925-41.
42. Santos CXC, Tanaka LY, Wosniak J, J., Laurindo FRM. Mechanisms and Implications of Reactive Oxygen Species Generation During the Unfolded Protein Response: Roles of Endoplasmic Reticulum Oxidoreductases, Mitochondrial Electron Transport, and NADPH Oxidase. ANTIOXIDANTS & REDOX SIGNALING. 2009;11(10).
43. Montezano AC, Touyz RM. Reactive oxygen species, vascular Noxs, and hypertension: focus on translational and clinical research. Antioxid Redox Signal. 2014;20(1):164-82.
44. Bravo-San Pedro JM, Kroemer G, Galluzzi L. Autophagy and Mitophagy in Cardiovascular Disease. Circ Res. 2017;120(11):1812-24.
45. van der Pluijm I, Burger J, van Heijningen PM, A IJ, van Vliet N, Milanese C, et al. Decreased mitochondrial respiration in aneurysmal aortas of Fibulin-4 mutant mice is linked to PGC1A regulation. Cardiovasc Res. 2018;114(13):1776-93.
46. Oller J, Gabande-Rodriguez E, Ruiz-Rodriguez MJ, Desdin-Mico G, Aranda JF, Rodrigues-Diez R, et al. Extracellular Tuning of Mitochondrial Respiration Leads to Aortic Aneurysm. Circulation. 2021;143(21):2091-109.
47. Siegert AM, Garcia Diaz-Barriga G, Esteve-Codina A, Navas-Madronal M, Gorbenko Del Blanco D, Alberch J, et al. A FBN1 3'UTR mutation variant is associated with endoplasmic reticulum stress in aortic aneurysm in Marfan syndrome. Biochim Biophys Acta Mol Basis Dis. 2019;1865(1):107-14.
48. Meirelles T, Araujo TLS, Nolasco P, Moretti AIS, Guido MC, Debbas V, et al. Fibrillin-1 mgDelta(lpn) Marfan syndrome mutation associates with preserved proteostasis and bypass of a protein disulfide isomerase-dependent quality checkpoint. Int J Biochem Cell Biol. 2016;71:81-91.
49. Ji F, Sadreyev RI. RNA-seq: Basic Bioinformatics Analysis. Curr Protoc Mol Biol. 2018;124(1):e68.
50. Geistlinger L, Csaba G, Santarelli M, Ramos M, Schiffer L, Turaga N, et al. Toward a gold standard for benchmarking gene set enrichment analysis. Brief Bioinform. 2021;22(1):545-56.
51. Askin L, Duman H, Ozyildiz A, Tanriverdi O, Turkmen S. Association between Omentin-1 and Coronary Artery Disease: Pathogenesis and Clinical Research. Curr Cardiol Rev. 2020;16(3):198-201.
52. Iyer NV, Leung SW, Semenxa GL. The Human Hypoxia-Inducible Factor 1α Gene: HIF1A Structure and Evolutionary Conservation. Genomics. 1998;52(2):159-65.
53. Gimenez M, Schickling BM, Lopes LR, Miller FJ, Jr. Nox1 in cardiovascular diseases: regulation and pathophysiology. Clin Sci (Lond). 2016;130(3):151-65.
54. Leone O, Corsini A, Pacini D, Corti B, Lorenzini M, Laus V, et al. The complex interplay among atherosclerosis, inflammation, and degeneration in ascending thoracic aortic aneurysms. J Thorac Cardiovasc Surg. 2020;160(6):1434-43 e6.

55. Waters KM, Rooper LM, Guajardo A, Halushka MK. Histopathologic differences partially distinguish syndromic aortic diseases. Cardiovasc Pathol. 2017;30:6-11.
56. Gabel G, Northoff BH, Weinzierl I, Ludwig S, Hinterseher I, Wilfert W, et al. Molecular Fingerprint for Terminal Abdominal Aortic Aneurysm Disease. J Am Heart Assoc. 2017;6(12).
57. Gabel G, Northoff BH, Balboa A, Becirovic-Agic M, Petri M, Busch A, et al. Parallel Murine and Human Aortic Wall Genomics Reveals Metabolic Reprogramming as Key Driver of Abdominal Aortic Aneurysm Progression. J Am Heart Assoc. 2021;10(17):e020231.
58. Sulkava M, Raitoharju E, Mennander A, Levula M, Seppala I, Lyytikainen LP, et al. Differentially expressed genes and canonical pathways in the ascending thoracic aortic aneurysm - The Tampere Vascular Study. Sci Rep. 2017;7(1):12127.
59. Huang X, Yu X, Li H, Han L, Yang X. Regulation mechanism of aquaporin 9 gene on inflammatory response and cardiac function in rats with myocardial infarction through extracellular signal-regulated kinase1/2 pathway. Heart Vessels. 2019;34(12):2041-51.
60. Tesse A, Gena P, Rutzler M, Calamita G. Ablation of Aquaporin-9 Ameliorates the Systemic Inflammatory Response of LPS-Induced Endotoxic Shock in Mouse. Cells. 2021;10(2).
61. Li Y, Chen B, Yang X, Zhang C, Jiao Y, Li P, et al. S100a8/a9 Signaling Causes Mitochondrial Dysfunction and Cardiomyocyte Death in Response to Ischemic/Reperfusion Injury. Circulation. 2019;140(9):751-64.
62. Salehipour P, Rezagholizadeh F, Mahdiannasser M, Kazerani R, Modarressi MH. Association of OLR1 gene polymorphisms with the risk of coronary artery disease: A systematic review and meta-analysis. Heart Lung. 2021;50(2):334-43.
63. Xie C, Ye F, Zhang N, Huang Y, Pan Y, Xie X. CCL7 contributes to angiotensin II-induced abdominal aortic aneurysm by promoting macrophage infiltration and pro-inflammatory phenotype. J Cell Mol Med. 2021;25(15):7280-93.
64. Qiao E, Huang Z, Wang W. Exploring potential genes and pathways related to calcific aortic valve disease. Gene. 2022;808:145987.
65. Xu Y, Ye J, Wang M, Wang Y, Ji Q, Huang Y, et al. Increased interleukin-11 levels in thoracic aorta and plasma from patients with acute thoracic aortic dissection. Clin Chim Acta. 2018;481:193-9.
66. Nunez J, de la Espriella R, Minana G, Santas E, Llacer P, Nunez E, et al. Antigen carbohydrate 125 as a biomarker in heart failure: a narrative review. Eur J Heart Fail. 2021;23(9):1445-57.
67. Nunez-Marin G, de la Espriella R, Santas E, Lorenzo M, Minana G, Nunez E, et al. CA125 but not NT-proBNP predicts the presence of a congestive intrarenal venous flow in patients with acute heart failure. Eur Heart J Acute Cardiovasc Care. 2021;10(5):475-83.
68. Huang F, Chen J, Liu Y, Zhang K, Wang J, Huang H. New mechanism of elevated CA125 in heart failure: the mechanical stress and inflammatory stimuli initiate CA125 synthesis. Med Hypotheses. 2012;79(3):381-3.
69. Li Y, He XN, Li C, Gong L, Liu M. Identification of Candidate Genes and MicroRNAs for Acute Myocardial Infarction by Weighted Gene Coexpression Network Analysis. Biomed Res Int. 2019;2019:5742608.
70. Klampatsa A, Dimou V, Albelda SM. Mesothelin-targeted CAR-T cell therapy for solid tumors. Expert Opin Biol Ther. 2021;21(4):473-86.
71. Wang Y, Liao H, Wang Y, Zhou J, Wang F, Xie Y, et al. KLK11 promotes the activation of mTOR and protein synthesis to facilitate cardiac hypertrophy. BMC Cardiovasc Disord. 2021;21(1):266.

72. Wang K, Bodempudi V, Liu Z, Borrego-Diaz E, Yamoutpoor F, Meyer A, et al. Inhibition of mesothelin as a novel strategy for targeting cancer cells. PLoS One. 2012;7(4):e33214.
73. Tan JJ, Guyette JP, Miki K, Xiao L, Kaur G, Wu T, et al. Human iPS-derived pre-epicardial cells direct cardiomyocyte aggregation expansion and organization in vitro. Nat Commun. 2021;12(1):4997.
74. Zhangyong X, Mingliang G, Xiaodong J, Xiaodong J, Xianting W, Chunxia W, et al. Integrated DNA methylation and gene expression analysis identifies SLAMF7 as a key regulator of atherosclerosis. Aging. 2018;10(6):1324 - 37.
75. Kang I, Chu CT, Kaufman BA. The mitochondrial transcription factor TFAM in neurodegeneration: emerging evidence and mechanisms. FEBS Lett. 2018;592(5):793-811.
76. Ngo HB, Lovely GA, Phillips R, Chan DC. Distinct structural features of TFAM drive mitochondrial DNA packaging versus transcriptional activation. Nat Commun. 2014;5:3077.
77. Sanchez-Infantes D, Nus M, Navas-Madronal M, Fite J, Perez B, Barros-Membrilla AJ, et al. Oxidative Stress and Inflammatory Markers in Abdominal Aortic Aneurysm. Antioxidants (Basel). 2021;10(4).
78. Hoshino S, Jain S, Shimizu C, Roberts S, He F, Daniels LB, et al. Biomarkers of inflammation and fibrosis in young adults with history of Kawasaki disease. Int J Cardiol Heart Vasc. 2021;36:100863.
79. Carbone F, Montecucco F. Inflammation in arterial diseases. IUBMB Life. 2015;67(1):18-28.
80. Heinz A. Elastic fibers during aging and disease. Ageing Res Rev. 2021;66:101255.

8. Supplementary

8.1. Quantity of the RNA in the samples

The quantity of the RNA in each sample was measured by NanoDrop 1000 Spectrophotometer (Thermo Scientific).

Table S1. RNA quantity of the samples.

Syndromic patients	RNA quantity (ng/uL)
TAA6	251
TAA12	299,7
TAA24	164
TAA26	130,1
TAA28	123
TAA32	432,1
TAA33	244
TAA44	261,1
Non-syndromic genetic patients	
TAA2	98,8
TAA41	55,9
TAA45	63,2
TAA50	122,8
TAA55	141,4
TAA60	256,9
TAA70	414,5
Patients with bicuspid aorta	
TAA9	35,8
TAA11	314,7
TAA27	304,8
TAA30	78,7
TAA31	188
TAA34	43,9
TAA42	347,9
TAA46	68,5
TAA47	395,7
TAA52	141,4
TAA58	74,6
TAA61	365,6
TAA71	47,3
TAA75	84,2

TAA81	205
TAA82	52,2
TAA83	156,8
Healthy donors	
DO1	685,1
DO2	301,5
DO3	303,1
DO4	41,8
DO5	515,6
DO6	352,7
DO7	107,6

8.2. RNA sequencing supplementary material

This section includes RNA sequencing data of the 50 most upregulated genes (Table S2-S4). The 50 most differentially expressed genes from each patient group were compared between patient groups.

Table S2. Top-50 most upregulated genes in AAT1 - Bicuspid vs. Donors (Healthy). **Green:** Gene only upregulated in this comparison study. **Blue:** Genes upregulated in AAT1 and AAT2 comparison groups. **Orange:** Genes upregulated in all comparison groups. **Pink**: Genes upregulated in AAT1 and AAT3 comparison groups.

gene_id	baseMean	log2FoldChange	FoldChange	lfcSE	stat	pvalue	-LOG pvalue	padj	status	control	comparison	gene_name	GSEA	TOP
ENSG00000181143.11	89,8795717	23,36786394	10825001,85	2,5247462	9,2555299	2,13E-20	19,6712731	3,45E-16	OK	1,66E-05	179,759127	MUC16	4,6911E+19	1
ENSG00000230259.2	50,869681	22,57914938	6266156,539	3,08119464	7,32805033	2,34E-13	12,6316666	1,26E-09	OK	1,62E-05	101,739346	AC008738.1	4,2822E+12	2
ENSG00000167757.9	48,6609758	22,50884967	5968138,858	2,72610944	8,25676671	1,50E-16	15,8248607	1,21E-12	OK	1,63E-05	97,3219352	KLK11	6,6813E+15	3
ENSG00000114638.3	52,221824	8,612841573	391,4926937	2,45119753	3,51372807	0,00044186	3,35471049	0,02025193	OK	0,26610342	104,177545	UPK1B	2263,13513	4
ENSG00000126353.3	115,302871	7,690265462	206,5382907	1,33624215	5,75514359	8,66E-09	8,06264171	2,80E-05	OK	1,11114793	229,494594	CCR7	115515884	5
ENSG00000179914.4	1871,61481	7,433335186	172,8450151	1,35708894	5,47741194	4,32E-08	7,36492696	7,76E-05	OK	21,5319928	3721,69762	ITLN1	23170049,3	6
ENSG00000186081.7	39,98299	7,41013256	170,0874117	1,64970911	4,49178131	7,06E-06	5,15101123	0,00137677	OK	0,46739838	79,4985815	KRT5	141583,04	7
ENSG00000177820.5	22,6323049	7,401377978	169,0584102	2,10997665	3,5078009	0,00045183	3,34502776	0,0204193	OK	0,26617096	44,9984388	AC004917.1	2213,23616	8
ENSG00000165390.11	136,868288	7,236000894	150,7486105	2,22349201	3,25434086	0,00113656	2,94440832	0,0384694	OK	1,80388192	271,932693	ANXA8	879,849358	9
ENSG00000271856.1	30,6247381	7,232499243	150,3831632	2,01301162	3,59287507	0,00032705	3,48538662	0,01658725	OK	0,404599	60,8448773	RP11-861A13.4	3057,64191	10
ENSG00000102854.10	188,221164	7,122369292	139,330693	1,76904144	4,02611783	5,67E-05	4,24637649	0,00533392	OK	2,68253736	373,75979	MSLN	17635,0418	11
ENSG00000268903.1	122,476613	7,099104326	137,1018593	2,02255413	3,50997	0,00044816	3,34856956	0,0203839	OK	1,77371418	243,179513	RP11-34P13.15	2231,35958	12
ENSG00000105369.5	318,9006	6,89185212	118,7556316	1,23700748	5,57139081	2,53E-08	7,59737116	6,23E-05	OK	5,32585559	632,475344	CD79A	39570465,9	13
ENSG00000148204.7	22,2096253	6,805996549	111,8945958	1,41191296	4,82040802	1,43E-06	5,8438602	0,00050696	OK	0,39345772	44,0257928	CRB2	698007,671	14
ENSG00000112486.10	21,182861	6,697395967	103,7808155	1,6430756	4,0761338	4,58E-05	4,33922293	0,00451736	OK	0,40432709	41,9613949	CCR6	21838,5062	15
ENSG00000141668.5	20,2342736	6,623238314	98,58104121	1,61112167	4,11094857	3,94E-05	4,40446303	0,00431074	OK	0,40638807	40,062159	CBLN2	25378,3295	16
ENSG00000254870.1	12,1441593	6,50431791	90,78096445	1,91127385	3,40313237	0,00066618	3,17640842	0,02635239	OK	0,26463351	24,0236851	ATP6V1G2-DDX39B	1501,09584	17
ENSG00000183813.6	26,8948076	6,485087164	89,57890735	1,51275598	4,2869354	1,81E-05	4,74194981	0,00273065	OK	0,59384262	53,1957726	CCR4	55201,3639	18
ENSG00000169594.8	57,1284587	6,393000421	84,03977656	1,47394257	4,33734702	1,44E-05	4,84099607	0,00228747	OK	1,34357029	112,913347	BNC1	69341,9534	19
ENSG00000211747.3	10,2041463	6,242063371	75,69170872	1,61099767	3,87465699	0,00010677	3,97153046	0,00796089	OK	0,2661082	20,1421844	TRBV20-1	9365,48912	20
ENSG00000184937.8	64,477634	6,119164162	69,51074786	1,2518315	4,88816919	1,02E-06	5,99234589	0,00042618	OK	1,82887392	127,126394	WT1	982530,148	21
ENSG00000160856.16	42,3443176	6,11207045	69,16980336	1,36797563	4,46796736	7,90E-06	5,10255794	0,0014728	OK	1,20690997	83,4817253	FCRL3	126636,22	22
ENSG00000132872.7	16,6565037	5,873981655	58,64684751	1,59426307	3,68444943	0,000229197520589034	3,63979008	0,0131496	OK	0,55850407	32,7545033	SYT4	4363,04894	23
ENSG00000243566.2	358,631783	5,872335627	58,57997317	1,21621662	4,82836325	1,38E-06	5,86119281	0,00050618	OK	12,0386688	705,224897	UPK3B	726428,389	24

ENSG00000105697.3	27,0888297	5,83842739	57,21919875	1,07523727	5,42989676	5,64E-08	7,24882363	9,12E-05	OK	0,93058064	53,2470787	HAMP	17734691,1	25
ENSG00000006555.6	10,0131169	5,716391393	52,578147	1,18617116	4,81919608	1,44E-06	5,84122199	0,00050696	OK	0,37377616	19,6524577	TTC22	693780,349	26
ENSG00000123405.9	33,6592588	5,669340102	50,89105172	1,25965966	4,50069197	6,77E-06	5,16920226	0,00136453	OK	1,29730494	66,0212126	NFE2	147639,395	27
ENSG00000135925.4	14,3177015	5,623869865	49,31210264	1,37041637	4,10376729	4,06E-05	4,39096474	0,00431074	OK	0,56915536	28,0662476	WNT10A	24601,6786	28
ENSG00000211898.3	95,5580874	5,582620706	47,92214919	1,05100918	5,31167643	1,09E-07	6,96408484	0,00012233	OK	3,90653677	187,209638	IGHD	9206293,92	29
ENSG00000104921.10	28,5403517	5,576421743	47,71667937	1,25767518	4,43391252	9,25E-06	5,03367901	0,00166353	OK	1,17168707	55,9090163	FCER2	108063,495	30
ENSG00000172137.14	203,772336	5,546811108	46,74729909	1,11209164	4,98772844	6,11E-07	6,21400598	0,00032948	OK	8,53544976	399,009223	CALB2	1636839,05	31
ENSG00000185245.6	13,7946243	5,523595232	46,00106101	1,65211728	3,34334329	0,00082775	3,08209855	0,03093504	OK	0,58699204	27,0022566	GP1BA	1208,08794	32
ENSG00000154639.14	17,8168656	5,485882172	44,81414205	1,24943722	4,39068254	1,13E-05	4,9469392	0,00194484	OK	0,7777889	34,8559422	CXADR	88499,1697	33
ENSG00000260655.1	25,2290151	5,457353044	43,93665228	1,47072966	3,71064323	0,00020673	3,68458958	0,01216268	OK	1,12287026	49,33516	CTA-250D10.23	4837,15031	34
ENSG00000163600.8	94,5925934	5,325214066	40,09121031	1,1529735	4,61867862	3,86E-06	5,41319734	0,00102429	OK	4,60403053	184,581156	ICOS	258938,923	35
ENSG00000174171.4	18,1125429	5,320060578	39,94825492	1,34141961	3,96599285	7,31E-05	4,13613578	0,00625683	OK	0,88465518	35,3404307	RP11-23P13.6	13681,5652	36
ENSG00000026751.12	258,55507	5,274216375	38,69878521	0,9549062	5,52328215	3,33E-08	7,47791487	6,73E-05	OK	13,0258429	504,084298	SLAMF7	30054871,2	37
ENSG00000133048.8	302,713514	5,186869246	36,4253075	1,07229013	4,83718827	1,32E-06	5,88045154	0,00049549	OK	16,176942	589,250086	CHI3L1	759366,689	38
ENSG00000186810.7	39,9563639	5,181823122	36,29812501	1,05152753	4,92790057	8,31E-07	6,08030546	0,00039552	OK	2,14254008	77,7701878	CXCR3	1203110,35	39
ENSG00000110448.6	124,512022	5,15488869	35,62674293	0,97380427	5,29355729	1,20E-07	6,92096485	0,00012233	OK	6,79896777	242,225077	CD5	8336137,12	40
ENSG00000197506.6	27,4980388	5,124653168	34,88785921	1,27758137	4,01121471	6,04E-05	4,21891171	0,00558473	OK	1,53244241	53,4636351	SLC28A3	16554,3338	41
ENSG00000116748.15	19,3758717	5,066869966	33,51813484	1,48621001	3,40925571	0,0006514	3,18614965	0,02595828	OK	1,12264882	37,6290945	AMPD1	1535,14587	42
ENSG00000125910.4	87,4641759	5,065037441	33,47558683	1,0988111	4,60956158	4,04E-06	5,39413601	0,00105299	OK	5,0739775	169,854374	S1PR4	247819,806	43
ENSG00000185905.3	147,864888	5,051742539	33,1685155	0,99501556	5,07704879	3,83E-07	6,41641308	0,00025842	OK	8,65503727	287,074738	C16orf54	2608633,59	44
ENSG00000174837.10	24,407523	4,985378047	31,67731272	1,27004016	3,92537039	8,66E-05	4,06250022	0,00697036	OK	1,4938513	47,3211947	EMR1	11547,8257	45
ENSG00000264198.1	188,351018	4,982587166	31,61609246	0,89611472	5,56021127	2,69E-08	7,5695246	6,23E-05	OK	11,5495759	365,152461	RP11-94L15.2	37112875,2	46
ENSG00000119866.16	29,7860007	4,924816482	30,37508375	1,24368312	3,95986437	7,50E-05	4,12498308	0,006327	OK	1,89870414	57,6732972	BCL11A	13334,6947	47
ENSG00000227507.2	218,787497	4,901543664	29,88901947	0,91598978	5,35108993	8,74E-08	7,0583591	0,00011787	OK	14,166037	423,408957	LTB	11438237,2	48
ENSG00000172215.5	17,4841403	4,895621446	29,76657746	1,16551437	4,20039563	2,66E-05	4,57438594	0,00339268	OK	1,13656713	33,8317136	CXCR6	37530,6375	49
ENSG00000153002.7	40,747285	4,840670583	28,65411798	1,26878793	3,81519281	0,00013608	3,86621642	0,0093487	OK	2,74817042	78,7463995	CPB1	7348,79989	50

Table S3. Top-50 most upregulated genes in AAT2 - Syndromic vs. Donors (Healthy). **Green:** Gene only upregulated in that comparison study. **Blue:** Genes upregulated in AAT1 and AAT2 comparison studies. **Yellow:** Genes upregulated in AAT2 and AAT3 comparison studies. **Pink:** Genes upregulated in AAT1 and AAT3 comparison studies.

Gene_id	BaseMean	log2FoldChange	FoldChange	lfcSE	Stat	Pvalue	-LOG pvalue	Padj	Status	control	comparison	gene_name	TOP
ENSG00000163736.3	50,714707	8,13519271	281,149313	1,62447621	5,00788664	5,50E-07	6,25939316	0,00010091	OK	0,35948843	101,069926	PPBP	1
ENSG00000244115.1	24,1594246	7,65774271	201,934374	2,42411742	3,15898176	0,00158321	2,80	0,02607271	OK	0,23810086	48,0807484	DNAJC25-GNG10	2
ENSG00000211933.2	39,5581694	7,20596841	147,642924	1,93470343	3,72458553	0,00019564	3,71	0,0063508	OK	0,53225769	78,5840811	IGHV6-1	3
ENSG00000254870.1	16,6970044	7,12514621	139,599137	3,10409783	2,29540002	0,02171021	1,66E+00	0,12912231	OK	0,23751219	33,1564967	ATP6V1G2-DDX39B	4
ENSG00000241294.1	36,0915835	6,53266339	92,5822286	2,04842283	3,18911863	0,00142707	2,85	0,0242098	OK	0,77133413	71,411833	IGKV2-24	5
ENSG00000196565.8	12,5823294	6,50958478	91,1129857	1,45922065	4,46100101	8,16E-06	5,09	0,00068274	OK	0,27319339	24,8914653	HBG2	6
ENSG00000211669.2	53,8328116	6,08126842	67,7086581	1,54748584	3,92977321	8,50E-05	4,07	0,00347786	OK	1,56698772	106,098635	IGLV3-10	7
ENSG00000163737.3	26,4562165	6,0529031	66,3904164	1,43344499	4,22262671	2,41E-05	4,62	0,0015157	OK	0,78516258	52,1272705	PF4	8
ENSG00000211950.2	29,8191575	5,93812174	61,3130277	2,09578583	2,83336286	0,00460611	2,34E+00	0,05092523	OK	0,95707619	58,6812388	IGHV1-24	9
ENSG00000211968.2	10,3022675	5,84160164	57,3452323	1,75977526	3,31951571	0,00090174	3,04	0,01743644	OK	0,35314856	20,2513864	IGHV1-58	10
ENSG00000180871.3	62,5979581	5,80418295	55,8770114	1,32228631	4,38950545	1,14E-05	4,94	0,00088713	OK	2,20116903	122,994747	CXCR2	11
ENSG00000163735.6	34,3145385	5,59417711	48,3075609	1,17676754	4,75385062	2,00E-06	5,70	0,0002585	OK	1,39185707	67,2372199	CXCL5	12
ENSG00000103569.5	172,609233	5,43699091	43,320888	0,80174678	6,78143153	1,19E-11	10,92	3,24E-08	OK	7,78906923	337,429396	AQP9	13
ENSG00000211946.2	18,2475176	5,42690098	43,0189669	1,8494368	2,9343533	0,00334244	2,48	0,04192816	OK	0,82907523	35,6659599	IGHV3-20	14
ENSG00000224650.2	78,8992896	5,32300871	40,0299721	1,26863383	4,19585901	2,72E-05	4,57	0,00161324	OK	3,84593435	153,952645	IGHV3-74	15
ENSG00000228078.1	10,0866882	5,21172244	37,0582394	1,5736406	3,31188866	0,00092668	3,03	0,01777143	OK	0,53006594	19,6433104	HLA-U	16
ENSG00000163464.7	28,6495302	4,89948583	29,8464167	1,05376511	4,6495047	3,33E-06	5,48	0,00037193	OK	1,8575597	55,4415007	CXCR1	17
ENSG00000188536.8	617,195342	4,87669596	29,3786451	0,60929133	8,00388206	1,21E-15	14,92	9,84E-12	OK	40,6335003	1193,75718	HBA2	18
ENSG00000196611.4	34,4545712	4,83308999	28,5039507	1,54675283	3,12466859	0,00178005	2,75	0,02804102	OK	2,33559034	66,573552	MMP1	19
ENSG00000211660.3	199,127117	4,79105996	27,6855247	1,52814861	3,13520552	0,00171734	2,77	0,02731671	OK	13,8834565	384,370778	IGLV2-23	20
ENSG00000206172.4	398,584247	4,75350082	26,9740608	0,70971168	6,69779148	2,12E-11	10,67	4,93E-08	OK	28,4967027	768,671791	HBA1	21
ENSG00000211659.2	48,273729	4,71411719	26,2476651	1,72460893	2,73344124	0,00626763	2,20E+00	0,06167667	OK	3,54332959	93,0041284	IGLV3-25	22
ENSG00000108688.7	18,7162026	4,57410805	23,820108	1,41163492	3,24029109	0,00119408	2,92	0,02129764	OK	1,50814836	35,9242568	CCL7	23
ENSG00000171049.8	20,0560615	4,55184284	23,4553129	0,90665708	5,020468	5,15E-07	6,29	9,56E-05	OK	1,64022122	38,4719019	FPR2	24

ENSG00000105697.3	11,5100813	4,52986118	23,1006443	0,99719896	4,54258515	5,56E-06	5,26	0,00052725	OK	0,95516794	22,0649948	HAMP	25
ENSG00000244734.2	1173,30485	4,46478271	22,0817516	0,82263747	5,42740011	5,72E-08	7,24	2,17E-05	OK	101,665148	2244,94455	HBB	26
ENSG00000167772.7	11417,6321	4,41297201	21,3028126	1,29631354	3,4042474	0,00066347	3,18	0,01434142	OK	1023,87374	21811,3904	ANGPTL4	27
ENSG00000211965.2	29,952048	4,40919776	21,2471548	1,75926865	2,50626745	0,01220133	1,91E+00	0,09154105	OK	2,69266325	57,2114328	IGHV3-49	28
ENSG00000170866.7	15,9070437	4,3909466	20,9800556	1,16943755	3,75475082	0,00017351	3,76	0,00580114	OK	1,44740705	30,3666803	LILRA3	29
ENSG00000211668.2	66,0018999	4,36489975	20,6046743	1,72022142	2,53740576	0,01116774	1,95E+00	0,08699645	OK	6,10996482	125,893835	IGLV2-11	30
ENSG00000085265.6	147,464077	4,32697943	20,070149	0,63284879	6,83730382	8,07E-12	11,09	2,63E-08	OK	13,9974403	280,930713	FCN1	31
ENSG00000211898.3	36,2703573	4,30795659	19,8072487	1,41183769	3,05131151	0,00227844	2,64	0,03276137	OK	3,4863194	69,0543952	IGHD	32
ENSG00000029559.5	14,4560124	4,25745444	19,1258829	1,29507968	3,28740734	0,00101114	3,00	0,01891811	OK	1,43655932	27,4754654	IBSP	33
ENSG00000101916.11	41,4446336	4,22810864	18,740774	0,7630565	5,54101645	3,01E-08	7,52	1,42E-05	OK	4,19888638	78,6903808	TLR8	34
ENSG00000211637.2	26,62983	4,22595882	18,7128685	1,18432435	3,56824447	0,00035938	3,44	0,00942028	OK	2,70177118	50,5578888	IGLV4-69	35
ENSG00000165685.4	10,363482	4,17563662	18,0714031	1,10658681	3,77343791	0,00016101	3,79	0,00547445	OK	1,08680855	19,6401555	TMEM52B	36
ENSG00000211679.2	1166,95711	4,16709574	17,9647349	1,27946331	3,25690914	0,00112632	2,95	0,02040136	OK	123,066008	2210,84821	IGLC3	37
ENSG00000211890.3	414,675775	4,07370851	16,8386959	1,38127841	2,94923057	0,00318566	2,50	0,04064895	OK	46,4917141	782,859836	IGHA2	38
ENSG00000186407.4	248,011038	4,05374641	16,6073089	1,07027113	3,78758829	0,00015212	3,82	0,00527079	OK	28,1713735	467,850702	CD300E	39
ENSG00000095752.2	15,2035884	4,05002255	16,5644977	1,16651556	3,47189759	0,00051679	3,29	0,01203148	OK	1,73117257	28,6760041	IL11	40
ENSG00000121807.5	42,0578014	4,04884879	16,5510265	0,88316148	4,58449434	4,55E-06	5,34	0,0004629	OK	4,79263153	79,3229713	CCR2	41
ENSG00000103888.11	434,241884	4,01639147	16,1828238	0,73294144	5,47982588	4,26E-08	7,37	1,69E-05	OK	50,543716	817,940052	KIAA1199	42
ENSG00000069482.6	23,1419925	4,00976982	16,1087185	1,19321213	3,36048361	0,00077806	3,11	0,01588675	OK	2,7052865	43,5786985	GAL	43
ENSG00000173391.4	124,114218	4,00495907	16,0550924	0,93523092	4,28232106	1,85E-05	4,73	0,00125247	OK	14,5545055	233,673931	OLR1	44
ENSG00000248323.1	35,2219511	3,99563021	15,9516108	1,0950033	3,64896636	0,0002633	3,58	0,00770075	OK	4,15558751	66,2883148	LUCAT1	45
ENSG00000162849.11	23,2895368	3,85769025	14,4970781	0,94274665	4,09196919	4,28E-05	4,37	0,00220901	OK	3,00566812	43,5734055	KIF26B	46
ENSG00000268903.1	12,1386948	3,83506414	14,2714908	2,11480248	1,81343845	0,06976422	1,16E+00	0,25714854	OK	1,58971969	22,6876698	RP11-34P13.15	47
ENSG00000110777.7	36,2056434	3,78724426	13,8061988	1,14869676	3,29699221	0,00097726	3,01	0,01852169	OK	4,89060613	67,5206807	POU2AF1	48
ENSG00000162747.5	69,513045	3,76149725	13,5619926	0,69427662	5,41786537	6,03E-08	7,22	2,24E-05	OK	9,54718864	129,478901	FCGR3B	49
ENSG00000211899.3	725,402208	3,65785256	12,6218595	1,32159523	2,76775558	0,00564438	2,25E+00	0,05771694	OK	106,505607	1344,29881	IGHM	50
ENSG00000250366.2	30,4300914	3,58519151	12,001905	0,9797313	3,65936203	0,00025284	3,60	0,00752995	OK	4,68086658	56,1793162	LINC00617	51

ENSG00000258227.2	331,986531	3,54016438	11,6331055	0,73640578	4,8073555	1,53E-06	5,82	0,00021333	OK	52,5581823	611,41488	CLEC5A	54
ENSG00000110427.10	32,2467489	3,47234318	11,0988876	0,78325632	4,43321436	9,28E-06	5,03	0,00075006	OK	5,33053121	59,1629666	KIAA1549L	56
ENSG00000106952.3	81,2424181	3,45991832	11,0037115	0,71349388	4,84926135	1,24E-06	5,91	0,00018554	OK	13,5362164	148,94862	TNFSF8	57
ENSG00000166920.6	19,3331856	3,41978175	10,7018014	0,94930298	3,60241339	0,00031528	3,50	0,00870611	OK	3,30430932	35,3620619	C15orf48	61
ENSG00000118785.9	2413,10671	3,410421	10,6325888	0,71797937	4,75002644	2,03E-06	5,69	0,00025937	OK	414,887306	4411,32612	SPP1	62
ENSG00000149418.6	148,94042	3,39938433	10,5515594	0,80865513	4,20375041	2,63E-05	4,58	0,00158667	OK	25,7870672	272,093772	ST14	63
ENSG00000224397.1	38,6412253	3,32489074	10,0205566	0,89254933	3,72516186	0,00019519	3,71	0,0063508	OK	7,01257239	70,2698782	RP11-290F20.3	65
ENSG00000124731.8	151,237618	3,30346992	9,87287268	0,77925982	4,23924066	2,24E-05	4,65	0,00144102	OK	27,8192567	274,65598	TREM1	67
ENSG00000163221.7	26,7929773	3,23178896	9,39432146	0,81928346	3,94465303	7,99E-05	4,10	0,00335276	OK	5,15531051	48,4306441	S100A12	70
ENSG00000143546.5	265,560004	3,22838656	9,37219234	0,71735337	4,5004132	6,78E-06	5,17	0,00060259	OK	51,2061472	479,913861	S100A8	72
ENSG00000128383.8	29,6832835	3,14891016	8,86985277	0,84934405	3,70746126	0,00020935	3,68	0,00668831	OK	6,01493948	53,3516276	APOBEC3A	77
ENSG00000026751.12	55,9507253	3,11992408	8,69342139	0,80335557	3,88361542	0,00010291	3,99	0,00396124	OK	11,5440613	100,357389	SLAMF7	81
ENSG00000163814.3	331,03497	2,95324985	7,7449174	1,02280366	2,88740641	0,00388432	2,41	0,04573746	OK	75,7091131	586,360827	CDCP1	92
ENSG00000128342.4	406,180989	2,91958304	7,56627408	0,7559063	3,86236104	0,0001123	3,95	0,00422276	OK	94,8325925	717,529386	LIF	94
ENSG00000125910.4	18,2558761	2,85689518	7,24454547	0,78747034	3,62794005	0,00028569	3,54	0,0081512	OK	4,42859493	32,0831574	S1PR4	99
ENSG00000148848.10	314,71678	2,75190799	6,73607403	0,76956854	3,57591019	0,00034901	3,46	0,00923634	OK	81,3634354	548,070125	ADAM12	106
ENSG00000185905.3	28,3678916	2,73085757	6,63850124	0,55075845	4,95835799	7,11E-07	6,15	0,00012288	OK	7,42760673	49,3081765	C16orf54	111
ENSG00000110448.6	19,1619227	2,68806715	6,44449429	0,87073786	3,08711414	0,0020211	2,69	0,03042289	OK	5,14794477	33,1759007	CD5	118
ENSG00000164283.8	216,239357	2,67941323	6,40595309	0,77507515	3,45697217	0,00054628	3,26	0,01241687	OK	58,3960915	374,082623	ESM1	122
ENSG00000264198.1	34,8113105	2,59063073	6,02361988	0,86003196	3,01224938	0,00259319	2,59	0,03532632	OK	9,91264079	59,7099801	RP11-94L15.2	133
ENSG00000138944.7	200,15346	2,56598268	5,9215821	0,68136899	3,76592233	0,00016594	3,78	0,00563007	OK	57,8345984	342,472322	KIAA1644	139
ENSG00000164171.6	521,007814	2,56360853	5,91184537	0,57249384	4,47796701	7,54E-06	5,12	0,00065417	OK	150,757949	891,25768	ITGA2	140
ENSG00000126262.4	10,7389558	2,50020715	5,65766656	0,88637335	2,82071561	0,00479167	2,32E+00	0,05215998	OK	3,22604195	18,2518696	FFAR2	153
ENSG00000137558.3	171,697303	2,30023294	4,92537285	1,09574498	2,09924113	0,03579565	1,45E+00	0,17403051	OK	57,9532488	285,441358	PI15	199
ENSG00000111863.8	12,7385652	1,75486177	3,37493981	0,81199067	2,16118466	0,03068108	1,51E+00	0,15881009	OK	5,82342422	19,6537062	ADTRP	405

Table S4. Top-50 most upregulated genes in AAT3 - Genetic vs. Donors (Healthy). **Green:** Gene only upregulated in that comparison study. **Blue:** Genes upregulated in AAT1 and AAT2 comparison studies. **Yellow:** Genes upregulated in AAT2 and AAT3 comparison studies. **Pink:** Genes upregulated in AAT1 and AAT3 comparison studies.

Gene_id	BaseMean	log2FoldChange	FoldChange	lfcSE	Stat	Pvalue	-LOG pvalue	padj	Status	Control	comparison	Gene_name	TOP
ENSG00000163736.3	37,8964499	7,98430841	253,230682	1,89218949	4,21961354	2,45E-05	4,61132795	0,00227773	OK	0,29812649	75,4947734	PPBP	1
ENSG00000163735.6	140,264554	7,91478074	241,316164	1,86528459	4,24320277	2,20E-05	4,65688268	0,00210963	OK	1,1576987	279,371409	CXCL5	2
ENSG00000244115.1	20,7352358	7,71045422	209,448859	2,04520333	3,77001842	0,00016324	3,78718539	0,00736504	OK	0,19705724	41,2734143	DNAJC25-GNG10	3
ENSG00000254870.1	11,9579227	6,91240201	120,459303	3,02888125	2,28216343	0,02247969	1,64820961	0,11916026	OK	0,19690419	23,7189411	ATP6V1G2-DDX39B	4
ENSG00000103569.5	169,202645	5,7196505	52,6970575	0,83002672	6,89092338	5,54E-12	11,2562442	9,03E-08	OK	6,30211981	332,10317	AQP9	5
ENSG00000069482.6	60,686916	5,71822978	52,6451886	1,37318746	4,16420187	3,12E-05	4,50522839	0,00273607	OK	2,26252969	119,111302	GAL	6
ENSG00000095752.2	38,0551457	5,70502321	52,1654685	1,49954048	3,8045143	0,00014208	3,84745879	0,00694769	OK	1,43157379	74,6787175	IL11	7
ENSG00000108688.7	30,5813852	5,527673	46,1312667	1,0360503	5,33533265	9,54E-08	7,02059025	6,23E-05	OK	1,29771115	59,8650593	CCL7	8
ENSG00000180871.3	37,0196244	5,38347364	41,7433256	1,62398582	3,31497576	0,00091651	3,03786246	0,0197854	OK	1,73218269	72,3070661	CXCR2	9
ENSG00000183019.3	53,6445168	5,28496752	38,9882506	1,51874624	3,47982263	0,00050175	3,29951622	0,01409041	OK	2,68301394	104,60602	C19orf59	10
ENSG00000196611.4	35,9578313	5,14743877	35,4432444	1,60334665	3,2104341	0,00132535	2,87767055	0,02472035	OK	1,9733606	69,9423019	MMP1	11
ENSG00000166670.5	13,5250107	4,89704461	29,7959555	1,39862877	3,50131838	0,00046296	3,33445428	0,01341767	OK	0,87836279	26,1716585	MMP10	12
ENSG00000186407.4	322,30619	4,69747334	25,9465953	1,22179759	3,84472303	0,00012069	3,91833348	0,00636075	OK	23,9218489	620,690532	CD300E	13
ENSG00000250366.2	48,0094646	4,48643831	22,4157102	1,40400576	3,19545577	0,0013961	2,85508291	0,02533945	OK	4,10061998	91,9183093	LINC00617	14
ENSG00000197632.4	39,2266491	4,43582006	21,6428721	1,38824841	3,19526391	0,00139703	2,85479418	0,02533945	OK	3,46481215	74,988486	SERPINB2	15
ENSG00000173391.4	123,39255	4,25108655	19,0416494	0,84938705	5,00488743	5,59E-07	6,25262949	0,00016421	OK	12,3136123	234,471488	OLR1	16
ENSG00000162747.5	74,0236238	4,20413581	18,4319373	0,96519104	4,35575514	1,33E-05	4,87742716	0,00148961	OK	7,618759	140,428489	FCGR3B	17
ENSG00000248323.1	27,8199993	4,14098197	17,6424862	1,01381658	4,08454749	4,42E-05	4,35494346	0,00337403	OK	2,98458039	52,6554183	LUCAT1	18
ENSG00000170866.7	11,1540657	4,10404008	17,1964645	1,15606918	3,54999525	0,00038524	3,41427076	0,01213686	OK	1,22595966	21,0821718	LILRA3	19
ENSG00000163464.7	13,8486873	4,07782843	16,8868512	1,10002674	3,70702664	0,00020971	3,67838731	0,00838971	OK	1,54847683	26,1488977	CXCR1	20
ENSG00000258227.2	362,864954	3,98453272	15,8293787	0,72981794	5,4596256	4,77E-08	7,32135446	4,57E-05	OK	43,1227987	682,60711	CLEC5A	21
ENSG00000211940.2	23,7980307	3,94545525	15,4063719	1,95469018	2,01845556	0,04354384	1,36107329	0,17260697	OK	2,90107171	44,6949896	IGHV3-9	22
ENSG00000166920.6	22,2716777	3,89522948	14,8792456	0,9762669	3,98992273	6,61E-05	4,17983255	0,00427203	OK	2,80513045	41,738225	C15orf48	23
ENSG00000085265.6	92,8727738	3,8884076	14,8090542	0,74243726	5,23735517	1,63E-07	6,78809482	8,89E-05	OK	11,7493143	173,996233	FCN1	24

ENSG00000149418.6	165,622163	3,84344697	14,3546572	1,05702305	3,63610517	0,00027679	3,55784747	0,00984362	OK	21,5728898	309,671437	ST14	25
ENSG00000188536.8	255,066313	3,8282858	14,2045951	0,73192779	5,2304146	1,69E-07	6,7717786	8,89E-05	OK	33,5512142	476,581412	HBA2	26
ENSG00000106952.3	77,040724	3,81705216	14,0944196	0,73408435	5,19974598	2,00E-07	6,69992419	9,85E-05	OK	10,2078419	143,873606	TNFSF8	27
ENSG00000251491.2	25,1878635	3,70493071	13,040531	2,19479675	1,68805184	0,09140128	1,03904774	0,26291513	OK	3,58787905	46,7878479	OR7E28P	28
ENSG00000118785.9	2436,04339	3,67768449	12,7965632	1,05486711	3,48639602	0,00048958	3,31018017	0,013944	OK	353,137714	4518,94907	SPP1	29
ENSG00000128342.4	579,977513	3,62381961	12,3275962	1,11011744	3,26435698	0,00109713	2,95974256	0,0219957	OK	87,0340765	1072,92095	LIF	30
ENSG00000124875.5	14,9731574	3,60985373	12,2088358	1,2787083	2,82304708	0,00475696	2,32267063	0,05187713	OK	2,26714264	27,6791721	CXCL6	31
ENSG00000164283.8	327,785607	3,57547873	11,9213749	0,75747621	4,72025218	2,36E-06	5,62791242	0,00045137	OK	50,7354068	604,835806	ESM1	32
ENSG00000167772.7	5420,81475	3,53659676	11,6043738	0,96989293	3,64637852	0,00026596	3,57518022	0,00958405	OK	860,148207	9981,48129	ANGPTL4	33
ENSG00000211943.2	14,3924883	3,5148893	11,431076	1,2288098	2,86040142	0,00423105	2,37355176	0,04879334	OK	2,31556599	26,4694107	IGHV3-15	34
ENSG00000224397.1	31,3012756	3,49210077	11,2519315	0,93157797	3,74858668	0,00017783	3,7499855	0,00773443	OK	5,10960668	57,4929445	RP11-290F20.3	35
ENSG00000162105.12	77,2469674	3,49024789	11,2374897	0,79844759	4,37129242	1,24E-05	4,90828648	0,00142372	OK	12,6246426	141,869292	SHANK2	36
ENSG00000137558.3	318,811956	3,4896749	11,2330275	1,11969494	3,11663006	0,00182931	2,73771277	0,02972076	OK	52,1231488	585,500762	PI15	37
ENSG00000126262.4	16,5918305	3,47197587	11,0960622	1,13766791	3,051836	0,00227446	2,64312106	0,03401879	OK	2,74334412	30,4403169	FFAR2	38
ENSG00000148848.10	375,948094	3,45448343	10,9623365	0,67419172	5,12388886	2,99E-07	6,52389698	0,00012761	OK	62,8552946	689,040893	ADAM12	39
ENSG00000138944.7	301,910768	3,4483081	10,9155135	0,68228139	5,05408493	4,32E-07	6,3640549	0,00013749	OK	50,6752423	553,146293	KIAA1644	40
ENSG00000206172.4	139,335263	3,43693634	10,8298123	0,79972986	4,29762159	1,73E-05	4,76285716	0,00175748	OK	23,5566313	255,113896	HBA1	41
ENSG00000143546.5	255,150023	3,41395076	10,6586348	1,00534725	3,39579262	0,0006843	3,16475228	0,01686579	OK	43,7701371	466,529909	S100A8	42
ENSG00000163221.7	25,287468	3,40029711	10,5582375	1,027875	3,30808427	0,00093937	3,02716544	0,02005293	OK	4,37566161	46,1992743	S100A12	43
ENSG00000111863.8	33,2399588	3,39771459	10,5393544	0,73587671	4,61723348	3,89E-06	5,41017362	0,00063982	OK	5,76114704	60,7187705	ADTRP	44
ENSG00000128383.8	32,9737571	3,39306715	10,505458	1,12971633	3,00346827	0,00266921	2,57361664	0,03700098	OK	5,7318461	60,2156682	APOBEC3A	45
ENSG00000163814.3	379,017618	3,37738986	10,3919167	1,06700368	3,16530291	0,00154922	2,80988809	0,02693023	OK	66,5415011	691,493736	CDCP1	46
ENSG00000164171.6	748,071031	3,36756042	10,3213546	0,52331078	6,43510611	1,23E-10	9,90873024	6,70E-07	OK	132,152213	1363,98985	ITGA2	47
ENSG00000102962.4	12,2422994	3,29915891	9,84341496	1,30524616	2,52761435	0,01148404	1,93990523	0,08227053	OK	2,25801547	22,2265833	CCL22	48
ENSG00000110427.10	24,0239492	3,28871576	9,77241925	0,89051353	3,69305536	0,00022158	3,65447774	0,00853198	OK	4,46027001	43,5876285	KIAA1549L	49
ENSG00000124731.8	121,313744	3,26689349	9,62571355	0,84850949	3,85015552	0,00011804	3,92796032	0,00626281	OK	22,8339948	219,793493	TREM1	50
ENSG00000101916.11	15,2914693	2,94328652	7,69161485	0,77457108	3,79989207	0,00014476	3,83935407	0,00697365	OK	3,51867164	27,064267	TLR8	69

ENSG00000121807.5	15,9529893	2,8554747	7,23741599	0,74159485	3,85045109	0,0001179	3,92848445	0,00626281	OK	3,87329943	28,0326793	CCR2	75
ENSG00000244734.2	266,041756	2,40922071	5,3118732	1,15988019	2,07712894	0,03778966	1,42262702	0,16004435	OK	84,2988279	447,784685	HBB	123
ENSG00000103888.11	126,390784	2,23186468	4,69740727	0,58028677	3,84614093	0,00011999	3,92084494	0,00634559	OK	44,3678248	208,413743	KIAA1199	154
ENSG00000211668.2	13,8051466	2,12323766	4,3567057	1,22834436	1,72853617	0,08389214	1,07627872	0,24980534	OK	5,154342	22,4559512	IGLV2-11	180
ENSG00000211660.3	24,7243095	1,71487668	3,28268583	0,98854808	1,73474282	0,08278637	1,08204117	0,24787212	OK	11,5461701	37,9024489	IGLV2-23	284
ENSG00000133048.8	26,1126972	1,67707881	3,197798	0,96861145	1,73142575	0,08337586	1,07895969	0,24876826	OK	12,4411404	39,784254	CHI3L1	303
ENSG00000185905.3	12,2918144	1,48733391	2,80370375	0,63446295	2,34424078	0,01906586	1,71974363	0,10849692	OK	6,46307663	18,1205521	C16orf54	412
ENSG00000026751.12	15,6622546	1,23875388	2,35994605	0,85356344	1,45127335	0,14670376	0,83355876	0,34067733	OK	9,32292028	22,0015888	SLAMF7	641
ENSG00000211679.2	163,94562	1,12766884	2,18505386	0,7829439	1,44029328	0,14978444	0,8245333	0,34429706	OK	102,946843	224,944397	IGLC3	798

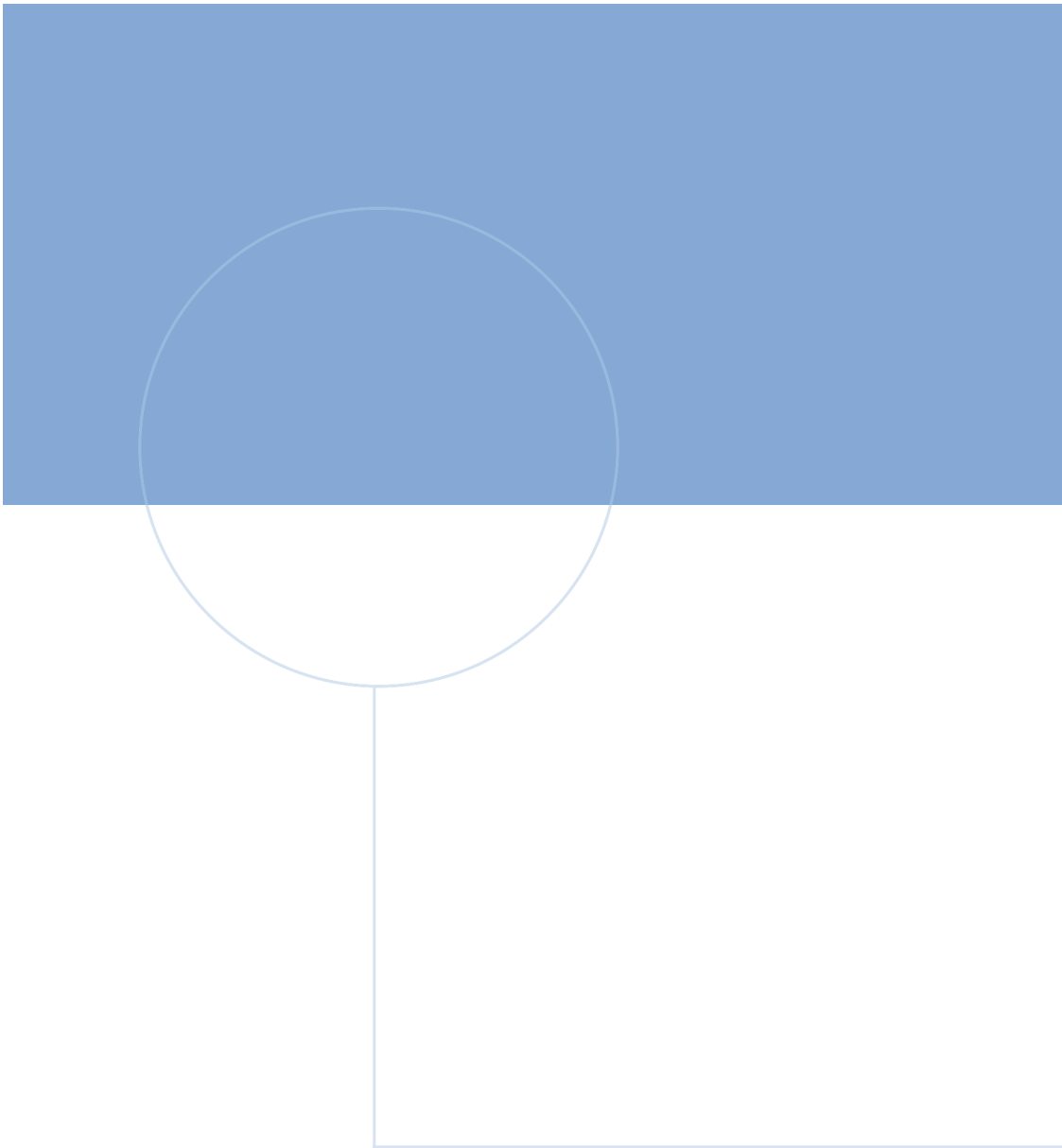

NTNU

Kunnskap for en bedre verden